Buoyancy driven bubbly flows: role of meso-scale structures on the relative motion between phases, and scaling of velocities in bubble columns operated up to the heterogeneous regime

Yann Mezui M'obiang, Martín Obligado, Alain H. Cartellier

▶ **To cite this version:**

Yann Mezui M'obiang, Martín Obligado, Alain H. Cartellier. Buoyancy driven bubbly flows: role of meso-scale structures on the relative motion between phases, and scaling of velocities in bubble columns operated up to the heterogeneous regime. 2022. ⟨hal-03615797⟩

HAL Id: hal-03615797

https://hal.science/hal-03615797v1

Preprint submitted on 21 Mar 2022

HAL is a multi-disciplinary open access archive for the deposit and dissemination of scientific research documents, whether they are published or not. The documents may come from teaching and research institutions in France or abroad, or from public or private research centers.

L'archive ouverte pluridisciplinaire **HAL**, est destinée au dépôt et à la diffusion de documents scientifiques de niveau recherche, publiés ou non, émanant des établissements d'enseignement et de recherche français ou étrangers, des laboratoires publics ou privés.

HAL Authorization

arXiv:2203.07417v1 [physics.flu-dyn] 14 Mar 2022

Buoyancy driven bubbly flows: role of meso-scale structures on the relative motion between phases, and scaling of velocities in bubble columns operated up to the heterogeneous regime

Y. Mezui[1], M. Obligado[1] and A. Cartellier[1]†

[1]Université Grenoble Alpes, CNRS, Grenoble-INP, LEGI, F-38000, Grenoble, France

(Received xx; revised xx; accepted xx)

The hydrodynamics of bubble columns is revisited, with an emphasis on the origin of the increase in the relative velocity observed in the heterogeneous regime. We focus on air-water systems, with no or limited coalescence and a quasi-fully developed region where the flow self-organizes when it reaches the heterogeneous regime.

We show from dimensional analysis that, in the heterogeneous regime, buoyancy equilibrates inertia, and that velocities scale as $(gD\varepsilon)^{1/2}$, where D is the bubble column diameter, ε the void fraction and g the gravitational acceleration. This scaling holds for both liquid and gas mean velocities and for their standard deviations, and it is valid over a large range of column diameter and of gas superficial velocities, corresponding to Froude numbers $Fr = V_{sg}/(gD)^{1/2}$ from 0.02 to 0.5.

To investigate further the analogy with turbulent convection, experiments are performed in a 0.4m diameter column with $O(10^3)$ particle Reynolds numbers bubbles. The self-organization prevailing in the heterogeneous regime is confirmed, with a recirculating liquid flow rate that only depends on the column diameter D. The void fraction at small scales is analysed using Voronoï tessellations, that allow to identify meso-scale structures (clusters), void and intermediate regions. A series of arguments are presented that demonstrate that the large relative velocity observed in the heterogeneous regime originates from the presence of meso-scale structures. Concerning velocity fluctuations, a flow picture is presented that seems consistent with a fast track mechanism which, for moderate Rouse numbers, leads to liquid velocity fluctuations proportional to the relative velocity.

Key words:

1. Introduction

In bubble columns, gas is injected at the bottom of an initially stagnant liquid. Such systems are often used in industry as reactors (chemical and biochemical transformations), in separation techniques (flotation...), to promote agitation and mixing (metallurgy)... Yet, the hydrodynamics of bubble columns operated in the heterogeneous regime remains difficult to predict. In such gravity driven bubbly flows, there is indeed

† Email address for correspondence: alain.cartellier@cnrs.fr

no imposed external forcing such as pressure gradient, heat flux at walls... Instead, the motion is driven by buoyancy only. Bubbles transfer momentum to the liquid and tend to impose their dynamics to the continuous phase, but their motion is strongly constrained by liquid inertia. The resulting dynamical equilibrium is hard to capture as it involves non-trivial momentum exchange as well as turbulence production and dissipation processes. That dynamics gives rise to complex flow structures: in a cylindrical column, secondary motions are superimposed on the mean recirculation arising at the reactor scale. These motions are said to be 'chaotic' by Noël De Nevers who noticed in 1968: 'In unbaffled systems these circulations are unstable and chaotically change in size, shape, and orientation. These chaotic circulations provide the principal mode of vertical bubble transport in bubble columns over a wide range of operating conditions' (De Nevers (1968)). The complexity of such dynamical structures is still beyond our understanding. Indeed, since the mid of the 20th century, more than 8000 articles have been published in connection with bubble columns and their hydrodynamics, with a current flux above 500 new contributions per year. These figures show that the exploitation of bubble columns in process engineering is expanding, and this is notably so in emerging biotechnologies. They also demonstrate that, in spite of a continuous and sustained scientific production over more than 70 years, the hydrodynamics of bubble columns operated in the heterogeneous regime is not yet mastered. In particular, there is still no consensus on the scaling of key variables such as void fraction, mean liquid velocity, velocity fluctuations. Indeed, the successive reviews by Deckwer & Field (1992); Joshi *et al.* (1998); Kantarci *et al.* (2005); Rollbusch *et al.* (2015); Kikukawa (2017); Besagni *et al.* (2018), all quote more than typically ten different correlations for the same variable. Similarly, and despite progresses in two-fluid modeling, the numerical simulation of bubble columns is not mastered as shown by the recent review of Shu *et al.* (2019). Such simulations require ad-hoc adjustments: the latter could notably be on the bubble size to modulate the relative velocity (e.g. Ekambara *et al.* (2005)), on the drag coefficient as a function of the local void fraction to represent an effective momentum exchange between phases that leads either to a decrease (e.g. Roghair *et al.* (2011)) or to an increase in the relative velocity due to a swarm effect (e.g. McClure *et al.* (2017); Gemello *et al.* (2018))... In addition, the question of the turbulence production and of its modeling is not settled, and very recently modeling attempts accounting for meso-scale structures and their impact on the dynamics started to appear (e.g. Capecelatro *et al.* (2015); Panicker *et al.* (2020)).

In this paper, the hydrodynamics of bubble columns is revisited in the light of recent experimental results: the latter support the idea that a strong analogy exists between a bubble column in the heterogeneous regime and turbulent buoyancy-driven flows in confined channels with zero mean flow. This prompted us to hypothesize that a dynamical equilibrium between inertia and buoyancy holds in the heterogeneous regime: such an equilibrium leads to a liquid velocity that scales as $V_{liquid} = (gD\varepsilon)^2$, where g is the gravitational acceleration, D the column diameter and ε stands for the void fraction (Cartellier (2019)). In this paper, that scaling proposal is analysed and tested against previous experimental data reported in the literature, as well as against gas phase velocities collected from a recently developed Doppler optical probe (Lefebvre *et al.* (2019, 2022)). We will notably show that, for bubble columns operated in the heterogeneous regime, both mean and fluctuating axial velocities of the liquid phase and of the gas phase closely follow the proposed scaling. Furthermore, by introducing gas velocity measurements conditioned by the local concentration, we will show that the presence of meso-scale structures in the heterogeneous regime induces a relative velocity that is significantly larger than the bubble terminal velocity. Finally, a scaling law for that relative velocity will be also proposed and discussed.

2. New velocity scaling proposal based on the equilibrium between inertia and buoyancy

Prior to the discussion on velocity scaling, let us first stress the analogy between hydrodynamics of bubble columns in the heterogeneous regime and turbulent convection in a vertical channel with zero mean flow. In a previous campaign (Raimundo *et al.* (2019)), controlled air-water experiments were performed over a wide range of column sizes (diameter D from 0.15 to 3m) and superficial velocities (V_{sg} from 3 to 35cm/s) while keeping a fixed bubble size. More precisely, the Sauter mean horizontal diameter was the same within $\pm 1mm$ in all columns at a given V_{sg}: it increased from 6 to 8mm over the range of V_{sg} with a mean eccentricity always close to 0.7. Accordingly, the equivalent diameter evolved from 4.7 to 7mm, and thus, the terminal velocity was nearly constant, equal to 0.21 ± 0.01cm/s whatever the flow conditions. Coalescence being avoided (or at least, it was too weak to influence the flow behavior), we have been able to clarify some key features of bubble columns operated in the heterogeneous regime, namely:

- The homogeneous-heterogeneous transition was observed with a fixed bubble size, meaning that coalescence is not necessary for such a transition to occur.
- In the heterogeneous, regime, local void fraction fluctuations, as quantified by a one-dimensional Voronoï analysis (Raimundo (2015); Mezui *et al.* (2018); Raimundo *et al.* (2019)), evolve between typically one tenth to ten times the average gas hold-up.
- The co-existence of 'dense' regions corresponding to clusters of bubbles with regions almost 'free of bubbles' called 'voids' induces strong differences in local velocities.
- As local velocity and void fraction are strongly correlated, the bubble transport is controlled by these clusters/voids meso-scale structures: this is the probable origin of the observed increase in the apparent relative velocity of the gas in the heterogeneous regime, an effect usually represented in two-fluid numerical simulations via a swarm coefficient.
- The presence of clusters and voids in the mixture induces strong local shear rates as well as intense 3D vortical structures that are expected to significantly contribute to turbulence production.

Clearly, the fluctuations in the mixture density induce strong spatial and temporal fluctuations in buoyancy (Figure 1): they are thus reminiscent of convective instabilities arising in turbulent buoyancy driven flows.

Some analogies also hold on the global flow structure. Indeed, a quasi-fully developed region exists in bubble columns operated in the heterogeneous regime. Such a region appears in systems that are not too strongly confined: according to Wilkinson *et al.* (1992), a minimum internal diameter of 0.15m is a necessary condition (possibly, that condition is helpful to avoid the development of a slug flow regime). In addition, the aspect ratio should be large enough so that end effects do not affect the flow organization in the central portion of the column: Wilkinson *et al.* (1992) argue that the dynamic height H_D of the mixture should exceed 5 diameters while Forret (2003) established that $H_D/D = 3$ is a sufficient condition for large (namely $D = 0.4$m and 1m) columns. When introducing the static liquid height H_0, these conditions transform into $H_0/D \geqslant 3.8$ or 2.3, respectively, indicating that the bubble column should not be operated in the shallow water limit for a quasi-fully developed region to exist. Moreover, when the above conditions are fulfilled, the way gas injection is performed has no impact on the flow organization outside the entrance region. That conclusion has been ascertained in air-water systems with a gas injection evenly distributed over the column cross-section, and for large enough injection orifices (orifice diameter above 1mm according to Wilkinson *et al.* (1992), above 0.5 mm according to Sharaf *et al.* (2016)). When one considers the so called 'pure' heterogeneous regime, i.e. flow conditions such that

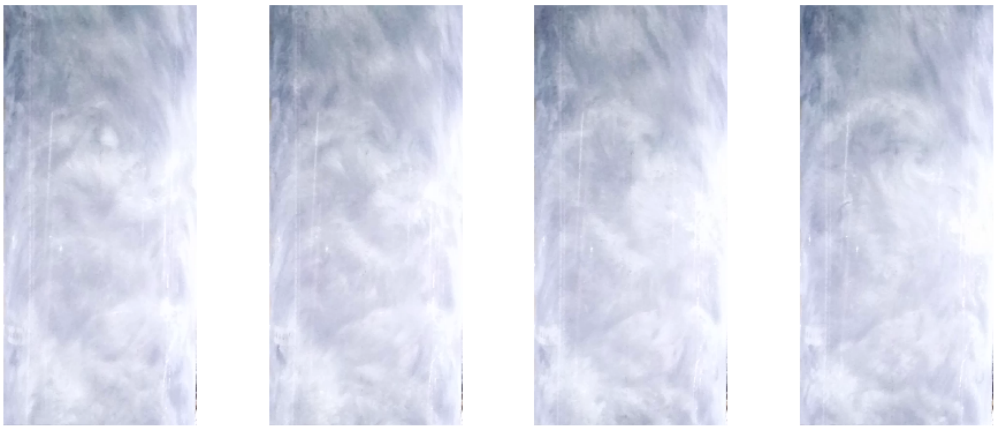

Figure 1: Illustration of the unsteady structures related with vorticity and/or void fraction appearing in bubble columns operated in the heterogeneous regime. Air-water bubble column D=0.4m, static liquid height $H_0 = 2$m, $V_{sg} = 23$cm/s. Visualization of the flow in the vicinity of column walls between about 0.8 and 2 meters above gas injection. The time increment between images is 1/30s.

the void fraction versus the superficial velocity is concave and that are far enough from the homogeneous/heterogeneous transition (Ruzicka (2013); Sharaf *et al.* (2016)), that conclusion seems to hold also when changing the coalescence efficiency by way of surfactants or of water purity (Sharaf *et al.* (2016)). The precise extend of the quasi-fully developed region is not precisely known: it is said to range from the end of the entrance region those extend is about one (Forret *et al.* (2006)) or two (see Guan *et al.* (2016) and references therein) column diameters, up to typically one column diameter below the free-surface (Forret *et al.* (2006)). Within that quasi-fully developed region, the self-similarity of the flow structure in the heterogeneous regime - in terms of transverse profiles of void fraction and liquid mean as well as fluctuating velocities - was shown to hold for diameters ranging from 0.15m up to 3m, and for superficial velocities spanning almost a decade, that is from the transition that arises for V_{sg} about a few cm/s up to about $35 - 40$cm/s (Forret *et al.* (2006); Raimundo *et al.* (2019)). In particular the mean liquid velocity profiles consistently exhibit an inversion of the velocity direction at distance from the column axis equal to $0.7R$ where R is the column radius. By design, there is no net liquid flow in a bubble column. In the homogeneous regime the back flow occurs everywhere in between ascending bubbles. In the heterogeneous regime, the two-phase flow auto-organizes itself at large scale by forming a global recirculation with an upward directed flow along the axis and a downward directed flow along the walls.

Such a large-scale organization is reminiscent of turbulent buoyancy-driven flows in confined channels with zero mean flow where density gradients are due to solute concentration Cholemari & Arakeri (2009) or to temperature Castaing *et al.* (2017). As for long channels or pipes, the translational invariance observed along the bubble column axis implies that the only characteristic length is the column diameter, provided that the column is high enough. Besides, and owing to that translational invariance, an uniform density gradient develops along the channel (Cholemari & Arakeri (2009); Castaing *et al.* (2017)). That expectation is corroborated in bubble columns. Indeed, in the quasi-fully developed region, the local void fraction measured on the column axis ε_{axis}, exhibits a linear growth with the vertical distance above the gas injector, and the

slope $d\varepsilon_{axis}/d(H/R)$ is proportional to the mean void fraction in the column (see figure 26 in reference Lefebvre *et al.* (2022)).

Neglecting the density of the gas compared to that of the liquid (all the experiments discussed hereafter were performed at ambient pressure conditions), the local density ρ of the mixture becomes $\rho \sim (1-\varepsilon)\rho_L$ (with ρ_L the density of the liquid phase). As the void fraction increases with the height above the injector, the density decreases with the height. Hence, the vertical stratification observed on the bubble column axis is stable. This contrasts with most investigations made on zero-mean flow buoyancy-driven turbulence in pipes. For the later, the boundary conditions imposed at the top and bottom ends of the vertical pipe or channel are fixed temperature or solute concentration corresponding to unstable situations. The output is to evaluate the vertical flux of heat or of solute concentration. In bubble columns, the boundary conditions are different since it is the gas volumetric flux through the system that is imposed, and the void fraction is the unknown parameter. The origin of the flow destabilization is not the same in bubble columns as it involves a radial reorganization of the two phases. Such a global structuration into clearly defined up and down flow regions is, in a sense, similar to the Boycott effect due to stratification. Yet, in both cases, up and down mean flows do appear those structuration could be intermittent (Gibert *et al.* (2009); Rusaouen *et al.* (2014)). In bubble columns, the self-organization observed in the heterogeneous regime leads to a stable recirculation. That circulation is related with a lateral gradient in void fraction that induces radially distributed axial buoyancy forces. In other words, in the liquid momentum balance, fluid inertia terms (namely $\rho\partial_t v_{Li}$, $\rho v_{Lj}\partial_j v_{Li}$ and $\partial_i p$) equilibrate buoyancy. Within a Boussinesq approximation, the later equals $g_i\Delta\rho$ where g is the gravitation acceleration and $\Delta\rho$ the difference in density at the origin of buoyant forces. Hence, the velocity scale for the liquid obeys:

$$V_L \propto \sqrt{(gD\Delta\rho/\rho)}, \tag{2.1}$$

where $\Delta\rho/\rho$ is evaluated at a large length scale. In turbulent buoyancy-driven flows in confined channels, the constant axial gradient of the mean density is used to evaluate $\Delta\rho$ (Cholemari & Arakeri (2009); Castaing *et al.* (2017)). In bubble columns, as the flow destabilization arises from lateral differences in density and thus in buoyancy, we sought a relevant scale from the radial void fraction profile. The void fraction typically evolves between ε_{axis} on the column axis and nearly 0 in the wall zone. Thus, the magnitude of the radial difference in density $\Delta\rho$ over a length scale of the order of the column diameter D is $\Delta\rho \sim D\partial\rho/\partial r \sim \rho_L D\partial\varepsilon/\partial r \sim \rho_L\varepsilon_{axis}$. Therefore, it shows that the void fraction on the axis ε_{axis} is a measure of the radial density gradient $\Delta\rho/\rho_L$. As ε_{axis} is proportional to the global void fraction (Raimundo *et al.* (2016)), one can use any characteristic gas fraction ε in the system to estimate the magnitude of the radial density gradient $\Delta\rho/\rho_L$. Consequently, the scaling from equation 2.1 becomes:

$$V_L \propto \sqrt{(gD\varepsilon)}. \tag{2.2}$$

The Boussinesq approximation is not mandatory for the derivation of Eq. 2.2. Indeed, for a bubbly flow, the dynamical equilibrium for the liquid phase balances at first order inertia terms (i.e. $\rho_L DV_L/Dt$) with the momentum transfer between phases. The later, homogeneous to a force per cubic meter, can be estimated as the void fraction times the force F exerted by a single bubble on the fluid divided by the bubble volume $\mathcal{V}$. Hence, the momentum equation for the liquid writes at first order:

$$\rho_L DV_L/Dt = -\nabla P + \mu_L \Delta V_L + \varepsilon F/\mathcal{V}, \tag{2.3}$$

where the pressure gradient term p includes the hydrostatic contribution. Along the vertical direction that force F corresponds to the buoyancy on a bubble, i.e. to $\rho_L g_i \mathcal{V}$. The momentum transfer amounts then to $\varepsilon \rho_L g_i$, and the Eq. 2.2 scaling is recovered by balancing inertia and buoyancy without using the Boussinesq approximation, that is without constraints on the relative velocity between phases.

Former experimental results support the velocity scaling proposed in Eq. 2.2. Indeed, in Raimundo *et al.* (2019), we evaluated the liquid flow rate Q_{Lup} in the core region of the flow that is in the zone where the mean liquid velocity is upward directed. Owing to the self-organization of the flow occurring in the heterogeneous regime, that region extends from the column axis up to a radial distance of $0.7R$ (that $0.7R$ limit was also identified by Kawase & Moo-Young (1986)). We have shown that, in the heterogeneous regime, Q_{Lup} is independent of the gas superficial velocity. Instead, Q_{Lup} only depends on the column diameter D and it scales as $D^{5/2}$: consequently, $(gD)^{1/2}$ was identified as the proper velocity scale for the mean flow circulation. Equation 2.2 is consistent with that result since the void fraction is known to be weakly sensitive (if any) to the column diameter. In the following, we test the relevance of Eq. 2.2 for bubble columns in the heterogeneous regime by examining a number of experimental results relative to the liquid and to the gas velocities including mean and fluctuating components. In section 3, we consider new experiments in which we succeeded to gather reliable statistics on bubble velocity. In section 4, we examine data sets extracted from the literature.

3. Test of the scaling on new gas and liquid velocity data collected in a $D = 0.4m$ bubble column

A new optical probe that combines accurate phase detection (its sensing length is very small, equal to 6μm) with gas velocity measurements based on Doppler signals collected from approaching interfaces has been recently developed based on a technology patented by A2 Photonic Sensors. The probe design, the signal processing and the sensor qualification are detailed in Lefebvre *et al.* (2022), where mean bubble velocity profiles in a $D = 0.4$m bubble column were also presented. In the following, we exploit further that probe to examine how bubble velocity statistics evolve with the gas superficial velocity. In parallel, classical Pavlov tubes are also used to access the liquid velocity. Let us first summarise the experimental conditions.

3.1. *Experimental conditions*

The experiment consisted in a 3m high and $D = 0.4$m internal diameter bubble column functioning with air and water. The gas injector was a 10mm thick plexiglass plate perforated by 352 orifices of 1mm internal diameter. These orifices were uniformly distributed over the column cross-section. The column was filled with tap water at an initial height $H_0 = 2.02$m. The surface tension of the tap water used was 67mN/m at 25°C, its pH evolves in the interval $[7.7, 7.9]$ and its conductivity varied in range $330 - 450\mu$S/cm, indicating the presence of a significant solid content. All the data presented here were gathered at $H = 1.45$m above injection that is at $H/D = 3.625$, a position well within the quasi fully developed region. Besides, and owing to the large ratio $H_0/D = 5.05$, the information collected in that zone is not sensitive to the static liquid height H_0. Experiments were achieved for superficial velocities V_{sg} ranging from 0.6cm/s to 26cm/s.

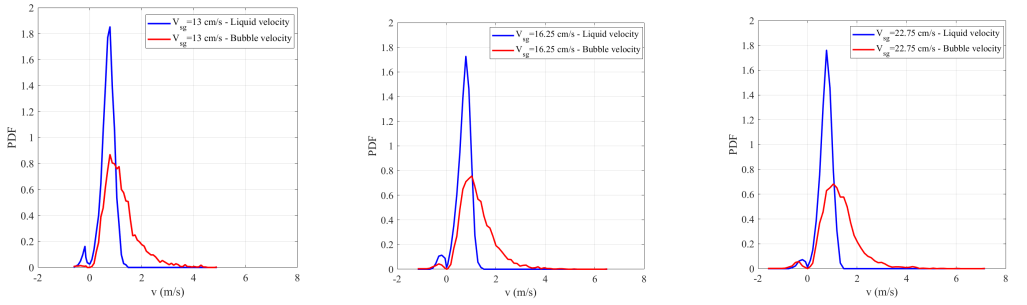

(a) (b) (c)

Figure 2: Velocity pdfs for the liquid and for the bubbles measured on the column axis at $H/D = 3.625$ for $v_{sg} = 13$cm/s (a), $v_{sg} = 16.25$cm/s (b) and $v_{sg} = 22.75$cm/s (c).

Information relative to bubbles was acquired with the Doppler probe. For each bubble detected, the probe gives access to the gas residence time t_G, that is the time spent by the probe tip inside the bubble. Besides, a Doppler signal is recorded from the rear interface (that is at the gas to liquid transition) for some bubble signatures, and its analysis provides the bubble velocity V_b projected along the fiber axis. When both the gas residence time t_{Gi} and the bubble velocity V_{bi} are available for the ith bubble, one can infer the gas chord $C_i = V_{bi}t_{Gi}$ cut by the probe through that bubble.

For the liquid, velocity statistics were measured with a Pavlov device made of two parallel tubes (external diameter 6mm, internal diameter 5mm), each drilled with a 0.5mm in diameter hole. These two orifices faced opposite directions: they were aligned along a vertical, and the vertical distance between them was 12mm. The pressure transducer was a Rosemount 2051 CD2 with a dynamics of $\pm$15000 Pa, a resolution of $\pm$9.75 Pa and a response time of 130ms. The differential pressure was transformed into the local liquid velocity using $v_L^2(t) = \pm 2|p(t)|/\rho_L$ (no correction dependent on void fraction was considered) with the appropriate sign. Hence, the dynamics in velocity was $\pm$5.48m/s and the resolution $\pm$0.14m/s.

Liquid and gas velocity pdfs measured with these sensors in the center of the column are illustrated Figure 2. By construction, the Pavlov tube detects both positive (upward directed, i.e. against gravity) and negative (downward directed, i.e. along gravity) velocities. For bubbles, as the Doppler probe detects only inclusions approaching it head on, the pdfs were built by cumulating the information gathered over the same measuring duration and at the same position with an upward directed probe and with a downward directed probe. More details and discussion concerning these measurements are presented in Lefebvre *et al.* (2022).

Concerning the bubble size, the analysis of the axial evolution of chords distributions along the column indicates that coalescence was absent (or at least extremely weak) in our experimental conditions (Lefebvre *et al.* (2022)), most probably because of the partial contamination of the tap water used. Over the investigated range of superficial velocities, the Sauter mean vertical diameter of bubbles remained in the interval $[6.2mm; 6.7mm]$ while their Sauter mean horizontal diameter measured with the correlation technique (Raimundo *et al.* (2016)) increased with V_{sg} from 6.6 to 7.8mm. Overall, the mean equivalent bubble diameter remained in the interval $[6.62mm; 7.35mm]$: that corresponds to a terminal velocity from 21cm/s to 23cm/s (Maxworthy *et al.* (1996)) and to particle Reynolds numbers in the range $1450 - 1550$.

The local void fraction measured on the column axis ε_{axis} is plotted versus the gas

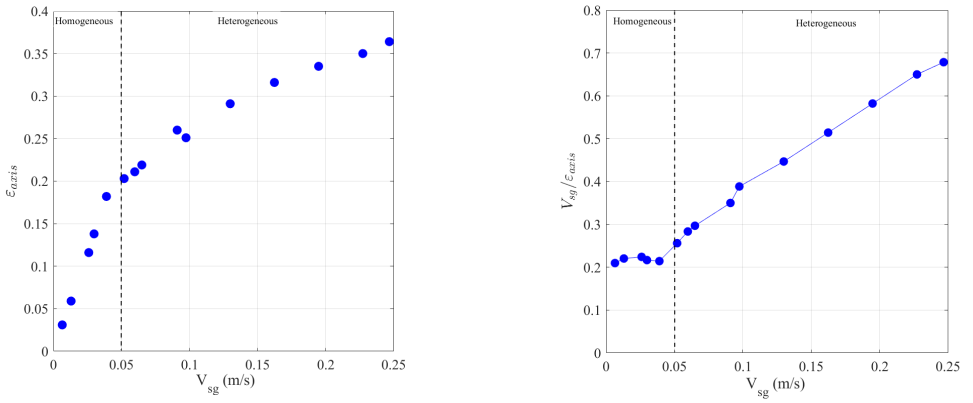

Figure 3: (a) Evolution of the local void fraction ε_{axis} on the column axis with the gas superficial velocity V_{sg}. (b) Plot of the apparent rise velocity estimated as $V_{sg}/\varepsilon_{axis}$ versus V_{sg}. Measurements with a downward directed Doppler probe at an height $H/D = 3.625$ above injection. The vertical dashed lines delineate the homogeneous to heterogeneous transition.

superficial velocity in Figure 3a. The homogeneous regime ends for V_{sg} between $\sim$ 4cm/s and $\sim$ 5cm/s, while the 'pure' heterogeneous regime starts at $V_{sg} \sim 6.5cm/s$. Following Krishna *et al.* (1991), these data are plotted as $V_{sg}/\varepsilon_{axis}$ versus V_{sg} in Figure 3b: they exhibit a constant rise velocity, close to the bubble terminal velocity U_T, up to $V_{sg} \sim$ 4cm/s that is within the homogeneous regime. Beyond that, the apparent rise velocity (called 'rise velocity of swarm' by Krishna *et al.* (1991)), monotonously increases with the gas superficial velocity. It reaches a magnitude about 3 times U_T at the largest V_{sg} investigated here (namely 24.7cm/s). That increase is the signature of the heterogeneous regime. Note also that the latter correspond to a void fraction on the axis that exceeds about 20%. In the following, the transition will be represented by a vertical dash line at $V_{sg} = 5$cm/s in figures as a guide to eye.

3.2. *Local gas and liquid velocity on the column axis versus V_{sg}*

Figure 4 provides the mean vertical velocities of bubbles V_G and of the liquid V_L on the column axis as well as the standard deviations V'_G for the gas phase and V'_L for the liquid phase. Two datasets are presented for the mean velocities.

For bubbles, a set named 'up flow' corresponds to measurements achieved with a Doppler probe pointing downward that collects only upward directed (i.e. positive) vertical velocities. A second set of data named 'up and down flow' was obtained by gathering direct (i.e. without interpolation) velocity measurements from a probe pointing downward, with direct (i.e. without interpolation) velocity measurements from the same probe pointing upward. In this process, the measuring duration was the same for the two probe orientations. In the flow conditions considered here, the mean velocities from these two sets are close, with a difference of at most 4% (Lefebvre *et al.* (2022)). Similarly, the difference on bubble velocity standard deviations from these two sets is at most 8%.

For the liquid, two sets of data are also presented for the velocity: one corresponds to moments evaluated over the entire distribution (named 'up and down flow') while the other concerns positive velocities only (named 'up flow'). In the heterogeneous regime, the difference between the two sets is at most 3.6% for the mean value and 18% for the

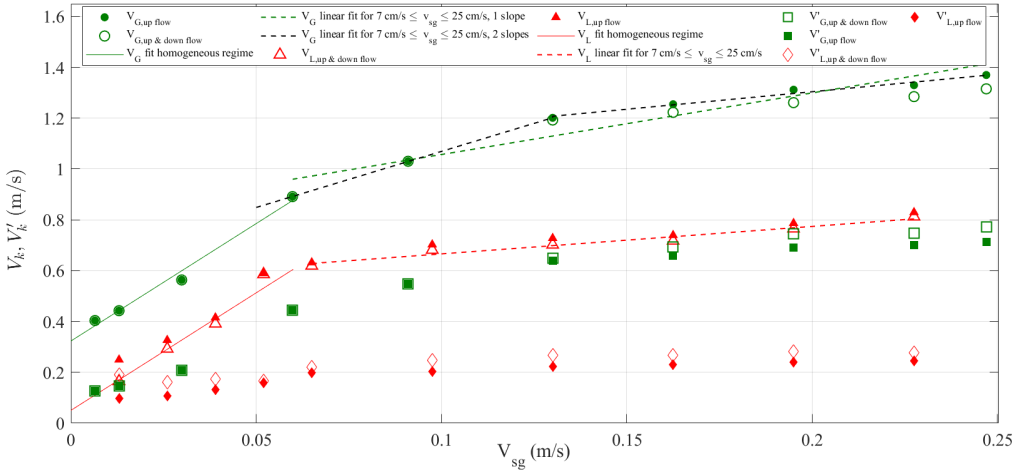

Figure 4: Evolution of the mean vertical velocities of the bubbles VG and of the liquid V_L, and of their standard deviation (V'_G for the gas, V'_L for the liquid), with the gas superficial velocity V_{sg}. Measurements performed in a $D = 0.4$m column, at $H/D = 3.625$ and on the column axis. The bubble velocities were measured with a Doppler probe and the liquid velocities with a Pavlov tube. The straight lines in the homogeneous (continuous lines) and in the heterogeneous (dashed lines) regime are linear fits of the data. Note that in the heterogeneous regime, two plausible trends (green and black dashed lines) are proposed for the mean bubble velocity. The difference between 'up flow' and 'up and down flow' sets is explained in the text.

standard deviation. Oddly, larger liquid velocity deviations between 'up flow' and 'up and down flow' statistics appear in the homogeneous regime. The difference is especially pronounced for V_{sg} below 3cm/s. These deviations are related with the unexpected apparition of a significant negative tail in the liquid velocity pdfs when V_{sg} becomes small, a defect that may possibly be due to the flow perturbation induced by the rather large probe holder used here.

Except for these low V_{sg} cases, the differences between the 'up flow' and the 'up and down flow' data sets remain weak. These small differences partly come from the fact that these data are all collected on the column axis, where the probability of occurrence of absolute negative velocities in the laboratory frame remains limited. Indeed, in our experiments, the probability to observe a downward directed liquid velocity on the axis was less than 3% for any V_{sg} in the heterogeneous regime. Similarly, Xue *et al.* (2008) found a probability for observing negative bubble velocities on the column axis about 4% to 4.5% at $V_{sg} = 14$cm/s and about 6% at $V_{sg} = 60$cm/s. For the gas phase, and because of the positive (upward directed) relative velocity, these probabilities should be lower than the above figures. Hence, considering either 'up flow' or 'up and down flow' data sets does not change the conclusions proposed hereafter. Yet, the distinction between the two series is worth to be kept in mind in the perspective of analyzing other radial positions where the probability of occurrence of downward flow increases.

From the data presented Figure 4, a series of comments and conclusions emerge.

(i) the local relative velocity $V_G - V_L$ remains nearly constant in the homogeneous regime. It is about 27cm/s, a magnitude comparable to the 'mean' terminal velocity U_T of the bubbles generated in the column.

(ii) in the heterogeneous regime, the relative velocity becomes larger than U_T. Even

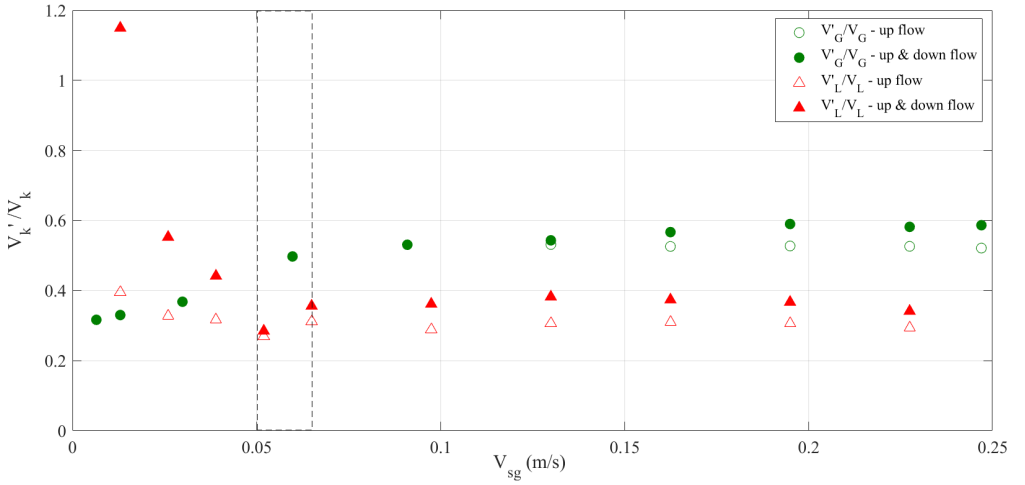

Figure 5: Vertical velocity fluctuations V'/V of liquid and gas phases versus the gas superficial velocity V_{sg}. Measurements performed in a $D = 0.4$m column, on the column axis at $H/D = 3.625$.

more, it seems to monotonously increase with V_{sg} (see the trend indicated by the green and red dashed lines in Figure 4). At about $V_{sg} = 19.5$m/s, the measured relative velocity amounts to 54.6 cm/s that is 2.5 times the terminal velocity U_T. Thus, these direct velocity measurements are consistent with the behavior of the 'rise velocity of swarm' $V_{sg}/\varepsilon_{axis}$ shown in Figure 3. They also confirm the conclusion we previously obtained (see Raimundo *et al.* (2019)) by analyzing the flow in the core region of the bubble column: the apparent relative velocity was indeed found to range between 2 and 8 times U_T using a conservative evaluation of the gas liquid flow rate in the core region of the bubble column.

(iii) the relative fluctuations in velocity V'/V are nearly constant in the heterogeneous regime as shown Figure 5. For the liquid phase, the average of V'_L/V_L over the data collected in the heterogeneous regime equals 36.5%, in agreement with previous findings (see the discussion in Raimundo *et al.* (2019)). For the gas phase, the average of V'_G/V_G is even higher; it equals 52-53% when considering positive velocities only, and it rises up to 56-57% when combining positive and negative velocities measurements (Lefebvre *et al.* (2022)). These strong figures confirm that intense turbulent motions take place in heterogeneous conditions.

(iv) from a closer examination of Figures 4 and 5, two different behaviors could possibly be distinguished in the heterogeneous regime. From the homogeneous/heterogeneous transition up to V_{sg} about $13 - 15$cm/s, the relative velocity $V_G - V_L$ and also to some extend the fluctuation V'_G/V_G exhibit a clear monotonous increase with the gas superficial velocity. Above $V_{sg} \sim 13 - 15$cm/s, these two quantities seem to become constant. In particular, the increase in the bubble velocity illustrated by the black dashed line in Figure 4 becomes nearly parallel to that of the mean liquid velocity (dashed red line in Figure 4): accordingly, the relative velocity seems to stabilize at a value about $2.3-2.4U_T$ at large V_{sg}. With regard to flow dynamics and scaling laws, it would be worthwhile to clarify whether the relative velocity reaches an asymptote, or if it continues to grow with V_{sg}: more experimental data covering an enlarged range of gas superficial velocities are required for that.

To test the scaling proposed in eq. 2.2 on these experimental data, we used local void fraction and velocities measured on the axis and at the same height H/D above the injector. Since the two sets 'up flow' and 'up and down flow' are close, let us consider only 'up and down flow' velocity statistics for the analysis. The mean velocities as well as the standard deviations scaled by $(gD\varepsilon)^{1/2}$ are represented for both phases in Figure 6. Clearly, all these quantities remain nearly constant for all flow conditions pertaining to the heterogeneous regime. For the mean bubble velocity on the column axis, one gets:

$$V_G/(gD\varepsilon)^{1/2} \sim 1.09 \pm 0.02, \tag{3.1}$$

while for the mean liquid velocity on the column axis:

$$V_L/(gD\varepsilon)^{1/2} \sim 0.68 \pm 0.01, \tag{3.2}$$

According to these results, it happens that the relative velocity on the column axis scales as $U_R \sim 0.41(gD\varepsilon)^{1/2}$, i.e. it monotonously increases with the void fraction ε. Such an increase of the relative velocity with the void fraction has been identified in bubble columns using indirect arguments (see for example Raimundo *et al.* (2019)). It has also been observed in others gas-liquid systems. Such a behavior is sometimes represented by a swarm coefficient that quantifies the decrease of the drag force acting on a bubble with the void fraction (Ishii & Zuber (1979); Simonnet *et al.* (2007)). Nowadays, ad-hoc swarm coefficients are routinely introduced in numerical simulations based on two-fluid models (e.g. McClure *et al.* (2017); Gemello *et al.* (2018)). We bring here direct experimental evidence of the increase of the relative velocity with the void fraction in a bubble column operated in the heterogeneous regime.

Concerning velocities, the standard deviation being proportional to the mean (see Figure 4), they also follow the same scaling with $V'_G/(gD\varepsilon)^{1/2} \sim 0.6 \pm 0.02$ and $V'_L/(gD\varepsilon)^{1/2} \sim 0.22 \pm 0.02$. Hence, all the above results obtained on the mean and on the fluctuating components of bubbles and liquid velocities confirm the soundness of the scaling proposed in eq. 2.2 with respect to void fraction.

The scaling resulting from an inertia-buoyancy equilibrium proposed above also includes an increase of velocities with the square root of the bubble column diameter. As the experiments presented in this section concern but a single bubble column diameter, the dependency with the column diameter cannot be tested. New experimental data gathered in bubble columns of variable diameters are needed to test the validity of the proposed scale. In that perspective, available experiments from the literature and relative to bubble columns of variable diameter will be analyzed in the next section. Yet, we already have accumulated strong experimental evidence of the relevance of the square root of the bubble column diameter as a scaling factor for the mean liquid velocity (Raimundo *et al.* (2019)). Indeed, the neat upward liquid flow rate Q_{Lup} in the column, where Q_{Lup} is obtained by integrating the liquid flux $(1-\varepsilon)V_L$ over the core region (i.e. from the axis up to $0.7 - 0.71R$), happens not to depend on V_{sg} in the heterogeneous regime. In the present experiments, we also found that Q_{Lup} is independent on V_{sg} in the heterogeneous regime. That conclusion was confirmed from data collected at three heights above injection, namely $H/D = 2.625$, $H/D = 3.625$ and $H/D = 4.875$. The result is $Q_{Lup} = 0.0122$ m3/s, with variations between $+0.001$ m^3/s and 0.0007 m^3/s depending on the set of data considered to evaluate the mean.

Moreover, we have previously shown (Raimundo *et al.* (2019)) that Q_{Lup} is proportional to $D^2(gD)^{1/2}$ over a significant range of column diameters (from $D = 0.15$m to 3m) and of gas superficial velocities (from $V_{sg} = 9$ to 25cm/s). As shown Fig. 7a, the present experiments confirm that finding in a $D = 0.4$m column, for V_{sg} between

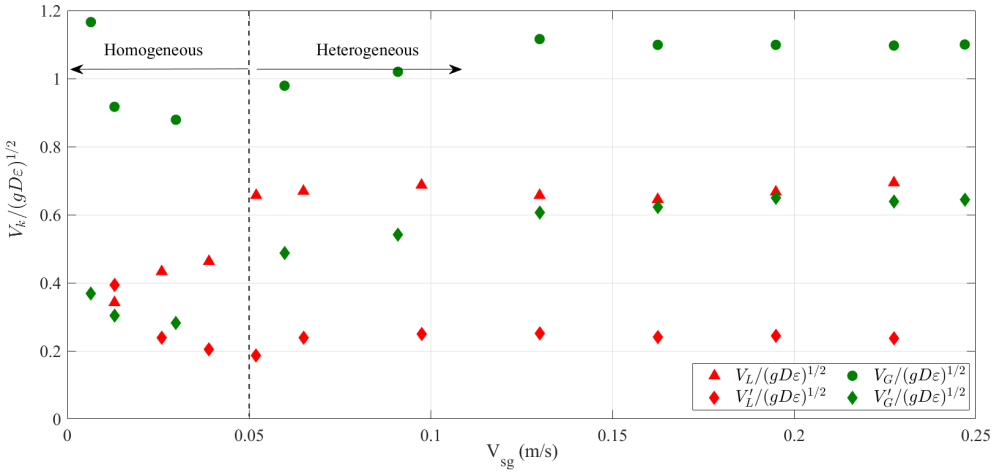

Figure 6: Evolution of phasic velocities ('up and down flow' velocity statistics) scaled by $(gD\varepsilon)^{1/2}$ versus the superficial velocity V_{sg}. The mean (V) and fluctuating (V') components of the bubble and the liquid vertical velocities as well as the void fraction ε are local quantities measured in a $D = 0.4$m column, on the column axis at $H/D = 3.625$.

6.5cm/s and 22.7cm/s and for $2.625 \leqslant H/D \leqslant 4.875$. The dependency of Q_{Lup} with D is further illustrated in Fig. 7b where we have reported the present data, the data collected by Raimundo *et al.* (2019), as well as one data produced by Guan *et al.* (2015) in the following flow condition: $V_{sg} = 47$cm/s in a $D = 0.8$m column and for $2.75 \leqslant H/D \leqslant 4.625$. All these data fall onto the same curve. Overall, the observed liquid flow rate - column diameter relationship writes:

$$Q_{Lup} = 0.0386 \pm 0.002 D^2 (gD)^{1/2}. \tag{3.3}$$

This result can also be expressed as a Froude number based on the average liquid velocity Q_{Lup}/S_{core} in the core region. Here, the cross section S_{core} of the ascending flow zone is evaluated as $\pi D^2/8$ (the mean liquid becomes zero at a radial position comprised between 0.7 and $0.71R$: that limit is well approximated as $2^{1/2}/2R = 0.707R$). Hence, $Fr_L = (Q_{Lup}/S_{core})/(gD)^{1/2} = 0.098$ † . All the above mentioned experiments bring a clear evidence that the velocity of the mean liquid circulation in a bubble column operated in the heterogeneous regime scales as $(gD)^{1/2}$ with the column diameter.

4. Confrontation of the proposed scaling with experimental data from literature

In this section, we examine whether available experimental data on local liquid or gas/bubble velocities obey the scaling proposed above when considering a larger range of flow conditions, and in particular variable column diameters. To this end, we target meaningful experiments in bubble columns in the sense that we seek conditions such that the flow dynamics is controlled by the same mechanisms as those discussed in section 2. More precisely, we select experiments pertaining to the 'pure' heterogeneous regime,

† There is a typo error in eq.(13) of Raimundo *et al.* (2019): the coefficient 0.024 should be replaced by 0.098.

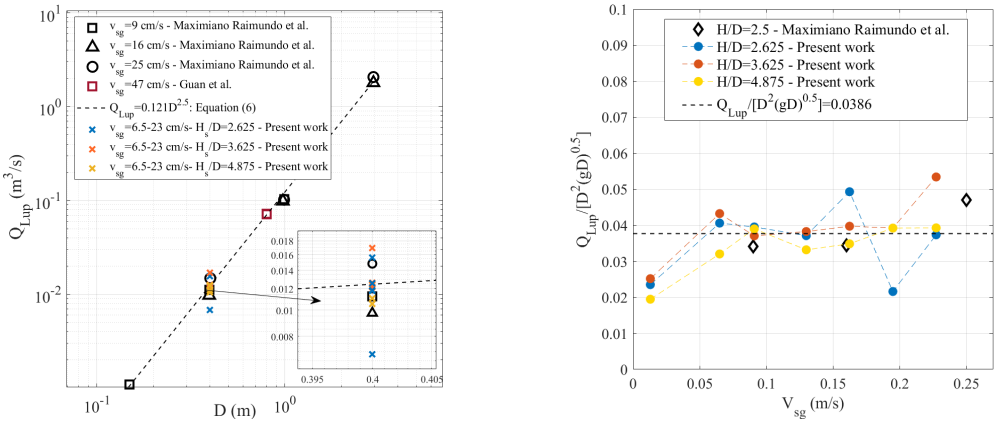

Figure 7: (a) Upward directed liquid flux $Q_{Lup}/[D^2(gD)^{1/2}]$ versus Vsg measured at different heights above injection in $D = 0.4$m columns. (b) Evolution of Q_{Lup} with the bubble column diameter from Raimundo *et al.* (2019), from Guan *et al.* (2015) and from present data.

a regime that occurs neatly beyond the transition region, and for which the global void fraction is an increasing and concave function of the gas superficial velocity. In addition, we consider only data collected in the quasi-fully developed region of the bubble column: as discussed in section 2, that condition implies a minimum column diameter, a minimum static liquid height as well as a proper range of measuring heights. Besides, and although it is known that in the heterogeneous regime the flow organization is weakly sensitive to the injector design, we also select experiments such that the gas injection is pretty well uniformly distributed over the column cross-section to avoid forcing of large-scale instabilities by an uneven gas repartition at injection and/or to avoid strong asymmetry of the mean flow such as the one observed by Chen *et al.* (2003) in their largest column. Another constraint in the search of relevant data is that both local velocity and local void fraction should be simultaneously available. In the following, we focus on local data gathered on the column axis. The sets of data fulfilling the above-mentioned constraints are presented in Table 4.1 for the liquid phase and in Table 4.2 for the gas phase. Note that almost all experimental conditions in Tables 4.1 and 4.2 correspond to air-water systems and to 'large' bubbles, i.e. with an equivalent diameter between 3mm and 10mm. Their terminal velocity typically ranges between 21cm/s and 27cm/s (Maxworthy *et al.* (1996)), so that all these flow conditions involve bubble dynamics at high (from 800 to 2100) particle Reynolds number. Yet, these experiments remain difficult to quantify with respect to coalescence. We qualitatively estimated the coalescence efficiency based on measurements of the axial evolution of the bubble size when such data were available. When such information was absent, we considered how the bubble size changes with the superficial velocity: a strong increase of the latter from homogeneous to heterogeneous conditions could be (but this is not certain) the mark of a neat coalescence. In addition, let us underline that when a significant coalescence is present, the flow regime may continuously evolve with the height above injection so that a quasi-fully developed region may not exist or may require column heights much larger than available in experiments. All the information collected is summarized in Tables 4.1 and 4.2 where the situation with respect to coalescence has been classified into three main categories: none or weak

coalescence, medium coalescence, strong coalescence, and the situation is said unclear when information was insufficient to conclude.

4.1. *Mean liquid velocity on the column axis*

Table 4.1 lists the experiments that obey the above constraints and that provide the liquid velocity and the local void fraction on the bubble column axis. Some choices were made to exploit the data. For Hills (1974), we considered only the data acquired with the 'plate B' that corresponds to a uniform gas injection over the column cross section. In Forret *et al.* (2006), the only quantitative data on gas hold-up are global void fractions deduced from static and dynamic liquid heights. We transformed the global void fraction into a local void fraction on the axis by multiplying it by 1.5 as done by the authors (see their eq.(4)), but this factor could be inappropriate. The local void fractions for the data of Vial *et al.* (2001) were collected in Camarasa *et al.* (1999). For Yao *et al.* (1991), we present the data they collected at various heights with H/D from 2.6 up to 12, and we use an extrapolation to evaluate the void fraction at $V_{sg} = 10$cm/s. Note also that these authors imposed a forced liquid motion but the mean velocity of 1cm/s is negligible compared with the measured liquid and gas velocities on the column axis: these data are therefore believed to be representative of a bubble column operated in a batch mode and they have been kept in the analysis. Finally, all the measurements mentioned in Table 4.1 considered positive and negative velocity realizations, although some (hard to evaluate) bias may be present notably with Pavlov tubes, as evoked by Hills (1974). To be consistent, we compared with our data series named 'up and down flow' (see Section 3).

Figure 8 provides the quantity $V_L/(gD\varepsilon)^{1/2}$ versus the superficial gas velocity with V_L and ε measured on the axis. The figure includes all the contributions listed Table 4.1, and that have been collected in the homogeneous regime as well as in the heterogeneous regime. The data concern column diameters from 0.1 to 3m and superficial velocities varying from 1.2 to 62cm/s. In the limit of small superficial gas velocities, $V_L/(gD\varepsilon)^{1/2}$evolves between 0.01 and 1.02. As V_{sg} increases, the range of variation of $V_L/(gD\varepsilon)^{1/2}$ smoothly diminishes. Above $V_{sg} \sim 15$cm/s, $V_L/(gD\varepsilon)^{1/2}$ evolves within the interval $[0.48; 0.77]$. Note that this interval corresponds to bubble column diameters ranging from 0.1m to 3m. Above $V_{sg} \sim 20$cm/s, that interval further narrows and the quantity $V_L/(gD\varepsilon)^{1/2}$ tends to be constant in the pure heterogeneous regime: that feature supports the scaling argument presented in Section 2. Although experimental data are lacking at very large V_{sg} to precisely define the asymptotic behavior, the latter corresponds to:

$$V_L \sim 0.58(gD\varepsilon)^{1/2}, \tag{4.1}$$

as shown by the insert in Figure 8 that provides V_L versus $(gD\varepsilon)^{1/2}$ for all available data at V_{sg} above 8cm/s: the proportionality factor equals 0.5774 (and the correlation coefficient is 0.867). Note that the same plot but for all data available at V_{sg} above 6cm/s also provides a linear behavior with a proportionality factor equals to 0.5786 (and a correlation coefficient of 0.87). Alternately, when the quantity $V_L/(gD)$ is plotted versus the local void fraction for all the data shown Fig. 8, $V_L/(gD)$ is found to evolve as $\varepsilon^{0.50\pm0.01}$: this is fully consistent with the $\varepsilon^{1/2}$ dependency predicted.

It is worth discussing the uncertainty on these figures as the data presented in Figure 8 come from different operators and from various measuring techniques. The typical dispersion in the measurements can be appreciated by comparing the data collected in identical bubble columns. For example, in the $D = 0.15$m column and at $V_{sg} \sim 20cm/s$,

Authors	Reference(s)	Column diameter (m)	Column height (m) / static or dynamic height (m)	Fluids	Gas injection	Measuring height H/D	Typical bubble size	Coalescence	Regime	Local Void fraction measurement technique	Liquid velocity measurement technique
Hills J.H.	Trans. Instn Chem. Engrs., 1974	0.138	1.37 m / ??	Cambridge tap water / air	Perforated plate B = 61 holes, diameter of oridfices = 0.4mm	H/D=4.3	No information	No information	Transition at Vsg ≈ 5cm/s. Heterogeneous conditions for Vsg above ≈ 6cm/s.	Local void fraction from needle resistivity probe	Pavlov tube (calibrated, correction for void fraction accounted for)
Menzel TH., in der Weide Th., Staudacher O., Wein O. and Onken U.	Ind. Eng. Chem. Res., 1990	0.6m	3.35/??	water / air and water + 0.22 wt% propanol / air	Not detailed	Not indicated	No information	No information	Transition at Vsg≈ 4.8cm/s for water. Smooth evolution of the void fraction with Vsg for water + 0.22 wt% propanol => no clear transition in that case.	Local void fraction from single tip conductivity probe	Hot film anemometer - triple split probe
Yao B.P., Zheng C., Gashe H.E. and Hofmann H.	Chemical Engineering and Processing, 1991	0.29 NB enforced weak liquid circulation in the column (superficial liquid velocity = 1cm/s)	4.5m / ??	deionized water / air	uniform injection through orifices 0.2mm internal diameter	Selected data at H/D= 2.6 ; 5.2 and 12.	Mean bubble diameter ≈ 3.2 - 4mm at H/D=2.6. Bubble size increases up to 4.0-4.4mm at H/D=12.	**Weak coalescence**. The authors indicate that some coalescence is present. Yet the data they provide indicate a limited increase of the bubble size : the latter increases by about 1mm between H/D=2.6 and H/D=12.	Transition not indicated. May be at Vsg≈ 3cm/s according to void fraction profiles.	Local void fraction from single tip conductivity probe	Hot film anemometer (processing not detailed)
Vial Ch., Lainé R., Poncin S., Midoux N., and Wild G.	Chem. Eng. Sc., 2001	0.1m	2m	tap water / air	multiple-orifice nozzle = 50 holes of 1 mm diameter uniformly spaced	Data at H/D=10	No information. If the conditions are the same as in Camarasa et al 1999, then, the equivalent diameter Deq measured from images is ≈ 4-5 mm beyond Vsg≈ 5cm/s.	No information. **Unclear** if the conditions are the same as in Camarasa et al 1999 [33].	Transition with the multiple orifices injector starts at Vsg≈ 4 cm/s. Established heterogeneous regime beyond Vsg≈11-12cm/s.		LDA
Forret A. Forret A., Schweitzer J.-M., Gauthier T., Krishna R. and Seweich D.	PhD thesis 2003 Chem. Eng. Sci. 2003 Oil & Gas	0.15 ; 0.4 ; 1m	0.9 ; 3.2 ; 6 m / dynamic height = 4 or 5 D in all columns	tap water / air (ambiant T,P conditions)	Perforated plates with 313 orifices 2mm in diameter uniformly spaced over the cross section.	Measurements taken in the "fully-developed" region	Bubble size not reported. The same facilities were later used by Maximiano Raimundo at IFPEN Lyon using slightly different spargers. Assuming that the tap water quality remained the same over years, the data collected by Maximiano Raimundo et al. on bubble size probably apply to the experiments performed by Forret et al.	**Weak coalescence** According to the gas hold-up versus superficial velocity graph, the coalescence is probably weak. In addition, the water quality was presumably similar as the one used during the experiments of Maximiano Raimundo et al.	Heterogeneous regime for Vsg higher than about 4-5cm/s	The local void fractions data acquired with an optical fiber probe are all normalized by the void fraction value on the axis. The quantitative data on gas hold-up is provided by global void fractions deduced from the static and dynamic liquid heights.	Home made Pavlov tube calibrated in situ. Estimated uncertainty on velocity = 10%.
Guan X., Gao Y., Tian Z., Wang L., Cheng Y. and Li X.	Chemical Engineering Research and Design, 2015	0.8m	5m / fixed dynamic height = 4.1m	presumably tap water / air	Uniform aeration : perforated plate, orifices of 2.5 mm in diameter, opening ratio 0.53%	Data at H/D=2.75	No information	No information	Pure heterogeneous regime according to their Fig.3.	Local void fraction from conductivity probe	Pavlov tube
Maximiano Raimundo P., Maximiano Raimundo P., Cartellier A., Beneventi D., Forret A., Augier	PhD thesis 2015 Chem. Eng. Sci. 2019	0.15m ; 0.4m ; 1m ; 3m	1m ; 3.2m ; 5.7m ; 12m / static height = 4 D in all columns except in the 3m I.D. column where the static height was 2.2 D.	tap water / air (ambiant T,P conditions)	Perforated plates (with 60 orifices 1mm in diameter uniformly spaced over the cross section that provide similar bubble size distributions whatever Vsg and/or the column diameter	Selected data at H/D= 2.5	Sauter mean diameter ranging from 4.8mm to 6mm. NB the mean bubble size almost the same whatever the column diameter or Vsg.	**No or weak coalescence** according to the axial evolution of chord distributions and of Sauter mean horizontal diameter in columns 0.15 ; 0.4 and 1 m in diameter. Although, the axial evolution of chords / bubble size was not quantified in the 3m diameter column, mean bubble sizes similar to those found in other columns were measured at H/D=2.5. It is therefore likely that the condition **No or weak coalescence** also prevails in the 3m diameter column.	The homogeneous region ends at Vsg ≈ 4cm/s. Pure heterogeneous regime observed for Vsg above ≈ 4-5cm/s except in the D=0.4m column where the transition region exhibits a peak in a plot void fraction versus Vsg and pure heterogeneous flows are observed for Vsg above ≈ 10cm/s.	Local void fraction from monofiber optical probe (conical)	Home made Pavlov tube.

Table 1: List of references and flow conditions exploited to extract liquid velocity and local void fraction on the column axis.

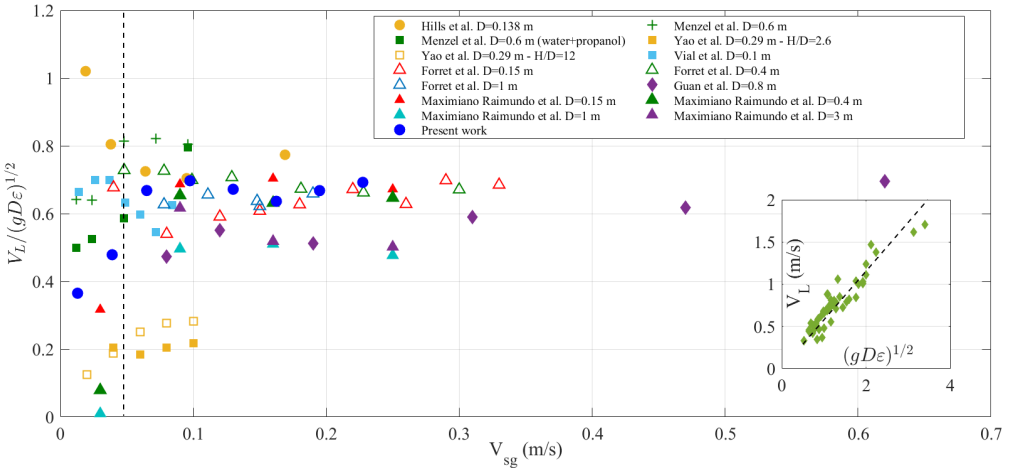

Figure 8: Evolution of $V_L/(gD\varepsilon)^{1/2}$ where V_L and ε are measured on the column axis versus the superficial gas velocity from the contributions quoted in Table 4.1. The insert plots V_L versus $(gD\varepsilon)^{1/2}$ for all data collected on the column axis in the heterogeneous regime for $V_{sg} \geqslant 8$cm/s and for $0.1m \leqslant D \leqslant 3m$: the dash line in the insert corresponds to the fit $V_L = 0.577(gD\varepsilon)^{1/2}$.

there is a 0.2 difference in $V_L/(gD\varepsilon)^{1/2}$ between the data from Forret *et al.* (2006) and those from Raimundo *et al.* (2019). Similarly, in the $D = 0.4$m column and at $V_{sg} \sim 20$cm/s, the values of $V_L/(gD\varepsilon)^{1/2}$ deduced from the data of Forret *et al.* (2006), from those of Raimundo *et al.* (2019) and from the present work all fall within a 0.1 band. These are quite reasonable dispersions especially when considering that the water quality was not always the same, so that the coalescence efficiency varied. Finally, as far as we can judge from the available information given in articles, all the experimental conditions in Figure 8 correspond to no or weak coalescence. The monotonous allure of the evolution of the local void fraction on the axis with V_{sg} shown in Figure 9 also supports that statement.

4.2. *Mean gas velocity on the column axis*

Experiments providing statistics on the bubble velocity are not common. This is due to the lack of reliable measuring techniques giving access to bubble velocity in the difficult conditions encountered in the heterogeneous regime, in particular with respect to high void fractions, flow unsteadiness and 'chaotic' 3D trajectories of bubbles. Each bubble velocity technique has its own limitations, and their respective uncertainty and resolution in such flow conditions are not well known. For example, for phase detection techniques based on immersed probes either single, double or multiple, it is well known that erroneous velocity data are collected in heterogeneous conditions because of the unsteady 3D motions of these two-phase flows. Yet, average quantities relative to velocity or size seem to be meaningful (Chaumat *et al.* (2007); Raimundo *et al.* (2016)). Moreover, some bias may alter the statistics and when the latter occurs, it is usually hard to quantify. For all these reasons, we will not discuss further the respective merits of each measuring technique: instead we report all available raw data as given in the original papers, keeping in mind that some issues on resolution, accuracy or bias remain an open question.

The Table 4.2 summarizes the set of experiments used to analyze the gas velocity

Authors	Reference(s)	Column diameter (m)	Column height (m) / static height (m)	Fluids	Gas injection	Measuring height	Typical bubble size	Coalescence	Regime	Local void fraction	Bubble size measurements	Local gas/bubble velocity
Yao B.P., Zheng C., Gashe H.E. and Hofmann H.	Chemical Engineering and Processing, 1991	0.29 NB enforced weak liquid circulation in the column (superficial liquid velocity = 1cm/s)	4.5m/??	deionized water / air	Uniform injection through orifices 0.2mm internal diameter	Selected data at H/D= 2.6 ; 5.2 and 12.	Mean bubble diameter ≈ 3.2 - 4mm at H/D=2.6. Bubble size increases up to 4.0-4.4mm at H/D=12.	**Weak coalescence.** The authors indicate that some coalescence is present. Yet the data they provide indicate a limited increase of the bubble size : the latter increases by about 1mm between H/D=2.6 and H/D=12.	Transition not indicated. Possibly for Vsg≈ 4-5cm/s.	Conductivity probe	Five-point conductivity probe. Signal processing not detailed.	Bubble velocity : Ultrasound Doppler probe. Signal processing not detailed. Gas flux velocity : from five-point conductivity probe. Velocity weighted by the gas residence time.
Camarasa E., Vial C., Poncin S., Wild G., Midoux N. and Bouillard J.	Chemical Engineering and Processing, 1999	0.1	2.0m /??	tap water / air and water+pentano l / air	Selected data acquired with the multiple orifices injector = perforated plate 62 holes of 1mm uniformly spaced	Not indicated. Probably in the quasi-fully developped region	In water, the equivalent diameter Deq (as deduced from the projected area in images) is ≈ 4-5 mm beyond Vsg≈ 5cm/s. In water + pentanol, the equivalent diameter Deq decreases in the range 3-4mm to about 0.5mm.	**Unclear for water** No undisputable evidence as the bubble size at injection is not given. Possibly some coalescence in water according to bubble size distributions that extend from 1 up to 8mm at Vsg ≈ 8cm/s. **No or weak coalescence** for water + pentanol	Transition with the multiple orifices injector at Vsg≈ 4 cm/s for water and at Vsg≈5-6cm/ for water + pentanol. "Pure" heterogeneous regime beyond Vsg≈14cm/s.	Single optical fiber probe	Direct imaging (photography) + DGD (dynamic gas disengagement) technique.	Dynamic gas disengagement technique.
Chen W., Tsutsumi A., Otawara K. and Shigaki Y.	The Canadian Journal of Chemical Engineering, 2003	0.2 ; 0.4 ; 0.8	3.0m/2.0m	tap water / air	Perforated plates with 0.5 mm holes (equilateral triangular pitch of 16 mm, opening ratio about 0.09%) were employed as the gas distributor for the three columns.	Selected data at H/D=2.6 for D=0.4m	Mean bubble chord length from 2 to 3 mm. The latter does not change much with flow conditions (including Vsg) except in the D=0.8m column where the flow happens to be strongly non symmetrical.	**Unclear** No clear quantitative information on coalescence. Possibly weak in the D=0.2 and 0.4m columns and significant in the D=0.8m column in which the authors observed much wider chord lengths distributions. Yet, the enhanced coalescence in the D=0.8m column may result from the strong flow asymmetry.	Transition at Vsg ≈ 5cm/s	Single tip cleaved optical probe.	Chords as detected by the probe. No statistics provided.	Velocity determined from Doppler signals collected by a cleaved optical probe. Signal processing not detailed. Successive use of upward directed and downward directed probe.
Chaumat H., Billet A.-M. and Delmas H. Chaumat H., Billet-Duquenne A.-M., Augier F., Mathieu C. and Delmas H.	Int. J. Chemical Reactor Engineering, 2006 Experimental Thermal Fluid Sci. 2007	0.2	1.6m/??	tap water / air	Sparger consisting of two toric rings with orifices 0.5mm or 1mm in diameter.	Selected data at H/D= 3.25 and 5.75, and in the batch mode.	Sauter mean diameter ranging from 4 to 10mm. The authors mention wide bubble size distributions but the standard deviation is not quantified.	**Unclear** Coalescence may be present but no clear evidence. NB The bubbles detected at low altitude (0.25m) are larger than at higher altitude (0.65m) - see their Fig. 9 and 10: this may be due to break-up at injection.	Transition occurs over the interval $2 \leq Vsg \leq 6.4$cm/s for the injector with 1mm I.D. orifices, and over the interval $6.4\text{cm/s} \leq Vsg \leq 16$ cm/s for the injector with 0.5mm I.D. orifices.	Optical probe	Mean Sauter diameter deduced from the most probable bubble velocity and from the mean detection frequency.	Double optical probe. Vertical distance between tips 1.7mm. Evaluation of the most probable bubble velocity.
Xue J., M. Al-Dahhan, M.P. Dudukovic and R.F. Mudde	AIChE J., 2008	0.162 m	2.5m/1.8m	tap water -air (atmospheric pressure)	Selected data with sparger n°2 : 163 holes of 0.5mm I.D., hole pattern = 10mm triangle pitch.	Selected data at H/D=5.1 NB: Gas velocity and void fraction profiles are *non symmetrical* at that height.	Mean bubble chord length between 5 and 6mm, standard deviation on the chord length from 6.5 to 10mm.	**Significant coalescence.** There is no data on the evolution of the bubble size along a vertical at fixed Vsg. Yet, the mean bubble chord neatly increases from 2-3mm in the homogeneous regime (Vsg=2cm/s) up to 6-10mm in the heterogeneous regime. There is also a significant increase in the chord standard deviation from ≈ 1mm to 10mm as Vsg increases. The bubble chord distribution remains the same for Vsg≥30cm/s, i.e. for pure heterogeneous conditions.	Heterogeneous regime for the data collected at Vsg from 8cm/s to 60cm/s	Optical probe	Chords as detected by the multiple tips probe.	Four tips optical probe (axial distance 2 mm, radial distance 0.6mm)
Maximiano Raimundo P., Maximiano Raimundo P., Cartellier A., Beneventi D., Forret A., Augier F.	PhD thesis 2015 Chem. Eng. Sci. 2019	0.15 ; 0.4 ; 1	1m ; 3.2m ; 5.7m / static height = 4 D in all columns	tap water / air (ambiant T,P conditions)	Perforated plates (see details in [13]) providing similar bubble size distributions whatever Vsg and/or the column diameter	Selected data at H/D= 2.5	Sauter mean diameter ranging from 4.8mm to 6mm. NB the mean bubble size remains almost the same whatever the column diameter or Vsg.	**No or weak coalescence** according to the axial evolution of chord distributions in columns 0.15 ; 0.4 and 1 m in diameter.	The homogeneous region ends at Vsg ≈ 4cm/s. Pure heterogeneous regime observed for Vsg above ≈ 4-5cm/s except in the D=0.4m column where the transition region exhibits a peak in a plot void fraction versus Vsg and where pure heterogeneous flows are observed for Vsg above ≈ 10cm/s.	Single fiber optical probe	Direct imaging technique + Correlation technique using two parallel probes / Single fiber optical probe	Velocity deduced from the dewetting time of an optical probe.
Guan X. and Yang N.	Chemical Engineering Research and Design, 2017	0.15 m	1.6 m / fixed dynamic height = 1.4m	tap water / air	Perforated plate, 73 holes of 1.5 mm in diameter, distributed in a triangular pitch, with total free area of 0.73%	Selected data at H/D=5.3	In heterogeneous conditions, the mean volume equivalent bubble diameter evolves from ≈4.5mm to less than 6mm as Vsg increases.	**No or weak coalescence** (see their fig.13).	Transition around 5cm/s. Pure heterogeneous regime	Dual tip conductivity probe	Reconstructed from the double phase detection probe assuming a one-to-one relationship between size and eccentricity	Horizontal double conductivity probe. Distance between probe tips 1.5mm. Holder tubes 4mm O.D.

Table 2: List of references and flow conditions exploited to extract the gas velocity and the local void fraction measured on the column axis.

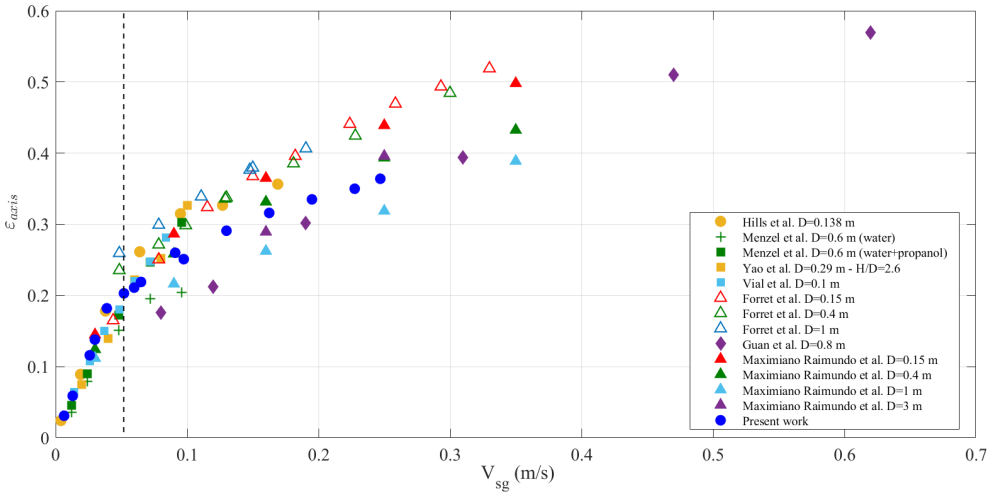

Figure 9: Evolution of the local void fraction on the column axis versus the superficial gas velocity for all the contributions quoted in Table 4.1 and exploited Figure 8. For Forret *et al.* (2006), the local void fraction has been estimated as the global void fraction divided by 1.5.

that corresponds here to the velocity of bubbles. The corresponding data on the mean bubble velocity scaled by $(gD\varepsilon)^{1/2}$, where both the velocity and the void fraction were measured on the column axis, are reported versus V_{sg} in Figure 10 irrespective of the flow regime. Let us provide some information on how the data were exploited. First, when different injectors were tested, we always selected the data acquired with multiple-orifice injectors distributed over the entire column cross section. Second, original data were sometimes interpolated to estimate missing local void fraction data: that process was used only when the interpolation process was safe. If some extrapolation was required, the corresponding data were discarded unless otherwise specifically stated in the text in the legend. It is worth to notice that almost all data correspond to tap water and air (under ambient pressure and temperature conditions), with two exceptions: Yao *et al.* (1991) used deionized water, and one set of data from Camarasa *et al.* (1999) was gathered in an aqueous solution of alcohol (water and pentanol at a concentration 4×10^{-4} mol/l). Let us also mention some specific choices we made when extracting the data. For Yao *et al.* (1991), only the bubble velocity detected by the ultrasound technique is plotted because these authors found comparable results with their five-point conductivity probe. In Camarasa *et al.* (1999), the bubble velocity was measured by an ultrasonic Doppler technique for single orifice and porous plate gas injection but not for the multiple orifice nozzle that provides the injection conditions we are looking for here. For that sparger, the bubble velocity was measured by a DGD (dynamic gas disengagement) technique: Camarasa *et al.* (1999) report the velocity of 'large' bubbles and of 'small bubbles' but they do not explicitly specify how 'large' bubbles are distinguished from 'small' ones. It happens that, for a given flow condition, the mean velocity of 'small bubbles' measured by Camarasa *et al.* (1999) is 2 to 4 times (in water) and 2 to 2.5 times (in aqueous solution of alcohol) lower than the mean velocity measured for 'large bubbles'. Presumably, 'small' bubbles correspond to the 1-2mm bubbles at the lower end of the bubble size distributions they provide, while 'large' bubble can be as large as 8-10mm in water (see their Fig.10)

and 6-8mm in water plus pentanol (see their Fig.20). According to these comments, only the data for 'large' bubbles are reported in Figure 10. Let us finally mention that, for the data of Camarasa *et al.* (1999) gathered in the aqueous solution of pentanol, no data is given on the local void fraction and we used the global void fraction instead. Accordingly, the values of $V_G/(gD\varepsilon)^{1/2}$ are overestimated for that series. Chen *et al.* (2003) performed measurements in a $D = 0.4$m bubble column at $H/D = 2.6$, and in a $D = 0.8$m bubble column at $H/D = 1.3$: the later case, for which they observed non-symmetrical flows, was discarded because the data were not collected in the quasi-fully developed region. Concerning the experiments by Xue *et al.* (2008), all the data they collected in the heterogeneous regime at $H/D = 5.1$ correspond to strongly asymmetrical flows. Indeed, the velocity difference between the upward motion on one side of the column and the downward motion on the opposite side ranges between 20cm/s and 40cm/s: these figures are therefore quite significant compared with the mean bubble motion on the column axis that evolved between 40cm/s and 90cm/s. That asymmetry was further confirmed by void fraction and bubble detection frequency profiles. The only symmetrical bubble velocity profile reported by Xue *et al.* (2008) was collected at a larger distance from injection (namely $H/D = 8.5$) and at $V_{sg} = 30$cm/s. Unfortunately they do not provide the void fraction for these conditions. Despite these shortcomings, all the data of Xue *et al.* (2008) collected at $H/D = 5.1$ have been integrated in our analysis. Let us also underline that these authors are among the very few who have explored large gas superficial velocities.

Among the contributions listed in Table 4.2, almost all gathered (at least in principle) positive and negative bubble velocities, except for Raimundo (2015); Raimundo *et al.* (2016) who collected positive velocities only since they exploited the dewetting of a single fiber tip. Yet, as the sources of bias are usually not analyzed for bubble velocity measurement techniques, it is difficult to ascertain that the information collected was indeed the faithful assembly of positive and negative realizations. An indication of these difficulties is that the standard deviation of bubble size distributions are never provided, nor discussed, except by Yao *et al.* (1991) who measured bubble velocity fluctuations with an ultrasound technique. As for the liquid phase, and to be consistent, we thus consider our data series from Section 3 named 'up and down flow' for the comparison.

The data presented Figure 10 concern column diameters from 0.1 to 1m and gas superficial velocities varying over two decades from 0.6 to 60cm/s. At low gas superficial velocities, say below a few cm/s, that is within the homogeneous regime, the quantity $V_G/(gD\varepsilon)^{1/2}$ evolves from 0.2 up to 1.8. That ratio significantly varies from one experiment to the other. For a given data series, the ratio $V_G/(gD\varepsilon)^{1/2}$ tends to become somewhat constant when moving towards large superficial velocities. For V_{sg} above around 10cm/s, that is well within the heterogeneous regime, the dispersion of the data significantly diminishes and $V_G/(gD\varepsilon)^{1/2}$ evolves inside a narrower band comprised between 0.6 and 1.4. Note that these last figures encompass bubble column diameters ranging from 0.15 to 1m. The trends are therefore the same as those detected when analyzing the liquid velocity. Yet, the fluctuations observed from one series to another are larger than those observed for the liquid velocity. This is probably because of the stronger uncertainties of gas velocity measuring techniques. Also, and compared with the mean liquid velocity presented Figure 8, it is more difficult to estimate the asymptotic value of $V_G/(gD\varepsilon)^{1/2}$. According to Xue *et al.* (2008) and to some runs of Raimundo *et al.* (2019), that limit is near 0.8 while from the present data, as well as from those of Yao *et al.* (1991), the limit is possibly closer to 1. Again, experimental data at very large V_{sg} are required to more accurately determine the asymptotic behavior of $V_G/(gD\varepsilon)^{1/2}$. Despite the limitations on available data, the trends observed on $V_G/(gD\varepsilon)^{1/2}$ for column

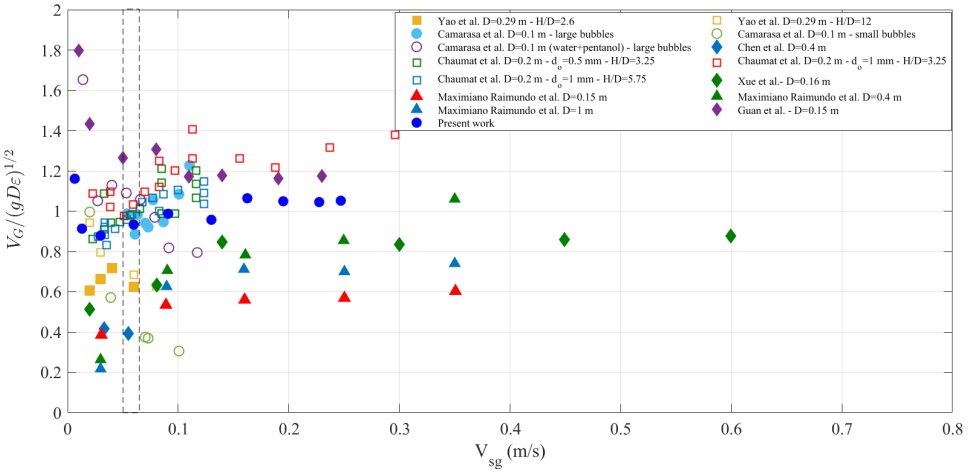

Figure 10: Evolution of $V_G/(gD\varepsilon)^{1/2}$ where V_L and ε are measured on the column axis versus the superficial gas velocity V_{sg} for all gas or bubble velocity measurements from the articles quoted in Table 4.2.

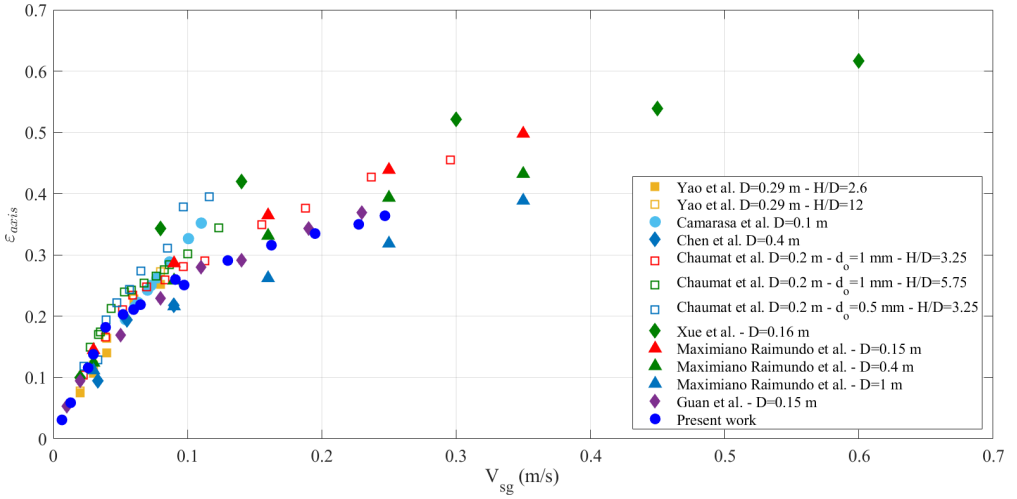

Figure 11: Evolution of the local void fraction on the column axis versus the superficial gas velocity for contributions quoted in Table 4.2 and exploited in Figure 10.

diameters between 0.1 and 1m are consistent with the scaling argument proposed in Section 2.

Figure 11 provides the evolutions of the void fraction on the axis with V_{sg} for all the experiments quoted in Table 4.2. As in Figure 9, all these evolutions are monotonous, so that they presumably all correspond to no or weak coalescence. Yet, in terms of local void fraction, one data series happens to be neatly above all others: this is the one from Xue *et al.* (2008). Contrary to all others experiments presented in Figure 10 (see also Table 4.2), the coalescence was probably significant in the experiments of Xue *et al.* (2008). Indeed, they observe an increase of the mean bubble chord length on the axis from 2-3mm in the homogeneous regime up to 6mm in the heterogeneous regime while the standard

deviation of the size distribution growths from about 1mm up to 10mm. Also, their bubble chord distributions indicate that bubbles up to 15mm are detected, and bubbles on the axis are significantly larger than near walls where their mean chord is less than 3mm. Let us also underline that the local void fractions measured by Xue *et al.* (2008) in the heterogeneous regime are among the largest of all data series presented Figures 9 and 11. Xue *et al.* (2008) used injectors made of orifices 0.5mm in diameter, and small orifices are known to produce smaller bubbles and thus to increase the maximum void fraction reached in the homogeneous regime (Joshi *et al.* (1998)). Chaumat *et al.* (2006) obtained similar large values of the local hold-up when using the same small orifices: yet, the values of $V_G/(gD\varepsilon)^{1/2}$ deduced from their measurements remain comparable with others contributions for V_{sg} below 0.13m/s (Fig. 10). These comments indicate that a characterization of flow conditions with respect to coalescence is not easy. In addition, experimental data on bubble velocity are missing to evaluate how much the magnitude of $V_G/(gD\varepsilon)^{1/2}$ may vary with the coalescence efficiency.

So far, the scaling of the liquid velocity has been discussed based on data collected on the axis. For the liquid, it is known that, in the heterogeneous regime, both the transverse liquid velocity and the local void fraction profiles assume self-similar shapes when scaled by their respective value on the axis (Forret *et al.* (2006)). Hence, all the above findings are expected to remain valid at any radial position in the column provided one remains in the quasi-fully developed region. For the gas phase, we have shown in Lefebvre *et al.* (2022) that the bubble velocity profiles collected in the quasi-fully developed region when in heterogeneous conditions also happen to be self similar when scaled by the bubble velocity on the column axis. Hence, the proposed scaling is also expected to remain valid at any radial position for the gas phase.

4.3. *Liquid and gas velocity fluctuations*

Experimental data on velocity fluctuations collected in bubble columns are scarce, and this is especially true in the heterogeneous regime. For the liquid phase, Menzel *et al.* (1990) provide two profiles of the axial liquid velocity fluctuations (quantified here by the standard deviation V' of the velocity distribution). Yet, these data were gathered in a 80 wt% glycerol/water mixture, and, unfortunately, the authors do not indicate the corresponding mean velocities and void fractions for that fluid. Otherwise, data for the liquid phase are available in Yao *et al.* (1991); Vial *et al.* (2001); Forret (2003); Raimundo *et al.* (2019) and from the present contribution. All these data concern deionized or tap water.

For the gas phase, single tip or multiple tips probes that exploit a transit time technique for velocity measurements are common, but, with these techniques, the measured velocity distributions are strongly biased by the detection of erroneous, large velocities (see for e.g. Chaumat *et al.* (2007); Raimundo *et al.* (2016)). It happens that the mean velocity is significant, but the standard deviation is not reliable. Also, some authors such as Chen *et al.* (2003); Xue *et al.* (2008); Guan & Yang (2017) provide velocity distributions but the standard deviations are not quantified. For these reasons, one is left only with the data from Yao *et al.* (1991) acquired from an ultrasound technique in a $D = 0.29$m column with de-ionized water / air as fluids, and the data we collected with the Doppler probe in a $D = 0.4$m column with tap water /air as fluids (see Lefebvre *et al.* (2022)).

The experiments of Menzel *et al.* (1990) indicate that, in the heterogeneous regime, the radial profiles of liquid velocity fluctuations remain self-similar when normalized by their maximum. One can also use the velocity fluctuations evaluated on the axis of the bubble column for that normalization. Hence, in the following, we focus our discussion on velocity fluctuations measured on the axis. The relative fluctuation V'_L/V_L in the

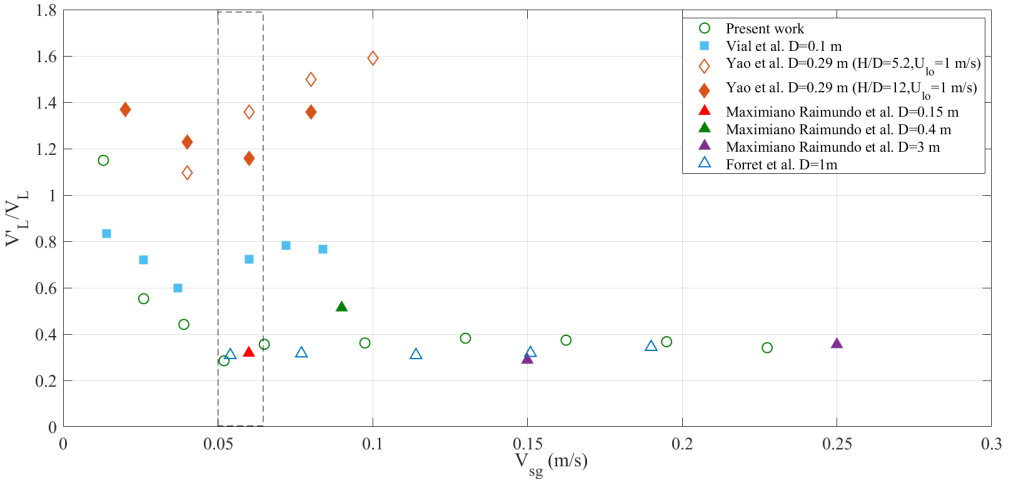

Figure 12: Evolution of the relative fluctuation in the liquid phase velocity V'_L/V_L measured on the column axis versus the superficial gas velocity.

liquid phase (respectively V'_G/V_G for the gas phase) measured on the column axis is presented Figure 12 (respectively Figure 13) versus the superficial gas velocity. All these measurements have been done in the quasi-fully developed region. Despite the limited number of independent data, each of the quantities V'_L/V_L and V'_G/V_G tends towards a constant value when moving inside the heterogeneous regime. That feature is well established for the liquid phase since the data come from different operators and from different sensors. Remarkably, the asymptotic behavior is the same whatever the column diameter ranging from 0.15 to 3m. The only series exhibiting a different trend are those from Yao *et al.* (1991) for the liquid phase. These data were obtained from hot-film probes, a technique that could be delicate to exploit in bubbly flows. The difficulties are expected to be even stronger in the conditions encountered in bubble columns at high gas superficial velocities. Unfortunately, Yao *et al.* (1991) do not comment on the signals they collected, nor on the signal processing they develop: it is therefore difficult to evaluate the reliability of their measurements.

Figures 12 and 13 show that, in the heterogeneous regime, the velocity fluctuations in the liquid as well as in the gas remain proportional to the mean velocity. Hence, all the findings on the scaling of mean velocities in the core region of the bubble column also apply to velocity fluctuations. One may be puzzled by such a result, but physical arguments similar to those evoked in section 2 can explain that feature. The idea is that, in the heterogeneous regime, the contributions to velocity fluctuations in the liquid by the relative motion at the bubble scale, i.e. the so-called bubble induced-turbulence, which is at the origin of large ratio V'_L/V_L observed Fig. 12 in the homogeneous regime (see Risso (2018)), is not the leading mechanism. Instead, in the heterogeneous regime, the agitation in the liquid is due to the presence of meso-scale structures. The later have been put in evidence and quantified with a 1D Voronoï analysis performed on the phase indicator function delivered by optical probes. With such Voronoï tesselations, we have shown that in the heterogeneous regime these flows as organized in clusters (high void fraction regions) and voids (low void fraction regions) (Raimundo *et al.* (2019)). The variations in void fraction from one meso-scale structure to the other induce buoyancy forces that spatially fluctuate, and hence a velocity field that changes from one structure

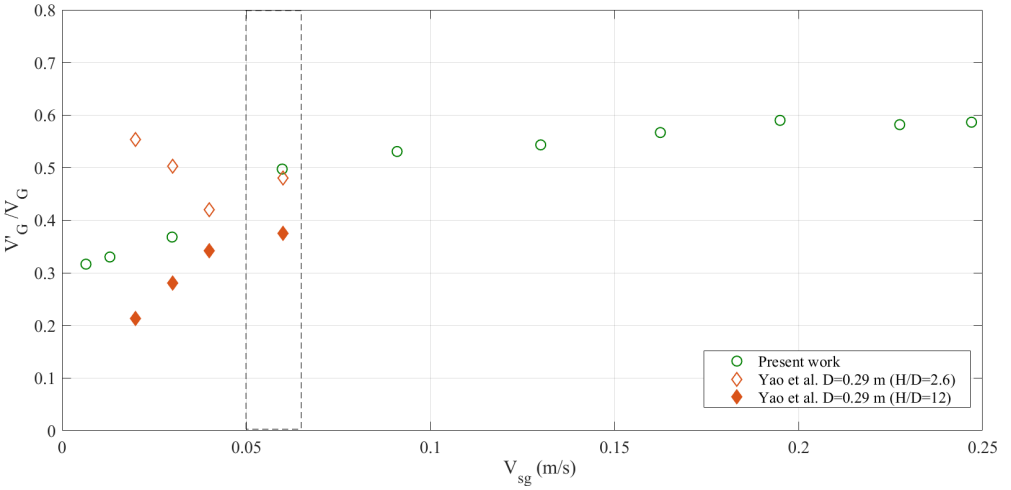

Figure 13: Evolution of the relative fluctuation V'_G/V_G of the velocity of bubbles measured on the column axis versus the superficial gas velocity.

to the other. These meso-scale structures are transported by the mean flow and they could also form and disappear. Hence, at a fixed point in space, the passage of successive structures induce the velocity fluctuations that are precisely those detected by an Eulerian measuring technique, i.e. they are the quantities V'_L and V'_G measured with local probes. We will come back to velocity fluctuations after having characterized the meso-scale structures and having analyzed their dynamics.

5. Scaling of the relative velocity and of velocity fluctuations: role of meso-scale structures dynamics

An inertia-buoyancy equilibrium similar to the one discussed in Section 2 is now applied at the scale of a meso-scale structure immersed in the two-phase mixture: such an equilibrium yields a velocity of that meso-scale structure relative to the mean flow of the mixture, that scales as $(gL\delta\rho/\rho)^{1/2}$. Here, L is the size of the structure and $\delta\rho/\rho$ is the difference in density between the structure and its surroundings. As noticed by Cholemari & Arakeri (2009) for turbulent flows purely driven by buoyancy, the velocity $(gL\delta\rho/\rho)^{1/2}$ corresponds to the 'free fall' velocity that a coherent region of density $\rho \propto \delta\rho$ sinking (or creaming) in a medium of density ρ reaches after a distance L, and L is such that the flow becomes uncorrelated at distances of order L.

In bubble columns, the density of meso-scale structures is $(1-\varepsilon_{structure})\rho_L$ where $\varepsilon_{structure}$ denotes the void fraction averaged at the scale of the meso-scale structure. Meanwhile, the mean density of the two-phase mixture is $(1-\varepsilon)\rho_L$. Hence, $\delta\rho/\rho_L = (\varepsilon - \varepsilon_{structure})$, meaning that the difference in density is proportional to the excess or to the deficit of void fraction in the structure compared with the mean void fraction ε in the surrounding medium. Typically, clusters - that are gas dominated regions - would have an upward directed (i.e. positive) relative velocity with respect to the mean flow of the gas-liquid mixture in the order of:

$$U_{relative\ cluster-mixture} = C_{cluster}(gL_{cluster}[\varepsilon_{cluster} - \varepsilon])^{1/2}, \tag{5.1}$$

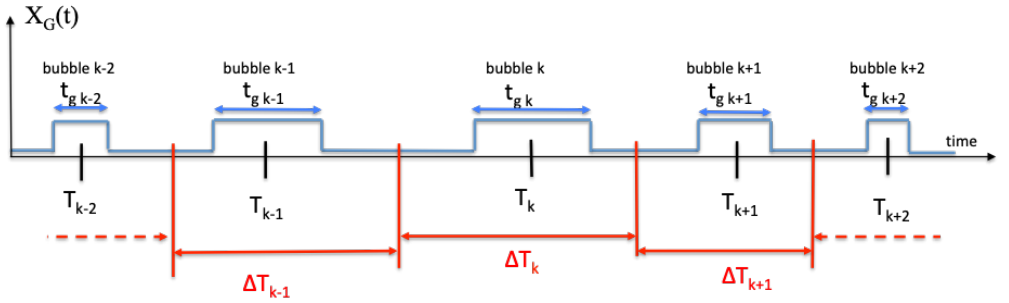

Figure 14: Construction of a 1D Voronoï tessellation from the gas phase indicator function.

where the prefactor $C_{cluster}$ is (a priori) of order one, while voids, that are liquid dominated regions, would have a downward directed (i.e. negative) relative velocity with respect to the mean flow of the gas-liquid mixture:

$$U_{relative\ void-mixture} = -C_{void}(gL_{void}[\varepsilon - \varepsilon_{void}])^{1/2}, \tag{5.2}$$

where C_{void} is a prefactor of order unity. The same reasoning can be applied to intermediate regions, so that the magnitude of the velocity between intermediate regions and the mixture obeys:

$$U_{relative\ intermediate-mixture} = C_{int}(gL_{intermediate}[\varepsilon_{intermediate} - \varepsilon])^{1/2}, \tag{5.3}$$

again with a prefactor C_{int} of order unity. A positive sign has been retained for eq. 5.3 because, as we will see below, the mean void fraction in intermediate regions $\varepsilon_{intermediate}$ is slightly larger than the local void fraction ε when in the heterogeneous regime (the opposite holds in the homogeneous regime). To exploit eq. 5.1, eq. 5.2 and eq. 5.3, the meso-scale structures need to be characterized: this is the purpose of the next section. After that, we will examine how the motions of these meso-scale structures relative to the mixture connect with the relative velocity of bubbles.

5.1. *Identification and characterization of meso-scale structures*

Paralleling what we did for turbulent laden flows (Monchaux *et al.* (2010); Sumbekova *et al.* (2017); Mora *et al.* (2018)) we exploit 1D Voronoï tessellations built from the gas phase indicator function $X_G(t)$ (Raimundo (2015); Mezui *et al.* (2018); Raimundo *et al.* (2019). $X_G(t)$ is deduced from the signal delivered by an optical probe. For the gas phase indicator function measurements presented here, the probe orientation was held fixed (the probe was downward directed). As shown Fig.14, Voronoï cells are then built as successive time intervals, each containing a single bubble. For that, the centers T_k of successive gas residence times t_{gk} are identified. The mid-distance between successive centers T_k and T_{k+1} defines a Voronoï cell boundary. That process is repeated for all detected bubbles, and the width of the k^{th} Voronoï cell that contains the k^{th} bubble is given by $\Delta T_k = (T_{k+1} - T_{k-1})/2$.

Pdfs of the Voronoï cell width ΔT_k normalized by the average $< \Delta T_k >$ are presented in Fig.15a for various gas superficial velocities: all these data have been collected on the bubble column axis at $H/D = 3.625$. Care was taken to ensure a correct convergence of these distributions. The latter comprises between 8000 and 13000 bubbles: these samples correspond to measuring durations from 95 to 950 seconds depending on flow conditions.

Qualitatively, the width ΔT_k of the time interval containing the k^{th} bubble is an indication of the local concentration as a short duration ΔT_k means the presence of a close-by bubble while a large duration indicates that the k^{th} bubble is somewhat isolated. We will come back later on the connection between normalised cell durations $\Delta T_k / < \Delta T_k >$ and concentration. For the time being, let us focus on the allure of these pdfs. The dash line in Figure 15a represents the pdf of normalized cell durations $\Delta T_k / < \Delta T_k >$ for a Random Poisson Process - RPP in short (Ferenc & Néda (2007)) - that has no correlation at any scale. Clearly, and as noted by Raimundo *et al.* (2019), measured distributions at large enough V_{sg} differ from the RPP case. In particular, both very large cell durations (corresponding to dilute conditions) and very small cell durations (corresponding to dense conditions) are more probable than for RPP.

Following Monchaux *et al.* (2010), the distance to RPP is commonly appreciated by examining the standard deviation $\sigma_{voronoi}$ of the pdf of Voronoï cells widths. As shown in Fig. 15b, such standard deviation drastically increases from a low value, comparable to that of RPP, to a much higher value (close to unity) when the system shifts from the homogeneous to the heterogeneous regime. In the homogeneous regime, the measured standard deviation of Voronoï cells pdfs evolves between 0.8 and 0.85. This is slightly larger than the 0.71 limit for a RPP of point particles as determined by Ferenc & Néda (2007) (according to Uhlmann (2020), the standard deviation for a RPP with finite size particles is even lower). The origin of that small difference is unclear. That could be the mark of an inhomogeneous spatial repartition of bubbles in the homogeneous regime because of some gas maldistribution at injection (Nedeltchev (2020)): such a scenario is supported by the analysis of liquid velocity profiles (Lefebvre *et al.* (2022)). Alternately, that small difference could be due to the measuring method itself because the optical probe allows detecting the centers of gas chords and not the centers of bubbles, and because most bubbles are not spherical. Hence, the value of the standard deviation measured in the homogeneous regime could be interpreted at the reference RPP level as detected with the probe technique. The key points in Fig. 15b are the very sharp increase in $\sigma_{voronoi}$ observed at the homogeneous-heterogeneous transition, and the large value, well above that of RPP, that $\sigma_{voronoi}$ reaches at high V_{sg}. The shortcomings of 1D Voronoï analysis in complex flows (Mora *et al.* (2018, 2019)) have been discussed elsewhere: one key result is that the neat difference observed with the standard deviation for RPP unambiguously demonstrates that clustering does occur in the present flow conditions. Furthermore, for all heterogeneous conditions investigated (that is for V_{sg} up to 24cm/s), the standard deviation $\sigma_{voronoi}$ remains nearly the same: that feature also indicates that clustering is a central characteristic of the heterogeneous regime. Finally, let us underline that, as for turbulent flows laden with inert particles (Sumbekova *et al.* (2017)), the main contribution to the standard deviation comes from cells at large $\Delta T_i / < \Delta T_i >$ corresponding to low void fractions, compared with the contribution from cells with intermediate $\Delta T_i / < \Delta T_i >$ (void fractions close to the mean value) or with low $\Delta T_i / < \Delta T_i >$ (high void fractions).

To quantify the connection between cell width $\Delta T_i / < \Delta T_i >$ and concentration, we consider two approaches. First, we follow what we did for turbulent flow laden with droplets (Sumbekova *et al.* (2017); Mora *et al.* (2018)), by connecting the ratio $\Delta T_k / < \Delta T_k >$ with linear number densities, i.e. with the number of inclusions detected per unit length. The length corresponds to the measuring duration multiplied by the axial velocity V_{axial} of inclusions. The local number density γ_k (number of inclusions per meter) in the k^{th} cell equals $1/[\Delta T_k V_{axial}]$ while $1/[< \Delta T_k > V_{axial}]$ is the mean number density γ. Therefore, the normalized cell width $\Delta T_k / < \Delta T_k >= \gamma/\gamma_k$ represents the inverse of the instantaneous (i.e. at the scale of the Voronoï cell) number density divided by the

mean number density. When applied to bubble columns (Raimundo (2015); Mezui *et al.* (2018); Raimundo *et al.* (2019)), we considered V_{axial} as the mean bubble velocity, and γ was assumed to be proportional to the mean dispersed phase concentration. Under these assumptions, the inverse of $\Delta T_k / < \Delta T_k >$, i.e. γ_k/γ, provides the magnitude of the local gas concentration (local at the scale of the Voronoï cell) with respect to the mean gas fraction at the measuring location. In Fig. 15, the abscissa $\Delta T_i / < \Delta T_i >$ varies from 0.07 to 10 so that γ_k/γ covers more than two decades as it evolves between 0.1 and about 14.

However, a second approach is required because, for the heterogeneous conditions considered here, γ_k/γ does not coincide with the ratio $\varepsilon_k/\varepsilon$ of the void fraction ε_k relative to the k^{th} cell to the mean gas hold-up ε at the measuring location. Indeed, in the turbulent laden flows we have previously analysed, all inclusions traveled with almost the same axial velocity. This is no longer the case for bubbles in the heterogeneous regime as their velocities experience strong variations (see the pdfs in Figure 2), leading to a standard deviation as large as 60% of the mean (Section 3.2). Hence, the selection of a mean bubble velocity to transform time into space induces very large distorsions on the concentration estimate by way of γ_k. To correct for these distortions and to evaluate reliable local void fractions, it is appropriate to rely on gas residence times as the latter naturally account for the actual velocity of each bubble. The void fraction relative to the k^{th} Voronoï cell equals the sum of gas residence times included in that cell divided by the cell duration ΔT_k. As shown in Annex B, the ratio $\Delta T_k / < \Delta T_k >$ is indeed related with $\varepsilon/\varepsilon_k$, but it does not coincides with $\varepsilon/\varepsilon_k$ as the prefactor between these two quantities varies with the gas residence time (see eq. B 1 in annex B). In the following, we will use the ratio γ_k/γ as a crude, qualitative characterisation of meso-scale structures in terms of concentration, while exact measurements of the gas fraction $\varepsilon_k/\varepsilon$ will be considered when equations 5.1, 5.2 and 5.3 will be exploited.

Going back to Fig.15a, and whatever the flow conditions, the measured pdfs of Voronoï cells cross the RPP at two fixed abscissa represented by vertical dashed lines. A third intersection sometimes occurs in the very dense limit (at $\Delta T_k / < \Delta T_k >$ about 0.1, that is for γ_k/γ about 10), but it will not be considered here because its occurrence is far too sensitive to the sample size. As for turbulent laden flows (Monchaux *et al.* (2010)), we define three populations out of the two stable thresholds. A Voronoï cell (and the bubble it contains) belongs to a 'dense' region when $\Delta T_k / < \Delta T_k >$ is below 0.51, or equivalently when γ_k/γ is higher than 1.96. A Voronoï cell (and the bubble it contains) belongs to an 'empty' or 'void' region when $\Delta T_k / < \Delta T_k >$ is above 2.89, or equivalently when γ_k/γ is lower than 0.34. In between, the cell (and its bubble) pertains to an 'intermediate' region. Owing to Fig. 15a, the probability for bubbles to belong to 'empty' or to 'dense' regions is larger than in RPP. This is confirmed by the data presented in Table 3. In average, 38% of the bubbles belong to dense regions, while 5% are within empty regions and 57% are in intermediate regions: these figures remain stable within about 5% over the whole heterogeneous regime that is for V_{sg} from 6cm/s to 25cm/s. As expected, the figures relative to dense and to empty regions are significantly larger than those for a RPP. Beside, in the heterogeneous regime, the contributions to the local void fraction are typically 17% for the dense regions, 10% for the empty regions and 70% for intermediate regions (Table 3). These figures correspond to average values for $V_{sg} \geqslant$ 9cm/s: they change by less than 1% when considering data over the interval $V_{sg} \geqslant 6cm/s$.

There is a slight decrease of the contribution of dense regions to the local void fraction as V_{sg} increases, which is compensated by a slight increase with V_{sg} of the contributions of empty and intermediate regions.

In the homogeneous regime, the repartition of bubbles in number between dense, empty

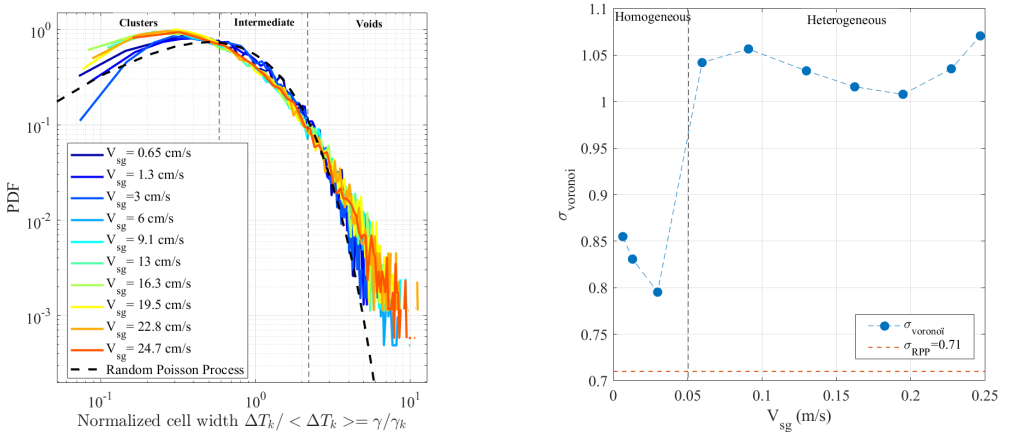

(a) (b)

Figure 15: (a) Centered pdfs of 1D Voronoï cells width $\Delta T_k / < \Delta T_k >$ built from Doppler probe signals at various gas superficial velocities. The dash line represents the 1D Voronoï distribution for an RPP, i.e. a Random Poisson Process. (b) Evolution of the standard deviation of 1D Voronoï distributions with the gas superficial velocity. The horizontal dash line indicates the standard deviation for an RPP while the vertical dashed lines delineate the homogeneous-heterogeneous transition. Measurements performed in a $D = 0.4$m column, on the column axis at $H/D = 3.625$.

	Dense regions	Intermediate regions	Empty regions
Repartition of bubbles in number in measured pdfs in the heterogeneous regime (average values for $V_{sg} \geqslant 9$cm/s)	38%	57%	5%
Repartition of the actual void fraction $\varepsilon_k/\varepsilon$ in the heterogeneous regime (average for $V_{sg} \geqslant 9$cm/s).	17%	73%	10%
Repartition of bubbles in number in RPP.	30%	68%	2%
Repartition of the actual void fraction $\varepsilon_k/$ in the homogeneous regime (average values for $V_{sg} \geqslant 3$cm/s).	29%	67%	4%
Repartition of bubbles in number in measured pdfs in the homogeneous regime (values for $V_{sg} = 1.3$cm/s)	33.60%	63.20%	3.20%

Table 3: Typical distributions of the dispersed phase between void regions, intermediate regions and dense regions in the heterogeneous and homogeneous regimes and comparison with a RPP. From measurements on the axis of a $D = 0.4$m bubble column at $H/D = 3.625$.

and intermediate regions is very close to the repartition in number for an RPP. The repartition in terms of void fraction is slightly different from the repartition in number (this is because the spatial extent of the three regions are not the same as shown in Fig.19b) but the two sets of figures remain close from each over.

Then, bubbles belonging to a 'dense' region and successive in time are assembled to form a 'cluster'. Similarly, successive bubbles belonging to an 'empty' region are assembled to form a 'void'. The same process was used for intermediate regions. The characteristics of the resulting meso-scale structures in terms of size and concentration are then extracted:

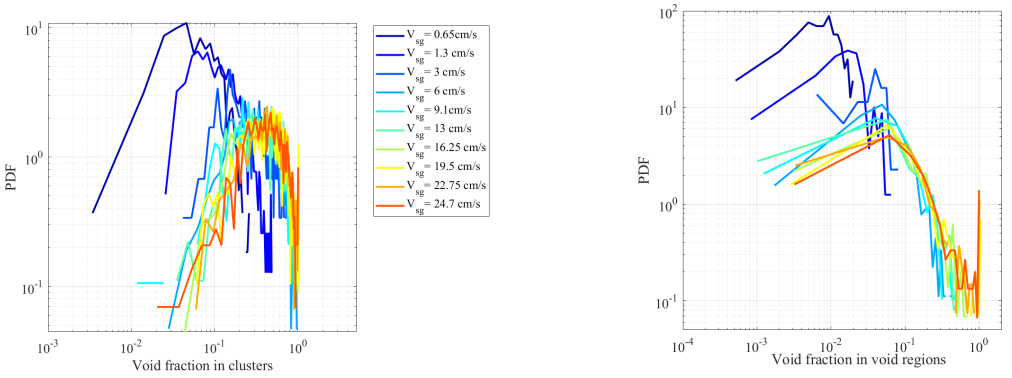

(a) (b)

Figure 16: Pdfs of void fraction (in absolute value) in clusters (a) and in void regions (b) for different superficial velocities. For these statistics, we considered clusters comprising at least two bubbles. Measurements performed in a $D = 0.4$m column, on the column axis at $H/D = 3.625$.

- The void fraction (in absolute value) in a given meso-scale structure is evaluated as the sum of gas residence times for all bubbles pertaining to that structure divided by the duration of that structure, the later being the sum of all involved ΔT_i. The distributions of void fraction in clusters and in voids are exemplified in Figure 16 for various V_{sg}.
- The size of a given meso-scale structure is estimated as the duration of the structure multiplied by the average bubble velocity, the latter being evaluated for the bubbles belonging to the structure considered (these conditional velocities are analyzed in detail in section 5.3). Length distributions for clusters and for voids are provided Figure 17 for various V_{sg}.

We considered two options for clusters: either the minimum number of bubbles in a cluster is set to 1 so that all Voronoï cells with a $\Delta T_k / < \Delta T_k >$ below the threshold are considered as clusters, or the minimum number of bubbles is set to 2 so that clusters involving a single bubble are excluded. That second option has been suggested to help distinguishing between 'coherent' and 'random' clusters in turbulent laden flows (Mora *et al.* (2019)). Here, and for all the flow conditions pertaining to the heterogeneous regime, it happens that 37% to 40% of clusters involve a single inclusion.

It should also be underlined that zones below or beyond the above-defined thresholds also exist for an RPP. Hence, one can still identify and statistically characterize 'dilute' and 'dense' regions in homogeneous conditions even though the corresponding Voronoï distributions are very close to and/or almost collapse with RPP. Using the same data processing routine to analyze homogeneous and heterogeneous conditions, the characteristics of clusters and of empty regions are presented over the whole range of V_{sg} from homogeneous to heterogeneous regimes, bearing in mind that different physical origins are associated with meso-scale structures for these two regimes. In particular, the data in the homogeneous regime are not expected to bear any particular significance as they could be of random origin, or they could be related to some correlation induced by 'defects' in the system (due for example to gas injection, see Lefebvre *et al.* (2022)).

Figures 16 and 17 clearly demonstrate that, for void regions as well as for clusters, the distributions in the heterogeneous regime markedly differ from the distributions observed in the homogeneous regime. Moreover, in the heterogeneous regime, the distributions tend

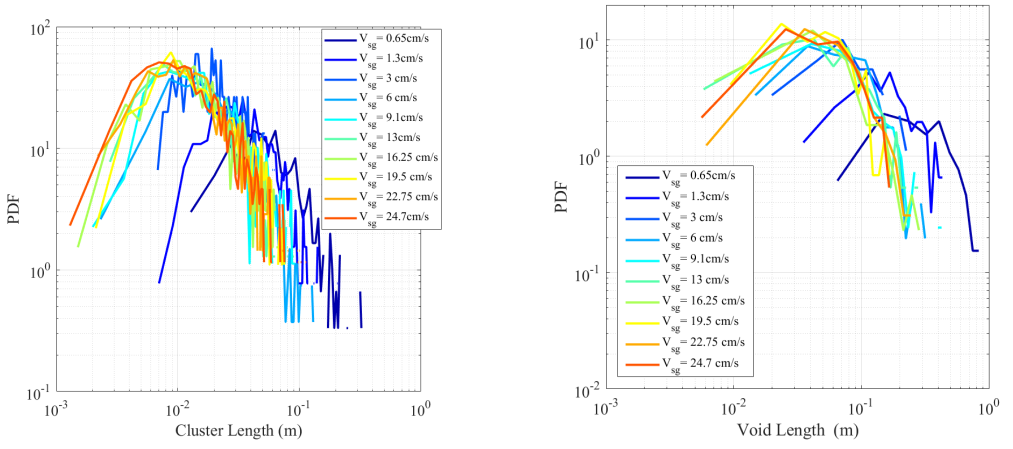

(a) (b)

Figure 17: (a) Pdfs of lengths of clusters (a) and of void regions (b) for different superficial velocities. For these statistics, we considered clusters that comprise at least two bubbles. Measurements performed in a $D = 0.4$m column, on the column axis at $H/D = 3.625$.

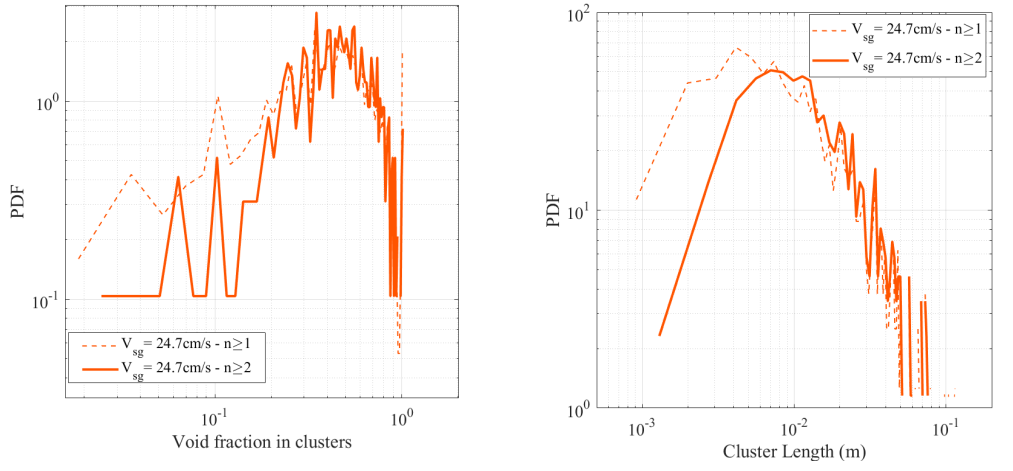

(a) (b)

Figure 18: Comparisons of the pdfs of void fraction in clusters (a) and of clusters lengths (b) when the minimum number of bubbles is set to 1 or to 2. Measurements performed in a $D = 0.4$m column, on the column axis at $H/D = 3.625$ and $V_{sg} = 24.7$cm/s.

to collapse indicating that clusters and void regions reach an asymptotic state when the gas superficial velocity becomes large enough. As shown Figure 18, that limiting state is almost the same when considering clusters with a minimum of 1 bubble or with a minimum of 2 bubbles.

The average characteristics of clusters and of void and intermediate regions are given Figure 19 as a function of the gas superficial velocity.

• The average number of bubbles is about 1.8 in void regions and about 4 in intermediate regions. In clusters, it is about 4.5 when $n \geqslant 2$, and it drops to 3.2 when

accounting for clusters consisting of a single bubble. The decrease from 4.5 to 3.2 is consistent with the fact that, as seen above, 2/3 of the clusters comprise more than one bubble. These average numbers of bubbles are quite low: they indicate that the clusters are not organized as compact assemblies of bubbles, but are more like thin sheets. The fact that the probability to find a cluster comprising N bubbles decays like $N^{-1.17}$, i.e. that it strongly drops with N, also supports the proposed picture. In particular, 1D clusters comprising more than 10 bubbles are very rare: they represent only 3.7% of the clusters (with $n \geqslant 1$) present in the heterogeneous regime.

• The size of void regions and of intermediate regions varies from 6-7cm to 20cm while the size of clusters ranges from a few millimeters up to 6-7cm. In the heterogeneous regime, the mean size of clusters $< L_{cluster} >$, that of void regions $< L_{void} >$ and that of intermediate regions $< L_{intermediate} >$ all remain fairly stable. The mean cluster length asymptotes at $21 \pm 3mm$: it is marginally affected if one considers a minimum of one bubble instead of two to form clusters. The asymptotic mean length of void regions is significantly larger as $< L_{void} > \sim$ 74mm$\pm$10mm, and similarly, for intermediate regions, $< L_{intermediate} >$ is about 62mm$\pm$4mm.

• The average concentration (in absolute value) in voids steadily increases with the gas superficial velocity. A similar behavior holds for intermediate regions. In clusters, the average concentration sharply increases at the homogeneous-heterogeneous transition, and for V_{sg} above $\sim$ 0.15m/s, it tends to stabilize at a large void fraction, say about 50%. Interestingly, when scaled by the local void fraction ε (here ε equals the void fraction on the axis ε_{axis}), the mean concentrations in voids and in intermediate regions increase with the mean gas hold-up, while the concentration in clusters slightly decreases: additional data are needed to confirm if the asymptotic trend corresponds to a decrease or to a plateau. The same question holds concerning the asymptotic behavior of the contrast in concentration between dense and dilute regions.

5.2. *Relative velocity between meso-scale structures and the mixture*

Before exploiting eq. 5.1 to 5.3, let us examine the average values of $< L_{cluster}[\varepsilon_{cluster} - \varepsilon] >$, of $< L_{void}[\varepsilon_{void} - \varepsilon] >$ and of $< L_{intermediate}[\varepsilon_{intermediate} - \varepsilon] >$. As all the data discussed here have been collected on the column axis, the local void fraction ε equals ε_{axis}. In the previous section, we have seen that the mean sizes $< L_{cluster} >$, $< L_{void} >$ and $< L_{intermediate} >$ do not change much with V_{sg} when in the heterogeneous regime, while the concentration in voids and in intermediate regions, and to a lesser extend the concentration in clusters, slightly evolve with V_{sg}. The products $< L_{void}[\varepsilon_{void} - \varepsilon] >$, $< L_{cluster}[\varepsilon_{cluster} - \varepsilon] >$ and $< L_{intermediate}[\varepsilon_{intermediate} - \varepsilon] >$ are shown versus V_{sg} in Figure 20a): they happen to remain fairly stable at large V_{sg}, say for V_{sg} above about 10-15cm/s.

The resulting relative velocities between meso-scale structures and the mixture, namely $U_{relative\ cluster-mixture}$ deduced from eq. 5.1 using clusters characteristics, $U_{relative\ void-mixture}$ deduced from eq. 5.2 using voids characteristics, and $U_{relative\ intermediate-mixture}$ deduced from eq. 5.3 using intermediate regions characteristics, are plotted versus V_{sg} in Figure 20b. Note that the present discussion relies on velocity estimates for which the prefactors entering eq 5.1 to eq. 5.3 are all considered as equal to unity (these prefactors will be quantified in Section 5.4). A number of features arise from Figure 20b:

• Setting the minimum number of bubbles in clusters to 1 or to 2 does not induce any significant difference on the velocity $U_{relative\ void-mixture}$ predicted.

• As expected from the behaviors of $< L_{cluster}[\varepsilon_{cluster} - \varepsilon] >$, of $< L_{intermediate}[\varepsilon_{intermediate} - \varepsilon] >$ and of $< L_{void}[\varepsilon_{void} - \varepsilon] >$, the three quantities

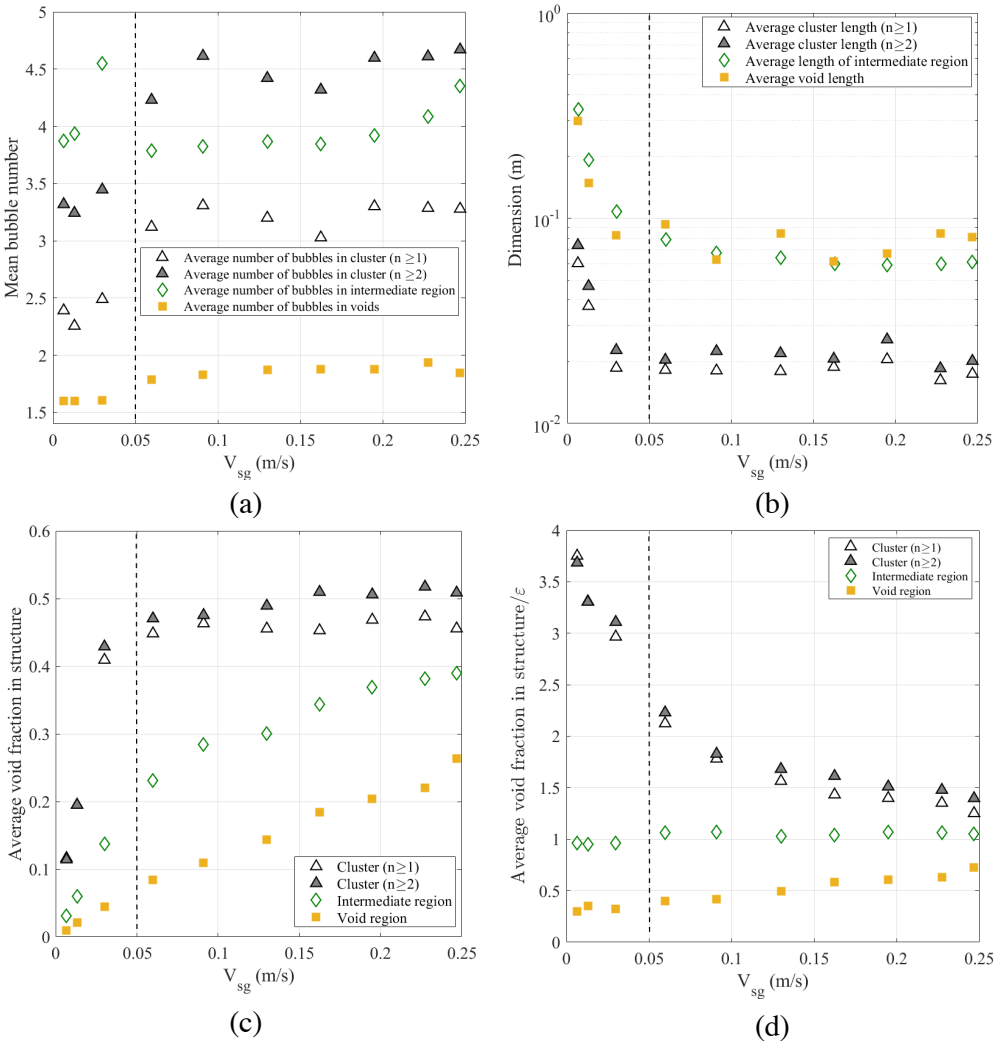

Figure 19: Mean characteristics of clusters, of void regions and of intermediate regions versus the gas superficial velocity: (a) Average number of bubbles in meso-scale structures, (b) average size, (c) average absolute gas concentration in meso-scale structures, (d) average concentration scaled by the void fraction on the column axis. Measurements performed in a $D = 0.4$m column, on the column axis, at $H/D = 3.625$. Vertical dashed lines delineate the homogeneous to heterogeneous transition.

$U_{relative\ cluster-mixture}$, $U_{relative\ intermediate-mixture}$ and $U_{relative\ void-mixture}$ stabilize to nearly constant values for V_{sg} above about 13-15cm/s.

• In the heterogeneous regime, the magnitude of $U_{relative\ cluster-mixture}$ is 0.15-0.20m/s while that of $U_{relative\ void-mixture}$ is -0.31m/s: the mean velocity difference between bubbles in clusters and bubbles in void regions is thus about 0.45-0.5m/s. This is the same magnitude as that of the mean relative velocity directly measured between the bubbles and the liquid from unconditional measurements (see Fig. 4).

This last observation provides credit to our initial guess that the relative velocity in

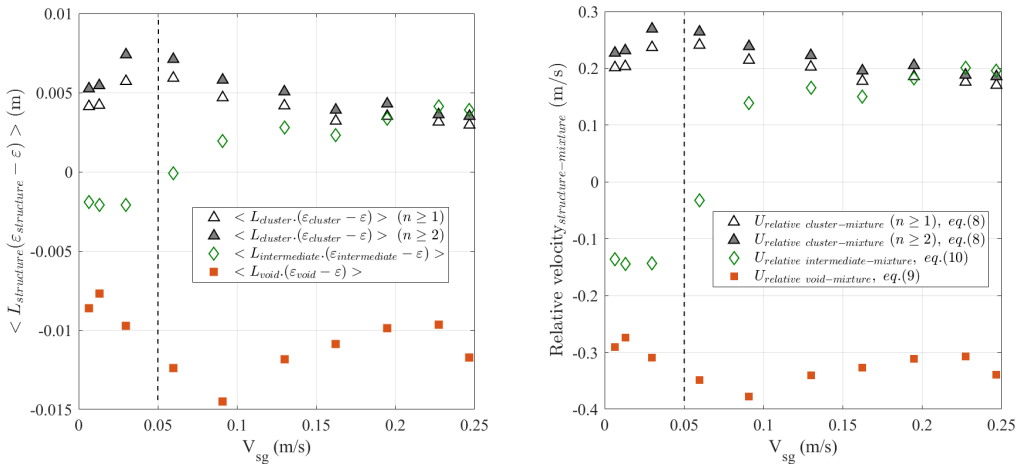

Figure 20: Evolution of the products $< L_{cluster}[\varepsilon_{cluster} - \varepsilon] >$ for $n \geqslant 1$ and for $n \geqslant 2$, $< L_{intermediate}[\varepsilon_{intermediate} - \varepsilon] >$ and $< L_{void}[\varepsilon_{void} - \varepsilon] >$ with V_{sg} (a). Corresponding relative velocities between bubbles pertaining to a given meso-scale structure with respect to the mixture assuming all prefactors in eq.(8) to (10) equal to unity (b). Measurements performed in a $D = 0.4$m column, on the column axis at $H/D = 3.625$.

these buoyancy driven bubbly flows is controlled by meso-scale structures dynamics. A more direct and quantitative analysis of that feature is developed in the next sections.

5.3. *Absolute and relative bubble velocities conditioned by the local concentration*

Paralleling what we did for turbulent laden flows (Sumbekova *et al.* (2016)), bubbles are classified into three populations namely clusters, void regions and intermediate regions. Bubble velocity pdfs are built for each of these populations using direct velocity measurements (no interpolation) performed with a downward oriented Doppler probe (Lefebvre *et al.* (2022)). Examples of such conditional pdfs are provided Figure 21. For both regimes, the minimum velocities are about the same for the three populations, while the most probable velocity as well as the maximum velocity drift to larger values when successively considering void regions, intermediate regions and clusters. This drift is weak in the homogeneous regime: the velocity at the peak increases from about 0.4m/s in void regions to 0.7m/s in clusters, so that the difference is of the order of the bubble terminal velocity. The drift is significantly larger in the heterogeneous regime as the most probable velocity goes from $\sim$ 0.5m/s in void regions up to 1.3m/s in clusters: in that case, the difference amounts to 3.5 times the bubble terminal velocity. Hence, the conditional bubble velocities gathered with the Doppler optical probe confirm our physical expectation that, in average, high void fraction regions are moving up must faster than low void fraction regions.

To quantify this effect, and for each meso-scale structure, we evaluated the mean bubble velocity $V_{b|structure}$ for bubbles pertaining to the selected meso-scale structure. These velocities, that represent absolute velocities in the laboratory frame, are shown Figure 22 as a function of the gas superficial velocity. It could be observed that the average conditional velocities relative to void regions $V_{b|voids}$, to intermediate regions $V_{b|intermediate}$ and to clusters $V_{b|clusters}$, all monotonously increase with V_{sg}. Beside, the velocity differences between any two out of these three populations remain limited, in

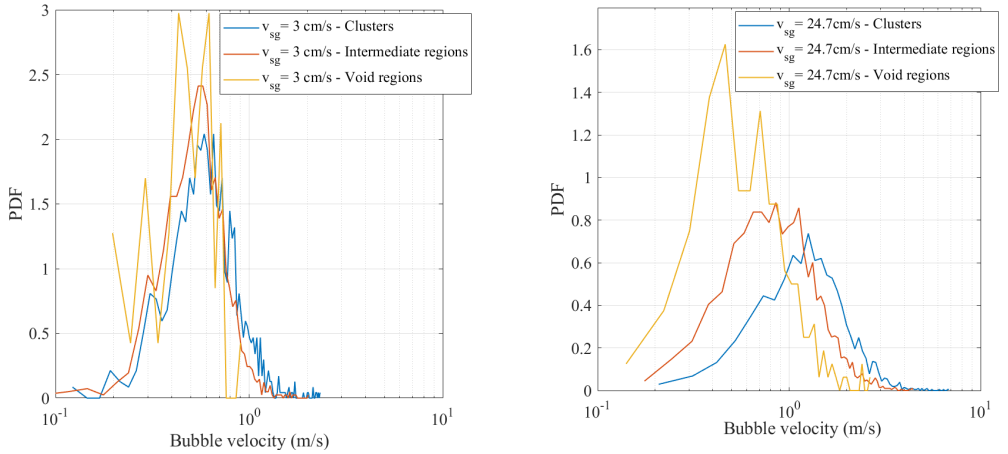

(a) (b)

Figure 21: Bubble velocity pdfs conditioned by the meso-scale structure they belong to, i.e. clusters, intermediate regions or void regions for $V_{sg} = 3$cm/s (a) and for $V_{sg} = 24.7$cm/s (b). Measurements performed in a $D = 0.4$m column, on the column axis at $H/D = 3.625$ with a downward directed Doppler probe.

the order of U_T, in the homogeneous regime. Beyond the homogeneous-heterogeneous transition, the velocity differences neatly increase with V_{sg}: bubbles embedded in dense regions are moving up faster than bubbles in intermediate regions, which are themselves moving up faster than bubbles in dilute regions. This observation provides an undisputable evidence of the central role of meso-scale structures on the actual dynamics of bubbles in the heterogeneous regime.

To quantitatively appreciate these velocity differences, let us consider the relative velocity of bubbles in a given meso-scale structure with respect to the liquid phase. The mean bubble relative velocities with respect to the liquid phase for each meso-scale structure are presented Figure 23. The two velocity differences $V_{b|clusters} - V_L$ and $V_{b|intermediate} - V_L$ increase with V_{sg} in a way similar to the unconditional relative velocity $U_R = V_G - V_L$. In particular, the differences in velocities remain moderate in the homogeneous regime, and they steeply increase at the transition. Both differences $V_{b|clusters} - V_L$ and $V_{b|intermediate} - V_L$ tend to become quasi-constant at large V_{sg} (roughly above $V_{sg} \sim 13 - 15$cm/s). In intermediate regions, the average bubble velocity exceeds that of the liquid by 0.3-0.4m/s. In clusters, the difference reaches about 0.7-0.8m/s that is 3 to 3.5 times the bubble terminal velocity.

In the heterogeneous regime, the unconditional mean bubble relative velocity $U_R = V_G - V_L$ happens to be comprised between $V_{b|clusters} - V_L$ and $V_{b|intermediate} - V_L$ (Figure 23). It is tempting to try to recover U_R from conditional measurements. Considering that a fraction $N_{clusters}$ of bubbles pertains to clusters, that a fraction $N_{intermediate}$ belongs to intermediate regions and a fraction N_{voids} to void regions (so that $N_{clusters} + N_{intermediate} + N_{voids} = 1$), one can write:

$$U_R = V_G - V_L = N_{clusters}(V_{b|clusters} - V_L) + N_{intermediate}(V_{b|intermediate} - V_L) + N_{voids}(V_{b|voids} - V_L). \tag{5.4}$$

The repartition of bubbles is given in Table 3 for both regimes. In the heterogeneous

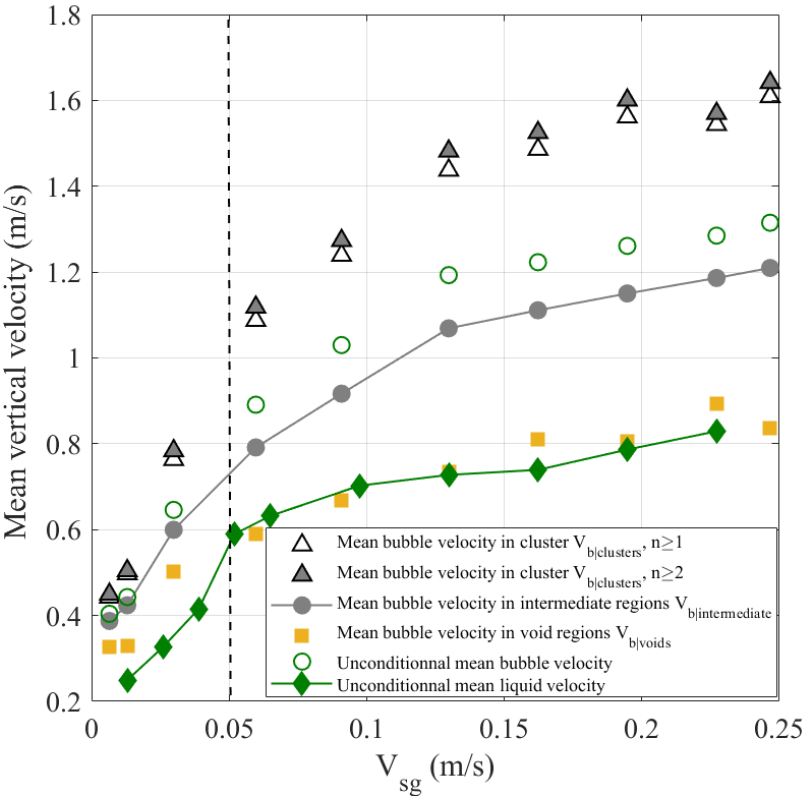

Figure 22: Average absolute bubble velocity for bubbles pertaining to clusters $V_{b|clusters}$, to intermediate regions $V_{b|intermediate}$ and to void regions $V_{b|voids}$ versus the gas superficial velocity. Measurements performed in a $D = 0.4$m column, on the column axis at $H/D = 3.625$ with a downward directed Doppler probe. The unconditional mean liquid V_L and gas V_G velocities (up & down series) from Figure 4 are also shown for sake of comparison.

regime, and in the limit of high V_{sg}, the relative velocities $V_{b|clusters} - V_L$, $V_{b|intermediate} - V_L$ and $V_{b|voids} - V_L$ are all nearly constant. When combining these results, U_R deduced from eq. 5.4 evolve between 0.49m/s and 0.51m/s depending on the range of V_{sg} considered (Table 4) while direct measurements of U_R (4 direct measurements are available between $V_{sg} = 0.13$cm/s and 0.227cm/s - see Figure 23) provide an average value of 0.52 m/s. There is thus an excellent agreement between the relative velocity predicted with eq.5.4 and direct measurements of the relative velocity.

We did the same in the homogeneous regime. We considered two ranges of V_{sg} to evaluate the mean values of the relative velocity per meso-structure, namelly $V_{sg} \leqslant 0.03$m/s and $V_{sg} \leqslant 0.06$m/s. The unconditional relative velocity U_R estimates are given in Table 5 for a RPP : in all cases, the resulting unconditional velocity predicted using eq. 5.4 evolves in the range $0.29 - 0.30$m/s. Very similar figures are obtained if one considers the measured repartition of bubbles that was measured in the homogeneous regime instead of the RPP repartition (see Table 3). The unconditional velocity deduced from eq. 5.4 happens to be close to the value extracted from direct measurements (the latter is 0.27m/s): the agreement in the homogeneous regime is also quite good.

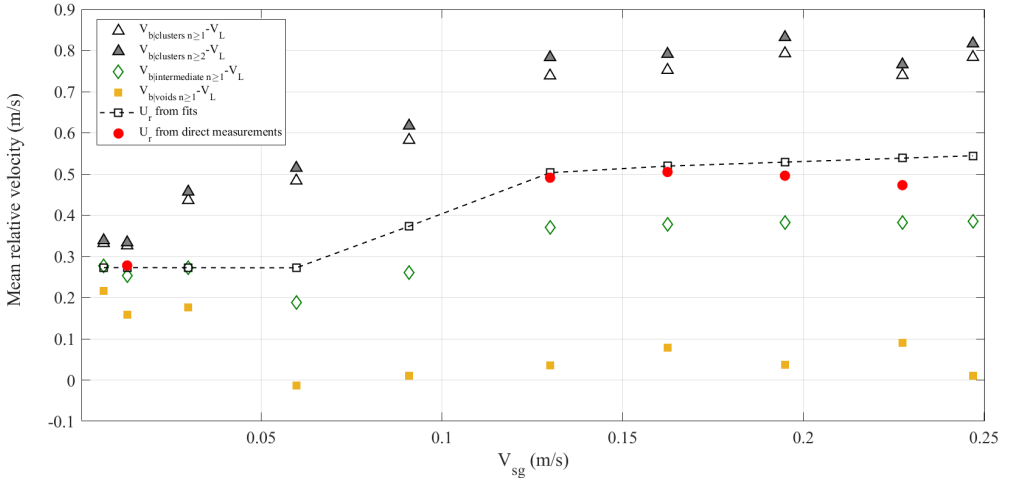

Figure 23: Mean relative velocity between bubbles pertaining to a meso-scale structure, namely clusters, intermediate regions and void regions, and the liquid phase: evolution with V_{sg}. The unconditional relative velocity U_R is also shown for comparison (red dots correspond to direct measurements while the dash line corresponds to the multiple slopes fit shown Figure 4). Measurements performed in a $D = 0.4$m column, on the column axis at $H/D = 3.625$.

Mean relative velocity $V_{b\|structure} - V_L$ (m/s)	clusters	intermediate regions	void regions	Unconditionnal relative velocity (m/s) deduced from eq. 5.4
mean value over the range $V_{sg} \geqslant 9$cm/s	0.732	0.360	0.044	0.49
mean value over the range $V_{sg} \geqslant 13$cm/s	0.762	0.379	0.050	0.51
mean value over the range $V_{sg} \geqslant 16$cm/s	0.767	0.381	0.054	0.51
repartition of bubbles in number:	38%	57%	5%	

Table 4: Estimations of the unconditional relative velocity U_R deduced from relative velocities conditionned by meso-scale structures using eq.5.4 in the heterogeneous regime.

Mean relative velocity $V_{b\|structure} - V_L$ (m/s)	clusters	intermediate regions	void regions	Unconditionnal relative velocity (m/s) deduced from eq. 5.4
mean value over the range $V_{sg} \leqslant 3$cm/s	0.367	0.270	0.186	0.30
mean value over the range $V_{sg} \leqslant 6$cm/s	0.391	0.244	0.131	0.29
repartition of bubbles in number for RPP	30%	68%	2%	

Table 5: Estimates of the unconditional relative velocity U_R deduced from relative velocities conditionned by meso-scale structures using eq. 5.4 in the homogeneous regime.

Hence, for both regimes, we recover the unconditional relative velocity from relative velocities conditioned by the three meso-scale structures we identified. As said above, the decomposition into meso-scale structures in the homogeneous regime is somewhat artificial. Indeed, owing to their definition, these structures can be identified as in any RPP process. Yet, the relative velocities conditioned by structures happen to be quite different in the two regimes. The relative velocity of bubbles in clusters is significantly larger in the heterogeneous regime than in the homogeneous regime. Meanwhile, the

relative velocity of bubbles in voids is significantly smaller in the heterogeneous regime than in the homogeneous regime. These features are clear indications that the physics at play are different, with collective effects present in the heterogeneous regime while the repartition of bubbles and their dynamics remain quasi uniform in the homogeneous regime. In both cases, the unconditional relative velocity is recovered by combining the repartition of bubbles between meso-scale structures with their relative velocity in each structure.

5.4. *Scaling of unconditional and conditional relative velocities of bubbles.*

On the one hand, thanks to conditional bubble velocity measurements, we gathered some direct experimental evidence of the impact of meso-scale structures on the relative velocity of bubbles with respect to the liquid in the heterogeneous regime. On the other hand, based on the inertia-buoyancy equilibrium, a tentative scaling for the velocity differences $U_{relative\ structure-mixture}$ is suggested in eq. 5.1 to 5.3 that relies on meso-scale structures characteristics. To combine these approaches and to identify the prefactors in eq. 5.1 to 5.3, one needs to evaluate $U_{mixture} - U_L$ that amounts for the slip velocity between the mixture and the liquid. By definition, $U_{mixture}$ is the mixture volumetric flux, that is the velocity of the center of volume of both phases (Ishii (1975)). Therefore, $U_{mixture}$ is related to unconditional phasic velocities by $U_{mixture} = (1-\varepsilon)U_L + \varepsilon U_G$. Thus, $U_{mixture} - U_L$ can be written as:

$$U_{mixture} - U_L = \varepsilon(U_G - U_L) = \varepsilon U_R. \tag{5.5}$$

The prefactors $C_{structure}$ in eq. 5.1 to 5.3 can now be evaluated. Indeed, for each meso-scale structure, one has:

$$\begin{aligned} U_{relative\ structure-mixture} &= U_{structure} - U_{mixture} \\ = U_{structure} + V_L - V_L - U_{mixture} &= V_{b|structure} - V_L - \varepsilon U_R. \end{aligned} \tag{5.6}$$

Note that, in the last equality of eq. 5.6, $U_{structure}$ has been identified with $V_{b|structure}$. Strictly speaking, these two quantities are not the same as $V_{b|structure}$ represents the mean velocity of bubbles within the structure considered while, as discussed in the introduction of Section 5, $U_{structure}$ corresponds to the velocity of the whole coherent region forming the structure meaning that $U_{structure}$ includes information on both gas and liquid phases. In clusters, owing to their large void fraction in the heterogeneous regime (see Fig. 19c), it is reasonable to assume that both phases move at nearly the same velocity and hence that $U_{clusters} \sim V_{b|clusters}$. A similar argument could be put forward for intermediate regions when V_{sg} is large. For void regions, experience shows that $V_{b|voids}$ and V_L nearly coincide when in the heterogeneous regime (see Fig. 22). Hence, assuming $U_{structure} \sim V_{b|structure}$ seems reasonable (to confirm that, liquid velocity measurements conditioned by the local gas concentration would be useful), and eq. 5.6 combined with eq. 5.1, 5.2 or 5.3 provides an estimate of the prefactor $C_{structure}$, namely:

$$C_{structure} = sign(\varepsilon_{structure} - \varepsilon) U_{relative\ structure-mixture} / (gL_{structure}|\varepsilon_{structure} - \varepsilon|)^{1/2}, \tag{5.7}$$

where the denominator has been quantified in section 5.2. The values $C_{structure}$ deduced from eq. 5.7 are given as a function of V_{sg} in Figure 24. They all tend to nearly constant values at large V_{sg}: the mean values of $C_{structure}$ in the heterogeneous regime are provided Table 6. All these mean values happen to be weakly sensitive to the range of V_{sg} selected

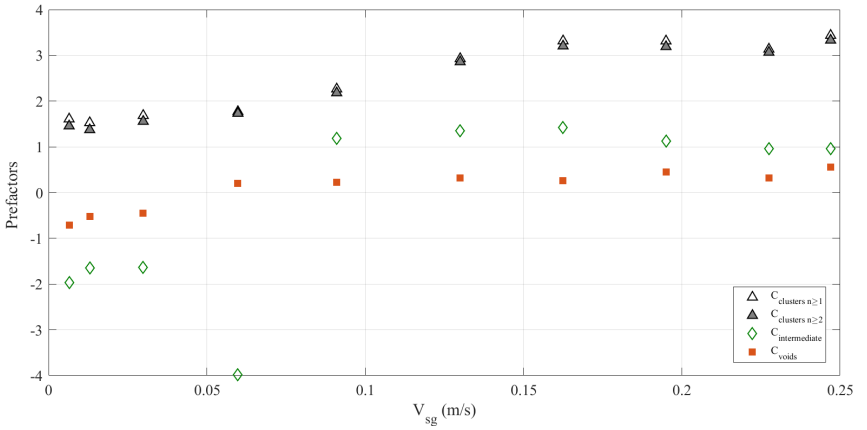

Figure 24: Evolution of the prefactors $C_{cluster}$, $C_{intermediate}$ and C_{void} deduced form eq. 5.7 combined with eq. 5.1 to 5.3 with V_{sg}.

Measured $U_{relative\ structure-mixture}/(gL_{structure}[\varepsilon_{structure}-\varepsilon])^{1/2}$	$C_{cluster}$ Dense regions $n \geqslant 1$, eq.5.1	$C_{cluster}$ Dense regions $n \geqslant 2$, eq.5.1	C_{int} Intermediate regions, eq.5.3	C_{void} Void regions, eq.5.2
Average prefactor for $V_{sg} \geqslant 6$ cm/s	2.87	2.78	1.26	-0.34
Average prefactor for $V_{sg} \geqslant 9$ cm/s	3.06	2.97	1.26	-0.36
Average prefactor for $V_{sg} \geqslant 13$ cm/s	3.22	3.13	1.17	-0.38

Table 6: Mean values of prefactors $C_{structure}$ in the heterogeneous regime when assuming $U_{structure} = V_{b|structure}$.

to compute the average. Moreover, all prefactors are of order unity, with $C_{cluster} \sim 3$, $C_{intermediate} \sim 1.2$ and $C_{void} \sim -0.35$. The scalings proposed in eq. 5.1 to 5.3 are therefore consistent. In other words, these equations provide the correct magnitude of the relative velocity of meso-scale structures with respect to the mixture, and the dynamics of these meso-scale structures is indeed controlled by an equilibrium between inertia and buoyancy.

Moreover, we succeeded to connect the conditional bubble dynamics with the characteristics of the meso-scale structures. Thanks to eq. 5.4, the unconditional bubble relative velocity also happens to be related with these characteristics combined with the repartition of bubbles between the three populations. Thus, the enhancement of the bubble relative velocity observed in the heterogeneous regime is the consequence of the collective dynamics occurring in these buoyancy driven bubbly flows when the gas fraction is large enough.

These findings and the associated scalings have been corroborated over a large range of gas superficial velocities but for a single bubble column diameter. As seen in Section 4, the existence of an asymptotic heterogeneous state at large V_{sg} is supported by many literature data on liquid and on gas velocities gathered over a significant range of bubble column diameter (say from 0.15m to 3m, see Table 4.1 and 4.2). However, measurements of the relative velocity in the heterogeneous regime are absent from the literature. Further experimental investigations are therefore required to test the proposed dependencies of meso-scale structures characteristics, and of both unconditional and conditional relative velocities on the bubble column diameter.

In that perspective, let us now examine how the relative velocities discussed above

Mean values evaluated for $V_{sg} \geqslant$ 9cm/s	Clusters with n$\geqslant$1	Clusters with n$\geqslant$2	Intermediate regions	Void regions
Mean size	0.018 m	0.022 m	0.062 m	0.074 m
Mean size / D	0.045	0.054	0.155	0.185
$< (\varepsilon_{structure} - \varepsilon)/\varepsilon >$	0.464	0.585	0.054	-0.42
$< gL_{structure}[\varepsilon_{structure} - \varepsilon] >^{1/2} /(gD\varepsilon)^{1/2}$	0.17	0.19	0.15	-0.3
$C_{structure}$ (from Table 6)	3.06	2.97	1.26	-0.36
prefactor $U_{relative\ structure-mixture}/(gD\varepsilon)^{1/2}$	0.520	0.564	0.189	-0.108

Table 7: Average characteristics of meso-scale structures in the heterogeneous regime measured on the axis of a D=0.4m bubble column and at H/D=3.625, pre-factors $C_{structure}$ et ratio $U_{relative\ structure-mixture}/(gD\varepsilon)^{1/2}$

are connected with the reference velocity $(gD\varepsilon)^{1/2}$ identified in Section 2. Table 7 provides the mean characteristics of meso-scale structures evaluated from all the data collected for $V_{sg} \geqslant 9$cm/s. Table 7 also provides the ratio $sign(\varepsilon_{structure} - \varepsilon) < gL_{structure}|\varepsilon_{structure} - \varepsilon| >^{1/2} /(gD\varepsilon)^{1/2}$ for each structure as well as the ratio $U_{relative\ structure-mixture}/(gD\varepsilon)^{1/2}$. All these ratio have a magnitude comprised between 0.1 and 0.6: such $O(1)$ values seem reasonable.

As before, the scaling for the unconditional relative velocity $U_R = V_G - V_L$ can be deduced from the above information. Starting from eq. 5.4 and still assuming that $U_{structure} = V_{b|structure}$, we have $U_R = N_{clusters}(U_{clusters} - V_{mixture}) + N_{intermediate}(U_{intermediate} - V_{mixture}) + N_{voids}(U_{voids} - V_{mixture}) + \varepsilon U_R$ that transforms into :

$$\begin{aligned}(1-\varepsilon)U_R = N_{clusters}(U_{clusters} - V_{mixture}) + N_{intermediate}(U_{intermediate} - V_{mixture}) \\ +N_{voids}(U_{voids} - V_{mixture}) = (N_{clusters}\left[(U_{clusters} - V_{mixture})/(gD\varepsilon)^{1/2}\right] \\ +N_{intermediate}\left[(U_{intermediate} - V_{mixture})/(gD\varepsilon)^{1/2}\right] \\ +N_{voids}\left[(U_{voids} - V_{mixture})/(gD\varepsilon)^{1/2}\right])(gD\varepsilon)^{1/2} = C_R(gD\varepsilon)^{1/2}\end{aligned} \tag{5.8}$$

The prefactor C_R has been evaluated over various ranges of V_{sg} within the heterogeneous regime: it is given in Table 8 where we have also considered the two options for clusters (namely $n \geqslant 1$ and $n \geqslant 2$). Overall, the dispersion is small, and one gets:

$$(1-\varepsilon)U_R \sim 0.30 \pm 0.01(gD\varepsilon)^{1/2}. \tag{5.9}$$

As the average void fraction in the heterogeneous regime ranges from 20 to 37% for the experimental conditions considered here, the ratio $U_R/(gD\varepsilon)^{1/2}$ evolves from 0.37 to 0.50, to be compared with the value $U_R \sim 0.41(gD\varepsilon)^{1/2}$ deduced from direct velocity measurements of both phases in Section 3.2. The difference between these two results remains in the interval $[-11\%; +23\%]$. Such a difference is quite acceptable owing to the variety of independent measurements involved in that analysis (the latter include void fraction, unconditional and conditional relative velocities, statistics on size and on concentration for the three meso-scale structures, repartition of bubbles among these

$U_{relative\ structure-mixture}/(gD\varepsilon)^{1/2}$	Cluster n$\geqslant$ 1	Cluster n$\geqslant$ 2	Intermediate regions	Void regions	$(1-\varepsilon)/(gD\varepsilon)^{1/2}$ n$\geqslant$ 1	$(1-\varepsilon)/(gD\varepsilon)^{1/2}$ n$\geqslant$ 2
mean value over the range $V_{sg} \geqslant$ 6cm/s	0.517	0.556	0.176	-0.105	0.292	0.307
mean value over the range $V_{sg} \geqslant$ 9cm/s	0.520	0.564	0.189	-0.108	0.300	0.317
mean value over the range $V_{sg} \geqslant$ 13cm/s	0.515	0.563	0.187	-0.110	0.297	0.315

Table 8: Prefactors for the relative velocities $U_{relative}$ structure-mixture and for the unconditional relative velocity U_R with respect to the velocity scale $(gD\varepsilon)^{1/2}$ in the heterogeneous regime (from measurements on the axis of a D=0.4m bubble column at H/D=3.625).

structures based on Voronoï tessellations) and possibly also owing to the assumption $U_{structure} \sim V_{b|structure}$ we made.

The above arguments indisputably demonstrate that the increase of the bubble relative velocity beyond the terminal velocity value originates from the meso-scale structures present in the heterogeneous regime. In this process, clusters bring the strongest contribution. Thanks to the significant proportion of bubbles they gather (Table 3) and thanks to their high relative velocity with respect to the mixture (Table 7), they contribute by 65-68% to U_R. Intermediate regions host the majority of bubbles but their relative velocity with respect to the mixture is about 3 times smaller than that of clusters: they contribute by 33-35% to U_R. Last, void regions are sinking in the mixture: they carry few bubbles and their (negative) contribution to U_R is almost negligible ($\sim$ a few percents).

Eq. 5.9 then provides a way to estimate the actual relative velocity in the heterogeneous regime when changing the column diameter (provided the void fraction is known or can be predicted). Although as said above, data are lacking to check how U_R evolves with D, we can nevertheless discuss the trend predicted by eq. 5.9. For that discussion, we assume, as it is commonly accepted, that the void fraction weakly varies with D (see Section 6). Hence, eq. 5.9 predicts that the relative velocity monotonously increases with D. At first sight, that prediction seems odd if one refers to a single bubble dynamics that is controlled by its interaction with the liquid at a scale commensurable with the bubble size, and not with the size of the domain. However, we have just seen that collective dynamics in these buoyancy driven bubbly flows plays a central role in the formation of meso-scale structures, and that the presence of both dense structures and void regions drives the momentum exchanges between phases and leads to an enhancement of the relative velocity. Although it is unlikely that the typical width of dense regions grows with D, the void regions have an extension of order D. This is supported by our experiments in the $D = 0.4$m column (see Fig. 19). In addition, we will show in section 5.5 that the void regions globally correspond to large scale vorticity regions that are of order D. Dense regions appears then as thin sheets (a few bubble diameter wide) located in between vortices, and those developed length is of order D. These arguments indicate that the relative velocity is indeed controlled by the lateral dimension of the column.

In conclusion, in the heterogeneous regime, the above analysis connects the relative velocity between phases with the characteristics in terms of size and concentration of dense, intermediate and dilute regions formed in these buoyancy driven bubbly flows. These meso-scale structures and the dynamics they induce are therefore at the origin of the swarm factor introduced in Eulerian two-fluid simulations to evaluate the momentum exchange between phases in the heterogeneous regime. Moreover, a number of experimental results support the existence of an asymptotic flow organisation at large

V_{sg}, in particular with the saturation of the gas concentration in dense regions, and with limiting values of the spatial extent of meso-scale structures. Additional investigations are however required to fully determine how these asymptotic values evolve with parameters, and in particular with the bubble column diameter. Let us finally underline that, in their simulations of heterogeneous conditions, Panicker *et al.* (2020) captured the presence of bubble swarms with a characteristic length scale of order U_G^2/g and predicted a significant increase of the mean gas velocity compared with homogeneous conditions: these findings are consistent with the experimental results presented here.

5.5. *Velocity fluctuations, internal structure in the heterogeneous regime and fast track mechanism*

So far, we have discussed the scalings of the mean transport velocity and of the relative velocities. Let us turn now towards velocity fluctuations. In sections 3.2 and 4.3, we have seen that experiments are compatible with unconditional standard deviations of velocity of the liquid V_L' as well as of the gas V_G' phase evolving as $(gD\varepsilon)^{1/2}$. However, these findings are based on a limited number of data.

As for mean values, we take advantage of the Doppler probe to examine the behavior of the standard deviation of the bubble velocity conditional to meso-scale structures.

For that, we first considered the mean unconditional bubble velocity V_G as the reference, and we evaluated the standard deviation $V'_{b|structure} = std(v_{b|structure} - V_G)$ where std denotes the standard deviation, and where $v_{b|structure}$ is the instantaneous bubble velocity in the selected structure. The standard deviations with respect to the unconditional mean bubble velocity are shown Figure 25 for clusters, intermediate regions and void regions. Their evolutions with V_{sg} have qualitatively the same allure as those of the mean conditional velocities. As expected, the differences between meso-scale structures remain slim when in the homogeneous regime. However, in the heterogeneous regime, they differ from one meso-scale structure to the other: the velocity fluctuations are larger in clusters than in intermediate regions, and in intermediate regions than in void regions. The differences are about 0.2 to 0.3m/s.

As for the mean velocity, the unconditional standard deviation of bubble velocity can be deduced from the contributions of the three meso-scale structures, weighted by the proportion of bubbles they contain. Indeed, the sum $N_{clusters}V'_{b|clusters} + N_{intermediate}V'_{b|intermediate} + N_{voids}V'_{b|voids}$ has been compared to the standard deviation V_G', and the agreement is good with a discrepancy of at most 25% in the homogeneous regime and at most 20% in the heterogeneous regime. In the latter case, the contributions to velocity fluctuation mainly originate from clusters for 35-36% and from intermediate regions for 45-47%, with a few percents only arising from void regions.

The fact that bubble velocity fluctuations are significantly larger than liquid velocity fluctuations has already been observed on unconditional phasic velocities (Figure 4). We show here that this is also true for conditional bubble velocities, with the exception of the very low V_{sg} limit that belongs to the homogeneous regime. This is not surprising owing to the overwhelming contributions of clusters and of intermediate regions to bubble velocity fluctuations in the heterogeneous regime. Oddly, this is even true in void regions, possibly because these statistics recover bubbles having quite diverse environments as the local void fraction typically ranges from 0.4 to 0.1 times the mean hold-up (see Figure 15 and associated comments).

The fluctuations in bubble velocity arise from bubble velocity variations between different types of meso-scale structures. They can also arise from velocity variations between meso-scale structures belonging to the same population as both buoyancy and

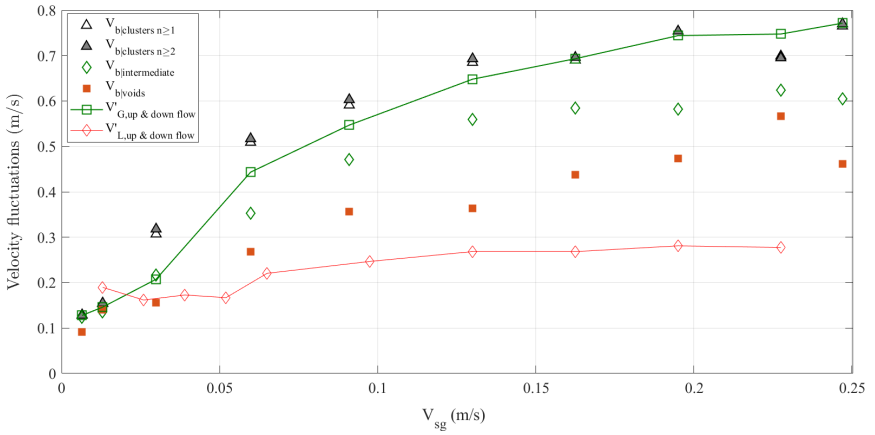

Figure 25: Standard deviations $std(v_{b|structure} - V_G)$ of bubble velocity conditioned by meso-scale structures i.e. clusters, intermediate and void regions with respect to the unconditional mean bubble velocity V_G versus the gas superficial velocity. Comparison with unconditional standard deviations of liquid and gas velocities. Measurements performed in a $D = 0.4$m column, on the column axis at $H/D = 3.625$.

inertia are variable from one structure to the other. In an attempt to evaluate that second contribution, we considered the quantities $L_{structure}[\varepsilon_{structure} - \varepsilon]$ that enter eq. 5.1 to 5.3 for the three meso-scale structures. Following the scaling rules given by 5.1 to 5.3, the velocity fluctuation associated with variations in size and concentration for a given meso-scale structure is evaluated as $w'_{structure} = gstd(L_{structure}[\varepsilon_{structure} - \varepsilon])^{1/2}$. These estimations are compared with the bubble velocity fluctuations conditioned by meso-scale structures in Figure 26. Figures are rather stable for V_{sg} above 10-15cm/s. It happens that for $w'_{structure}/V'_{b|structure} \sim 3$ for clusters, 1.5 for intermediate regions and about 1 for void regions. The contribution of the variability in size and in concentration of structures is therefore small for clusters, and it remains moderate but still higher than unity for intermediate regions. Hence, as clusters and intermediate regions bring the largest contribution to fluctuations, a significant fraction of bubble velocity fluctuations is therefore related with the velocity differences between the various types of meso-scale structures. Owing to the key contribution of the latter, we develop hereafter the idea that a fast track mecanisms is at play and that it connects the relative velocity with bubble velocity fluctuations.

As the starting point, let us come back to the structure of the flow in the heterogeneous regime. The spatial organization of the gas phase deduced from 1D Voronoï tesselations has demonstrated the presence of large regions at low void fraction. These void regions correspond to dark zones appearing when the flow near walls is examined with direct lightning (Figure 1). These dark regions correspond also to the large-scale vortical-like structures that have often been reported in the literature and that are illustrated in the cited figure. To quantify such vortical structures, we exploited the local liquid velocity provided by a Pavlov tube. Spatial correlations were not accessible with a single sensor, and liquid velocity measurements conditioned by the local gas concentration were not attempted. Instead, we considered time series collected from a single Pavlov tube even though its temporal resolution was low (about 14Hz). We detected the instants at which the instantaneous liquid velocity equals its mean value, and we measured the duration ΔT^+ (respectively ΔT^-) of successive intervals during which the liquid velocity stays

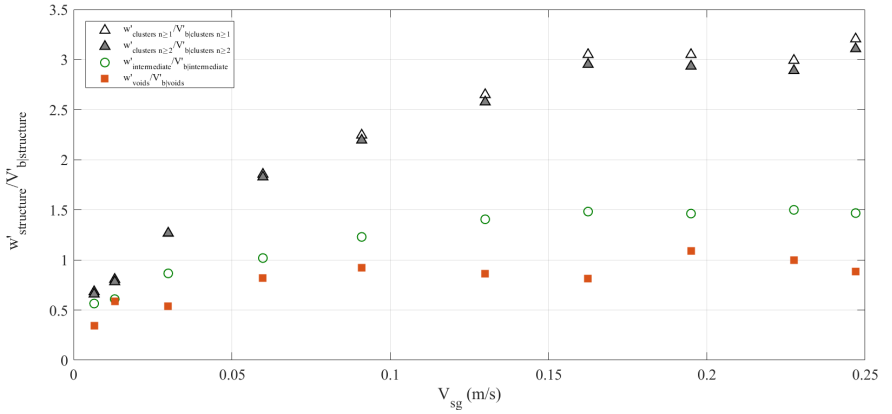

Figure 26: Comparison of the velocity variation $w'_{structure}$ due to size and concentration of meso-scale structures pertaining to the same population with bubble velocity fluctuations conditioned by meso-scale structures $V'_{b|structure}$. Measurements performed in a $D = 0.4$m column, on the column axis at $H/D = 3.625$.

above (respectively below) its average as illustrated in Figure 27. By multiplying these durations by the unconditionnal mean liquid velocity V_L, we deduced the vertical lengths $L^+ = V_L \Delta T^+$ (respectively $L^- = V_L \Delta T^-$) of liquid structures whose velocity is higher (respectively lower) than the average. A similar approach has been proposed by Liepmann & Robinson (1953) that related the Taylor microscale to the average distance between zero crossings of a streamwise velocity signal of a turbulent flow. In our case, it is not clear if the vertical spatial scale L we construct is related to any turbulence scale, as we are far from the conditions of homogeneity and isotropy required by the model from Liepmann & Robinson.

The distributions of L^+ and L^- measured in the $D = 0.4$m column are provided Fig. 28a for $V_{sg} = 19.5$cm/s. It can be observed that L^+ has significantly higher probability to have larger lengths, reaching values even larger than D, that can be as large as $2.5D$.

The mean values of L^+ and L^- are presented as a function of V_{sg} in Fig. 28b where the data for $D = 0.4$m and 1m columns extracted from Maximiano Raimundo's experimental campaign (Raimundo (2015)) have been added (Cartellier (2019)). Hence, such previous measurements performed in columns of diameter 0.4m and 1m, the mean size of vortical structures in the liquid phase increases with V_{sg} from $(0.07 \pm 0.02)D$ at $V_{sg} \sim 9$cm/s up to about $(0.11 \pm 0.02)D$ at large V_{sg} say between 25 to 35cm/s. Our present results are larger, as we find values of L^+ as big as 0.5D. The differences between our present dataset and the one from Maximiano Raimundo's campaign may be related to the spatial and temporal resolution of the Pavlov tube, but further studies are needed to properly address this difference. Nevertheless, all these structures have a magnitude comparable to the size of void regions in a $D = 0.4$m column as identified from Voronoï tessellations, that is about 0.18 D (Section 5.1). From these findings, a tentative cartoon of the spatial organization of phases in the heterogeneous regime emerges: bubbles accumulate in narrow (a few bubbles in size) regions located in between large ($\sim 0.1 - 0.4D$) vortical structures that are almost free of bubbles (Figure 29). The regions containing most bubbles are like thin "sheets" or "curtains". Let us try now to understand the consequences that such non-uniform spatial organization can have on the bubble dynamics.

Let us first show that the regions containing bubbles are not in the form of 'compact'

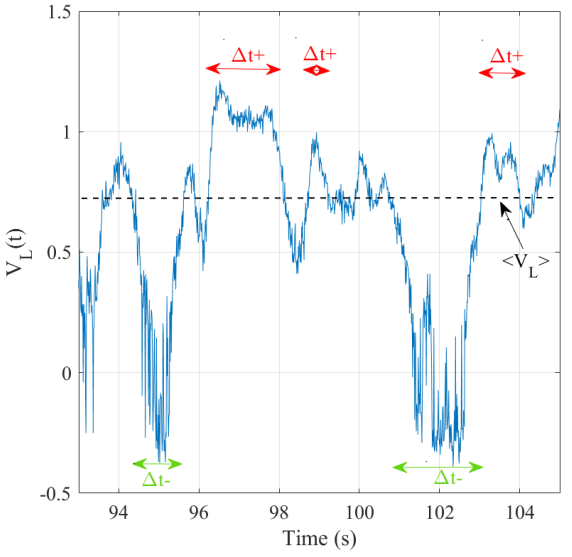

Figure 27: Example of the time evolution of the liquid velocity collected from a Pavlov tube for $V_{sg} = 16$ cm/s, and definition of successive time intervals ΔT^+ and ΔT^-. Measurements performed in a $D = 0.4$m column, on the column axis at $H/D = 3.625$.

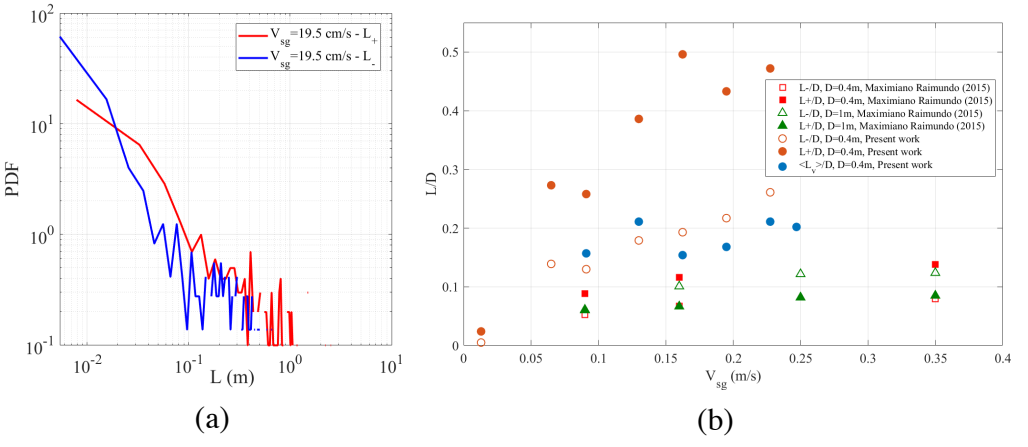

Figure 28: Dimensions of liquid structures deduced from the local liquid velocity versus time. (a) Distributions of L^+ and L^- for $V_{sg} = 19.4$cm/s measured in a D=0.4m column, on the column axis at $H/D = 3.625$. (b) Average size of liquid structures versus V_{sg} in $D = 0.4$m and $D = 1$m columns compared with the mean size of void regions measured in a $D = 0.4$m column.

clusters of bubbles. Indeed, the high particle Reynolds number bubbles considered here (see Section 4) are in a constant drag coefficient regime (when isolated). If one considers a compact, close to spherical assembly of N such bubbles, the dynamics of that ensemble would be also governed by a constant drag coefficient, and its relative velocity would be equal to $N^{1/6}U_T$. Therefore, the relative velocities between about $2U_T$ and $2.5U_T$ that

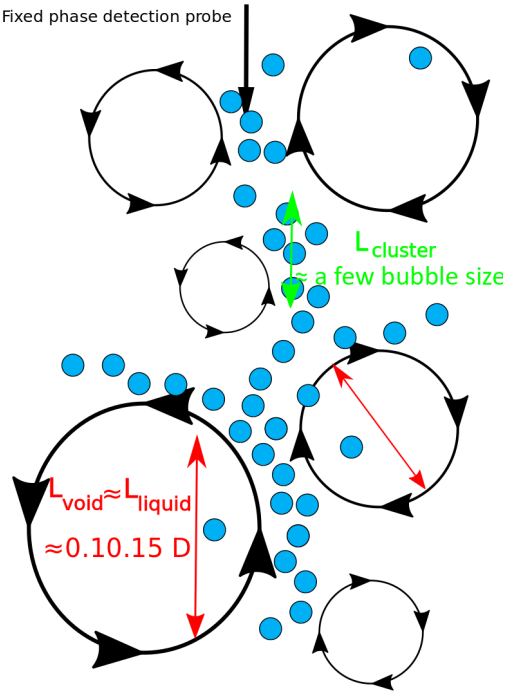

Figure 29: Tentative sketch of the flow organization.

we measured in heterogeneous conditions at large V_{sg} (for V_{sg} above 10cm/s, see Section 3), would be recovered with $N = 64$ for $2U_T$, or with $N = 244$ for $2.5U_T$: these figures are 10 to 50 times larger than the average number of bubbles present in clusters. Clearly, the existence of compact assemblies of bubbles does not correspond to observations. The question is now how thin bubbly sheets' could induce such an enhancement of the bubble relative velocity.

A plausible mechanism could be the following: as bubbles are mainly located between vortices, a fast track mechanism similar to the one observed in turbulent flow laden with inert particles (Wang & Maxey (1993)) takes place. Bubbles are channeling between vortices, and they preferentially pick up the side of eddies with an upward motion (choosing the downward side induces a much larger local relative velocity and hence a much larger drag). The neat result is a faster upward directed vertical bubble velocity. Such a picture is consistent with the conditional velocity measurements presented above. It also provides a physical background to the swarm coefficient often introduced in simulations to force the drag on a bubble to decrease with the local void fraction.

The proposed picture is also consistent with the impact a fast track mechanism has on the enhancement of the relative velocity. Indeed, in turbulent flows laden with inert particles, the enhancement of the settling velocity of dense particles is found proportional to the velocity fluctuations of the background turbulence, with a prefactor typically between 0.1 and 0.5 depending on particle and on flow characteristics (see for e.g. Wang & Maxey (1993); Mora *et al.* (2021)). Making a crude parallel with the present situation, we can consider V_L as the magnitude of external velocity fluctuations. In section 3, we have seen that, on the axis of a $D = 0.4$m column, the liquid fluctuations scale as $V_L' \sim 0.22(gD\varepsilon)^{1/2}$ while the mean relative velocity scales as $U_R \sim 0.3 - 0.4(gD\varepsilon)^{1/2}$:

these two results indicate that, when in the heterogeneous regime, U_R and V'_L remain proportional with a ratio about 0.5-0.7. This finding is therefore consistent with what is known about the impact of a fast track mechanism on the relative motion of inclusions with respect to a turbulent continuous phase. Beside, the velocity enhancement observed here is consistent with recent results concerning the frontier between enhancement and hindering (Mora *et al.* (2021)): the Rouse number of inclusions $Ro = U_R/V'_L$, that lies here between 0.5 and 0.7, is indeed small enough to avoid the triggering of a loitering scenario.

A question left open at this stage is why bubbles remain (in average) accumulated and stuck in between large-scale liquid structures. This is a counter-intuitive organization if one thinks of bubbles interacting with turbulent eddies in a denser fluid, as bubbles are preferentially moving towards low pressure zones, i.e. in the core of eddies. Our belief is that the situation in bubble columns is not the same as that of bubbles immersed in a weak turbulent field. We have shown in section 2 that, in the heterogeneous regime, buoyancy is the source of the mean motion and of velocity fluctuations by way of internal density gradients. In such flows, the accumulation or the depletion of bubbles are not governed by eddies interacting with independent, quasi-isolated bubbles, but by collective dynamics that imposes its forcing effect on the more inert phase. This is why, once formed, the (thin) clusters of bubbles as well as the empty regions are believed to persist for some time which is long enough compared with the transit time of the mixture from the bottom to the top of the bubble column. In our experiments, that transit time is about 1.5 to 3 seconds in the heterogeneous regime, and it is indeed small compared with the bubble response time a^2/ν_L that is about 10 seconds here. In other words, for the flow conditions considered here, there is not enough time available for bubbles to be significantly dispersed or to significantly diffuse outside dense regions. A companion argument is the following: the Rouse number evaluated above is small, and it would be even smaller if one considers the terminal velocity instead of the actual relative velocity. Such small Rouse numbers indicate that the turbulent field is quite intense compared with the (isolated) bubble motion relative to the liquid: hence, at first order, bubbles respond somewhat passively to the formation of turbulent eddies and they remain concentrated at their periphery.

The proposed scenario deserves to be tested further using experiments or direct numerical simulations. In particular, an in-depth investigation of the characteristics of the turbulence produced in such flows is also required. This scenario is expected to change when considering different flow conditions, notably in terms of bubble size at injection, or of coalescence efficiency. As a crude quantification of the limit of validity of this scenario, let us evaluate the size that would have bubbles so that their terminal velocity (when isolated) equals the relative velocity we measured in the $D = 0.4$m column. For a relative velocity about $2U_T$ where $U_T \sim 0.21 - 0.23$m/s, the bubble diameter should be multiplied by $44^{1/3} \sim 3.5$ compared with the size of the bubbles we considered. For a relative velocity about $2.5U_T$, the multiplication factor would be $244^{1/3} \sim 6$. Hence, the proposed scenario is expected to start to be altered when bubbles above 20 to 40mm in equivalent diameter appear in the flow.

6. Velocity scaling: further considerations

We have shown that, in the heterogeneous regime, all velocities, namely the mean velocity and its standard deviation in both phases as well as relative velocity between phases, scale with $(gD\varepsilon)^{1/2}$ as expected from an inertia-buoyancy equilibrium. We have shown that this scaling holds in a $D = 0.4$m column for all the flow conditions pertaining

to the heterogeneous regime that we investigated. The analysis of literature data has confirmed the validity of the proposed scaling for the mean and for the standard deviation of the liquid velocity in columns of diameter comprised between 0.1m and 3m, for the mean gas velocity in columns of diameter between 0.1m and 1m, and for the standard deviation of the gas velocity in columns of diameter $D = 0.29$m and 0.4m. For the relative velocity, the only data available concern the $D = 0.4$m bubble column considered here. Let us recall that almost all flow conditions analysed correspond to air-water systems with large bubbles at high particle Reynolds numbers (Section 4).

To reach a fully predictive status for velocities, one also needs the gas hold-up ε as a function of flow parameters. However, there is no consensus on the void fraction prediction in bubble columns operated in the heterogeneous regime as tens of different correlations involving various sets of parameters are proposed in the literature (as notably shown by the reviews by Joshi *et al.* (1998); Kantarci *et al.* (2005); Kikukawa (2017); Besagni *et al.* (2018)). There is even no clear consensus on non-dimensional parameters governing the response of the system. We propose in Annex A a dimensional analysis dedicated to the heterogeneous regime that is restricted to high aspect ratio bubble columns, to systems far from critical conditions, and without or with weak coalescence. We identify five independent non-dimensional parameters, and a possible choice could be:

- the Archimedes number $Ar = gD^3/\nu_L^2$, Ar is the square of a Reynolds number based on the column diameter D, on the liquid viscosity and on the velocity scale $(gD)^{1/2}$.
- the Froude number $Fr = V_{sg}/(gD)^{1/2}$, that quantifies the injected gas flow rate.
- Eötvös number $Eo = \rho_L g d^2/\sigma$, that measures the mean bubble size d relative to the capillary length.
- Morton number $M = g\mu_L^4/(\rho_L \sigma^3)$, that involves the physical properties of the couple of fluids selected and the gravitational acceleration.
- a non-dimensional parameter quantifying the degree of polydispersity in the system defined as the standard deviation of the bubble size distribution $std(d)$ divided by the mean bubble diameter d.

Among these, the Eötvös and Morton numbers completely define the dynamics, that is the shape, the trajectory and the relative velocity, of an isolated bubble having the mean equivalent diameter d immersed in the stagnant liquid and for the given gravitation field (strictly speaking, this holds for clean interfaces).

All the experimental conditions analysed here (see section 4) involve the same couple of fluids (i.e. air and water in ambient thermodynamic conditions) and earth gravity so the M parameter is the same ($\sim 10^{-11}$). The Eo parameter evolves in a rather narrow range, roughly from 1 to 10. For these M and Eo values, the bubbles are in the so-called wobbling regime, and they have similar dynamics with $O(10^3)$ particle Reynolds numbers (see Section 4). The polydispersity parameter $std(d)/d$ is scarcely quantified but, according to available bubble size distributions, it does not change much (the minimum bubble size is typically of the order of $0.5 - 1$mm while the maximum bubble size never exceeds ∼10mm). Hence, in the experiments quoted in Table 1 and 2, only the two parameters Ar and Fr have been significantly changed. The Ar number evolves between 9.8×10^9 and 2.6×10^{14}. Further, to be sure to analyse data pertaining to the heterogeneous regime (and thus to escape from the transition zone), let us consider gas superficial velocities above 7cm/s or 9cm/s. The corresponding Froude numbers span the range $[0.016; 0.475]$. According to Figures 7 and 9, the void fraction seems to be mainly driven by the superficial gas velocity V_{sg}. To check that, we first attempted a correlation with both Fr and Ar, and an exposant as low as 0.047 was found for the Ar number. We therefore examined how the void fraction evolves with the Froude number alone. As shown Fig. 30, the local void fraction correlates well with Fr as one gets:

$$\begin{aligned} \varepsilon_{axis} &= 0.853 Fr^{0.389},\ V_{sg} \geqslant 7cm/s, \\ \varepsilon_{axis} &= 0.838 Fr^{0.377},\ V_{sg} \geqslant 9cm/s, \end{aligned} \tag{6.1}$$

with correlation coefficients of about 0.8. The maximum deviation of these fits from measurements is ±30% except for two data collected in a $D = 3$m column at $V_{sg} =$ 16cm/s and 25cm/s for which the deviation reaches 35%. The measurements in large columns are not easy (probably due to vibration of the probe holder, and/or to flow perturbation induced by the latter when it is too large). If these two data are discarded, the correlation becomes:

$$\varepsilon_{axis} = 0.897 Fr^{0.415}, \tag{6.2}$$

with a correlation coefficient of 0.887. Eq. 6.2 holds for $V_{sg} \geqslant 7$cm/s as well as for $V_{sg} \geqslant 9$ cm/s. The deviation remains then within ±22% for all data. The correlation coefficients as well as the maximum deviations found here appear as acceptable, especially if one accounts for the fact that the data considered were collected at different heights above injection (see Table 4.1 and 4.2). Indeed, we have shown in Lefebvre *et al.* (2022) that the local void fraction on the axis linearly increases with the height in the quasi fully developed region of the flow. The impact of the measuring height on the local void fraction is illustrated in Fig. 30 by two data sets (closed symbols) gathered on the axis of the $D = 0.4$m column: the upper data set corresponds to $H/D = 6.37$ and the lower data set corresponds to $H/D = 2.85$. Clearly, the distance between these series is comparable with the dispersion.

The disappearance of the Archimedes number in the above empirical expressions for the void fraction is not unexpected. Indeed, as discussed in Annex A, the heterogeneous regime in a bubble column corresponds to a turbulent regime in free thermal convection. Thus, the Archimedes number somewhat controls the transition to that regime (the critical Rayleigh number introduced by Ruzicka & Thomas (2003) to identify the homogeneous-heterogeneous transition is proportional to Ar). However, once the turbulent regime is installed, buoyancy forcing overwhelms viscous effects, and the precise value of Ar is no longer relevant for setting the dynamical equilibrium: this is why its outcome, i.e. the void fraction, is no longer dependent on Ar.

There is also a debate as wether the void fraction should depend or not on the bubble column diameter D. For example, according to Besagni *et al.* (2018), the correlation proposed by Akita & Yoshida (1973) should be considered as the state of the art for determining the global gas hold-up. That correlation does not include any dependency of the void fraction on D. Yet, among the experiments quoted Table 4.1 and 4.2, huge differences (up to many times 100%) appear between gas hold-up measurements and predictions using the Akita and Yoshida's correlation. Beside, Ruzicka *et al.* (2001) unambiguously demonstrated that an increase in the column diameter advances the transition. Therefore, one expects some dependency of the void fraction on the bubble column diameter. According to the fits proposed here, ε_{axis} evolves as $\sim V_{sg}^{0.4}$ and as $\sim D^{-0.2}$.

Going back to the scaling for the mean liquid velocity (eq. 4.1) established in section 4.1, and using $\varepsilon_{axis} = 0.9 Fr^{0.4}$ as a convenient approximation of eq. 6.1 to eq. 6.2, we obtain:

$$V_L/(gD)^{1/2} \sim 0.58 \varepsilon^{1/2} \sim 0.55 Fr^{0.2}. \tag{6.3}$$

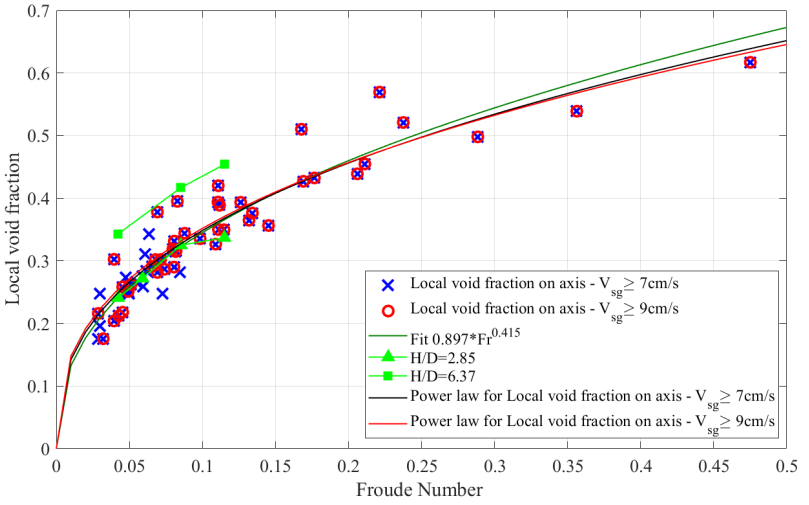

Figure 30: Correlation between the local void fraction on the axis of the column and the Froude number Fr=$V_{sg}/(gD)^{1/2}$ for all experiments quoted in Tables 1 and 2. Measurements performed for $1.3 \leqslant H/D \leqslant 12$. To illustrate the impact of H/D, the data with closed symbols correspond to measurements in the D=0.4m column performed at moderate (H/D=2.85, triangles) and at large (H/D=6.37, squares) distances from injection.

Eq.(19) leads to $V_L \sim 1.09 V_{sg}^{0.19} D^{0.3}$ which is close to the empirical fit proposed by Raimundo *et al.* (2019) that wrote $V_L \sim 1.35 V_{sg}^{0.16} D^{0.4}$. Hence, we recover a formula similar to that empirical fit by exploiting the inertia-buoyancy argument leading to the $(gD\varepsilon)^{1/2}$ velocity scaling, combined with an empirical relationship between the local void fraction and the Froude number. These findings are therefore consistent with each other.

Let us compare eq. 6.3 with available results from the literature. The majority of the correlations proposed for the mean liquid velocity are not in a dimensionless form. Among those that are dimensionally consistent, only one proposal uses the $(gD)^{1/2}$ velocity scale. The latter writes:

$$V_L/(gD)^{1/2} = 0.737 Fr^{1/3}. \tag{6.4}$$

Eq. 6.4 was proposed by Zehner (see Zehner & Benfer (1996)) and by Kawase & Moo-Young (1986) who quote an earlier publication by Zehner in 1982 that provides the same prediction. Eq. 6.4 was derived using modelling considerations: it is based on a simplified axial momentum equilibrium and on a global energy balance where the dissipation in the column is estimated from mean liquid velocity profiles using a mixing length approach. According to Kawase & Moo-Young (1986), Eq. 6.4 is reliable for column diameters from 0.1 to 1m, and for Newtonian fluids with a dynamic viscosity between 10^{-3} and 2×10^{-2} Pa s: the range of Fr is not indicated. Besides, Kawase & Moo-Young (1987) correlated the global gas hold-up R_{G3} for Newtonian fluids as:

$$R_{G3} = 1.07 Fr^{2/3}. \tag{6.5}$$

Let us first underline that the exponents of Fr appearing in equations 6.4 and 6.5 are compatible with the scaling (see eq. 2.2) derived from inertia-buoyancy equilibrium.

However, the 1/3 exponent of Fr in eq. 6.4 is significantly larger than the empirical value 0.2 found here (see eq. 6.3). Similarly, concerning the dependency of the void fraction on the Froude number, the exponent 2/3 found by Kawase & Moo-Young (1987), is somewhat larger than the empirical value ($\sim 0.38 - 0.4$) found here (see Fig. 30). Let us finally underline that Kawase & Moo-Young (1987) found eq. 6.5 valid for D between 0.1 and 1.07m and for Fr from 0.005 to about 0.05. It happens that these flow conditions mostly correspond to, or/and are very close to the homogeneous regime (see Kawase *et al.* (1987)), so that the comparison of their proposal with the results we obtained in a pure heterogeneous regime is poorly relevant.

Further investigations are therefore required to accurately determine how the void fraction evolves with non-dimensional parameters, and in fine to predict absolute as well as relative velocities in bubble columns operated in the heterogeneous regime. However, the proposals made here are believed to be a rather robust first step in that direction.

7. Conclusions

We revisited the hydrodynamics of bubble columns operated in the heterogeneous regime. Conditions with large enough aspect ratio were selected to ensure the presence of a quasi-fully developed region where transverse profiles of void fraction, liquid and bubble mean velocities remain self-similar. We also focused the analysis on air-water systems in ambient thermodynamic conditions involving bubbles in the wobbling regime with large, $O(10^3)$ particle Reynolds numbers.

We have shown first that the dynamical equilibrium in these gravity driven bubbly flows balances liquid inertia with buoyancy. Contrary to thermal convection in tubes involving an unstable vertical stratification, the driving force in bubble columns arises from the radial difference in density induced by the transverse gradient in void fraction. The resulting scaling for velocities is $V \sim (gD\varepsilon)^{1/2}$, where D is the diameter of the bubble column, ε the void fraction and g the gravitational acceleration.

Using new experiments performed in a $D = 0.4$ bubble column, as well as data extracted from litterature, this scaling proposal is shown to hold for the large-scale motion of both liquid and gas phases. Moreover, it is valid over a wide range of flow conditions, namely for D from 0.1 to 3m and for gas superficial velocities V_{sg} up to 60cm/s: the corresponding Froude number $Fr = V_{sg}/(gD)^{1/2}$ spans a range from ~ 0.02 to ~ 0.5. The same scaling applies to velocity fluctuations, as the latter were found proportional to the mean velocity both in the gas and in the liquid.

We also confirmed the finding of Raimundo *et al.* (2019) that the recirculating liquid flow rate Q_{Lup} in the heterogeneous regime is uniquely set by the column diameter, namely $Q_{Lup} = 0.098 S_{core}(gD)^{1/2}$, where S_{core} is the cross-section of the mean recirculation cell of radius $0.7R$. That result further reinforces the fact that $(gD)^{1/2}$ is the natural velocity scale of the vertical transport.

The concentration field at small scales and its connection with the relative motion between phases was investigated in a $D = 0.4$m column for gas superficial velocities up to 25cm/s with a quasi-identical bubble size distribution. From Voronoï tessellations in one-dimension built from the signal delivered by an optical probe, the homogeneous - heterogeneous transition was shown to correspond to a standard deviation of the probability density of Voronoï cell widths that levels off from its value for a Random Poisson Process (RPP). That departure from RPP allows to unambiguously identify meso-scale structures, namely clusters (i.e. regions where bubbles tend to accumulate), void regions (i.e. regions including only few bubbles) and intermediate regions. These meso-scale structures were characterised in terms of size and of concentration. Within the

heterogeneous regime, length and concentration pdfs seem to asymptote as V_{sg} increases. In particular, the lengths of these meso-scale structures tend towards constant values for V_{sg} higher than $\sim$ 0.1m/s. Also, the absolute concentration in clusters saturates to 45-50% while the concentration in voids and in intermediate regions slightly but continuously increases with the mean gas hold-up. The picture that comes out from conditional measurements using optical probes and Pavlov tubes, comprises void regions that correspond to vortices in the liquid those size is a fraction of D, and 'thin' clusters – typically a few bubbles wide – structured as sheets in between these vortices. This picture is consistent with a fast track mechanism that, for moderate Rouse numbers, leads to liquid velocity fluctuations that are a fraction of the relative velocity between phases.

The origin of the large relative velocity observed in the heterogeneous regime has been for a long time a central question in the hydrodynamics of bubble columns. A series of arguments demonstrating the key role of meso-scale structures on the relative velocity of bubbles have been presented:

(i) Direct measurements of the unconditional mean relative velocity show that the relative velocity levels off at the homogeneous-heterogeneous transition. Beside, the relative velocity asymptotes at large V_{sg}: the limit, in the $D = 0.4$m column, is about 2.4 times the terminal velocity of bubbles.

(ii) Bubble velocity measurements conditional upon the local gas concentration indicate that bubbles in clusters are moving up must faster, up to 3 to 3.5 times the terminal velocity, than bubbles in void regions those speed is nearly equal to the unconditional liquid velocity. Similarly, bubbles in intermediate regions are moving up faster, up to 1.5 to 2 times the terminal velocity, than bubbles in void regions.

(iii) The mean unconditionnal relative velocity of bubbles is recovered from conditional mean relative velocities weighted by the proportion of bubbles present in each meso-scale structure.

(iv) Assuming equilibrium between inertia and buoyancy at the scale of each meso-scale structure allows recovering the mean bubble velocity conditional upon local gas concentration from the characteristics of meso-scale structures in terms of size and concentration.

These findings indicate that the flow dynamics in the heterogeneous regime originates from collective effects linked with the apparition of meso-scale structures. Besides, our proposal connects the relative velocity with the characteristics of these meso-scale structures: that result opens the way to the identification of the proper scaling of the relative velocity. In particular, the spatial extension of meso-scale structures stays proportional to the bubble column diameter, so that one expects a relative velocity evolving as $(gD\varepsilon)^{1/2}$. However, that proposal needs to be tested over a wider range of conditions. In particular, the meso-scale structures need to be characterized for different bubble column diameters. It would also be worthwhile to understand what controls the limits in concentration of meso-scale structures in the asymptotic state by examining higher gas superficial velocities. Further, a prediction of the gas hold-up is still lacking. An empirical proposal has been made for air-water systems involving wobbling bubbles, in which the local void fraction ε is a function of the Froude number alone. Further investigations of the flow structure, notably along the radial direction, and of the flow dynamics, including turbulence production and turbulence characteristics, are needed to understand the origin of the global self-organisation prevailing in the heterogeneous regime.

Let us finally mention another issue of importance concerning the impact of coalescence on the above finding and in particular on the structuration of the concentration field and on its consequences on the flow dynamics. We anticipate that the flow dynamics discussed

here and the proposed scalings would remain valid as far as bubbles do not become too large. This statement is already partly supported by the experiments we analysed as the latter cover various situations in terms of coalescence efficiency. From an analogy with collective effects in turbulent laden flows, we can tentatively propose a criterium. Indeed, the relative velocity could be affected if the Rouse number becomes large enough. If coalescence efficiency is strong enough to produce say 5 to 10cm diameter bubbles (as already observed in some flows), then their terminal velocity would be about 0.5-0.7m/s and it would become comparable to the magnitude of velocity fluctuations in a $D = 0.4$m column. In other words, with a Rouse number of order one or above, loitering could happen instead of fast track, and that may lead to a decrease in the relative velocity. Pushing the limit further, the bubble size would become of the order of D (as observed in fluidized beds), and the dynamic would drastically change as one approaches slug flows.

Acknowledgements

The LEGI is part of the LabEx Tec21 (Investissements d'Avenir - grant agreement n. ANR-11-LABX-0030). That research was also partially funded by IDEX UGA (n. ANR-15-IDEX-0002) The authors report no conflict of interest.

Appendix A. Dimensional analysis

A tentative dimensional analysis of bubble column hydrodynamics may be the following. First, we consider that a quasi-fully developed region does exist when in the heterogeneous regime. We restrict the analysis to situations where coalescence is not playing a key role. More precisely, there is no or weak coalescence in the quasi fully developed region of the column. Coalescence may be present in the entrance region just above injection and thus control the 'equilibrium' bubble size distribution, but it is not active in other regions of the column. In such circumstances, the flow in the quasi-fully developed region becomes insensitive to the detail of the injector design (provided some precautions on the design of that device). The relevant physical quantities are the following:

- D column diameter,
- Ho static liquid height in the column,
- Q_G injected volumetric gas flow rate or superficial velocity $V_{sg} = Q_G/(\pi D^2/4)$
- g gravitation acceleration,
- d mean bubble size,
- $std(d)$ standard-deviation on bubble size distribution
- ρ_L liquid density
- ρ_G gas density
- μ_L liquid dynamic viscosity
- μ_G gas dynamic viscosity
- σ surface tension

Note that because coalescence is discarded (assuming it has not a significant impact on the flow dynamics when it is weak enough), we do not account for physical quantities such as surface tension gradients nor surfactant concentration and transport and their consequences on interfacial rheology that can affect coalescence efficiency. We keep the standard-deviation std(d) of the bubble size distribution as a parameter. Indeed, some suggestions by Lucas *et al.* (2005) supported by experiments from Lucas & Ziegenhein (2019) tend to indicate that the extent bubble size distribution has an impact on the transition from the homogeneous to the heterogeneous regime. Also, the approach developed by Krishna *et al.* (1991) based on a bi-modal bubble size distribution requires

$std(d)$ as a parameter. Yet, it is not ascertained that the extent bubble size distribution has an impact on the dynamics in the heterogeneous regime. Without clear evidence in one direction or in the other, that parameter is kept in the list.

We restrict the analysis to ambient pressure and temperature that is far from critical conditions. Hence, the gas to liquid density and dynamic viscosity ratio remain much smaller than unity: we assume that they have an asymptotic behavior and therefore the two parameters ρ_G and μ_G disappear from the analysis.

We are left with 9 physical parameters: D, Ho, Q_G, g, d, $std(d)$, ρ_L, μ_L and σ. That list leads to 6 non-dimensional parameters. A possible choice could be:

- Archimedes number $Ar = gD^3\rho_L\delta\rho/\mu_L^2 = [gD^3/\nu_L^2](\delta\rho/\rho_L)$, with $\delta\rho = \rho_L - \rho_G$. Far from critical conditions, $\delta\rho/\rho_L \sim 1$ and thus, $Ar = gD^3/\nu_L^2$.
- Aspect ratio Ho/D
- Froude number $Fr = V_{sg}/(gD)^{1/2}$
- Eötvös number $Eo = \rho_L g d^2/\sigma = (d/a_c)^2$, where a_c is the capillary length scale.
- Morton number $M = g\mu_L^4/(\rho_L\sigma^3)$
- Non-dimensional width of the size distribution $std(d)/d$

We have seen that the response of the system does not depend on the static liquid height Ho when the aspect ratio Ho/D is large enough. We are thus left with 5 independent non dimensional parameters, namely Ar, Fr, Eo, M and $std(d)/d$.

Within that list, the Eötvös and the Morton numbers control the dynamics of an isolated bubble in a quiescent fluid (Clift *et al.* (2005)): in particular, they control the shape of the bubble and its terminal velocity U_T in the selected fluids and gravity field. Almost all experimental data mentioned in Tables 4.1 and 4.2 concern large (say 3 to 10mm) air bubbles in water for which the particulate Reynolds number is quite high ($\sim 800 - 2100$): they thus all correspond to bubbles in the same regime. The polydispersity is also significant in the experiments presented Tables 4.1 and 4.2: the parameter $std(d)/d$ is not often quantified, but available measured size distributions indicate that this parameter keeps the same magnitude even though coalescence efficiency varies. In particular, let us underline that the flow conditions in Tables 4.1 and 4.2 never concern bubbles whose size becomes of the order of the bubble column diameter (in other words, the flow conditions never correspond to slug flow).

Thus, over the conditions mentioned in Tables 4.1 and 4.2 that almost exclusively concern high aspect ratio bubble columns operated with a few millimeters in size air bubbles in water under ambient T, P conditions, only two non-dimensional parameters have been significantly varied, namely:

- the Archimedes number $Ar = gD^3\rho_L\delta\rho/\mu_L^2 = [gD^3/\nu_L^2](\delta\rho/\rho_L)$
- the Froude number Froude number $Fr = V_{sg}/(gD)^{1/2}$.

Note that the Archimedes number equals Re^2, where Re is the Reynolds number based on the velocity scale $(gD)^{1/2}$, on the size D of the column and on the viscosity ν_L of the liquid. For the data shown Figure 8, Ar ranges from 9.8×10^9 to 2.6×10^{14} when in the heterogeneous regime. The Archimedes number Ar is the equivalent of the Grashof number used in thermal convection where changes in density arise from differences in temperature and from fluid dilation instead of differences in local void fraction. In free thermal convection, the transition from laminar to turbulent regime corresponds to a Grashof number about 10^9 (Metais & Eckert (1964)). The magnitude of the Archimedes number in the heterogeneous regime discussed above exceeds indeed that critical Grashof limit: the heterogeneous regime in a bubble column can be seen as equivalent to the turbulent regime in thermal free convection.

Owing to that observation, one could be tempted to associate the homogeneous/heterogeneous transition with a critical Grashof or Archimedes number. However,

the above analysis was achieved in the asymptotic limit of a large aspect ratio. As far as the transition is concerned, both the column height (more precisely the static liquid height) and its diameter do affect the transition as demonstrated by Ruzicka *et al.* (2001). Consequently, the parameter Ho should be accounted for when discussing the transition, and the Grashof/Archimedes numbers definition should be adapted accordingly. Under such conditions, and as shown by Ruzicka & Thomas (2003), the homogeneous/heterogeneous transition can be seen as an equivalent of thermal layers instability those transition is driven by a Rayleigh number.

Appendix B. Evaluation of the gas concentration in a Voronoï cell

B.1. *Connection between cell width and cell concentration*

The magnitude of ΔT_k is related with the local and instantaneous concentration, that is the concentration at the scale of the k^{th} Voronoï cell. A large ΔT_k means that neighbouring bubbles are far from the test bubble, or equivalently that the concentration in the vicinity of the test bubble is low. Inversely, a small ΔT_k indicates the presence of close neighbours, that is a high void fraction in the vicinity of the test bubble.

In Raimundo *et al.* (2019), it is argued that the quantity $\Delta T_k / < \Delta T >$ equals the ratio of the local and instantaneous gas concentration ε_k to the average gas hold-up ε at the measuring location, i.e. $\Delta T_k / < \Delta T >= \varepsilon/\varepsilon_k$. This equality must be replaced by the equation B 1 below. Indeed, let us consider N bubbles detected over a measuring duration T_{probe}. By definition, the void fraction ε equals $(\sum_i t_{gi})/T_{probe}$ where i goes from 1 to N. By construction, the Voronoï cells map all the space (that is the whole measuring duration) so that $T_{probe} = \sum_k \Delta T_k$ where k goes from 1 to N. Hence $\varepsilon = (\sum_i t_{gi})/T_{probe} = (\sum_i t_{gi})/\sum_k \Delta T_k = N < t_g > /[N < \Delta T >]$ where mean values have been introduced in the last equality. Meanwhile, the local void fraction ε_k (i.e. at the scale of the k^{th} cell) is $t_{gk}/\Delta T_k$. Therefore :

$$\varepsilon_k/\varepsilon = [t_{gk}/\Delta T_k] \,/\, [< t_g > / < \Delta T >] = [t_{gk}/ < t_g >] \,/\, [< \Delta T > /\Delta T_k] \,. \qquad \text{(B 1)}$$

The concentration ε_k in the k^{th} cell scaled by the local concentration ε is indeed proportionnal to $< \Delta T > /\delta T_k$, but these quantities are not equal. The proportionality coefficient happens to depend on the gas residence time t_{gk} divided by the mean gas residence time $< t_g >$. That coefficient changes from one bubble to another in a given record. Therefore, it is not possible to univocally transform a threshold in $\Delta T_k / < \Delta T >$ (such a threshold is used to distinguish the three populations, namely clusters, voids and intermediate regions) into a threshold in terms of cell concentration. Instead, the distributions of actual concentrations in each population need to be analysed (see Fig. 16 and associated text).

B.2. *Gas concentration in a Voronoï cell*

Here above, the void fraction ε_k at the scale of the k^{th} cell is estimated as $t_{gk}/\Delta T_k$. That formula is exact for the situation of the bubble indicated as A in Fig. 31. Let us consider the three successive bubbles $k-1$, k and $k+1$. Let us increase the residence time of bubble k while maintaining everything else fixed. In particular, the centers of the three bubbles remain located at T_{k-1}, T_k and T_{k+1}, so that the k^{th} Voronoï cell keeps its width ΔT_k. When the k^{th} bubble grows and reaches the situation B (Fig. 31), the right hand side of the gas residence interval becomes located outside the cell. When the bubble grows further and reaches the situation C (Fig. 31), the residence time of

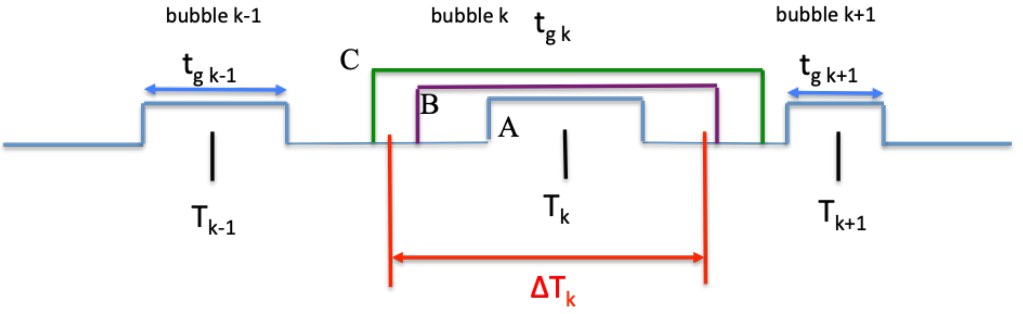

Figure 31: Void fraction at the scale of a Voronoï cell.

the bubble k exceeds the Voronoï cell width and ε_k becomes larger than unity. Hence, the formula $t_{gk}/\Delta T_k$ becomes incorrect when dealing with large bubbles (large t_{gk}) in a dense surrounding (small ΔT_k). In practice, one should account only for the fraction of the gas residence located inside the Voronoï cell. In Section 5, we used a somewhat crude correction as we simply set $\varepsilon_k = 1$ whenever $t_{gk}/\Delta T_k$ exceeded unity. However, the number of events concerned by that issue is quite limited (it is always less than 12% of the population) so that this approximation does not affect the trends identified nor the mean values.

REFERENCES

Akita, Kiyomi & Yoshida, Fumitake 1973 Gas holdup and volumetric mass transfer coefficient in bubble columns. effects of liquid properties. *Industrial & Engineering Chemistry Process Design and Development* **12** (1), 76–80.

Besagni, Giorgio, Inzoli, Fabio & Ziegenhein, Thomas 2018 Two-phase bubble columns: A comprehensive review. *ChemEngineering* **2** (2), 13.

Camarasa, E, Vial, Ch, Poncin, S, Wild, G, Midoux, N & Bouillard, J 1999 Influence of coalescence behaviour of the liquid and of gas sparging on hydrodynamics and bubble characteristics in a bubble column. *Chemical Engineering and Processing: Process Intensification* **38** (4-6), 329–344.

Capecelatro, Jesse, Desjardins, Olivier & Fox, Rodney O 2015 On fluid–particle dynamics in fully developed cluster-induced turbulence. *Journal of Fluid Mechanics* **780**, 578–635.

Cartellier, Alain H 2019 Bubble columns hydrodynamics revisited according to new experimental data. In *Recent advances in bubble columns organized by EFCE and SFGP*.

Castaing, Bernard, Rusaouën, E, Salort, Julien & Chillà, Francesca 2017 Turbulent heat transport regimes in a channel. *Physical Review Fluids* **2** (6), 062801.

Chaumat, Hélène, Billet, Anne-Marie & Delmas, Henri 2006 Axial and radial investigation of hydrodynamics in a bubble column; influence of fluids flow rates and sparger type. *International Journal of Chemical Reactor Engineering* **4** (1).

Chaumat, Hélène, Billet-Duquenne, AM, Augier, Frédéric, Mathieu, Charles & Delmas, Henri 2007 On the reliability of an optical fibre probe in bubble column under industrial relevant operating conditions. *Experimental Thermal and Fluid Science* **31** (6), 495–504.

Chen, Wei, Tsutsumi, Atsushi, Otawara, Kentaro & Shigaki, Yoshiki 2003 Local bubble dynamics and macroscopic flow structure in bubble columns with different scales. *The Canadian Journal of Chemical Engineering* **81** (6), 1139–1148.

Cholemari, Murali R & Arakeri, Jaywant H 2009 Axially homogeneous, zero mean flow buoyancy-driven turbulence in a vertical pipe. *Journal of fluid mechanics* **621**, 69–102.

Clift, Roland, Grace, John R & Weber, Martin E 2005 *Bubbles, drops, and particles*. Courier Corporation.

De Nevers, Noel 1968 Bubble driven fluid circulations. *AIChE Journal* **14** (2), 222–226.

Deckwer, Wolf-Dieter & Field, Robert W 1992 *Bubble column reactors*, , vol. 200. Wiley Chichester.

Ekambara, K, Dhotre, Mahesh T & Joshi, Jyeshtharaj B 2005 Cfd simulations of bubble column reactors: 1d, 2d and 3d approach. *Chemical Engineering Science* **60** (23), 6733–6746.

Ferenc, Járai-Szabó & Néda, Zoltán 2007 On the size distribution of poisson voronoi cells. *Physica A: Statistical Mechanics and its Applications* **385** (2), 518–526.

Forret, Ann 2003 Hydrodynamic scale-up of slurry bubble columns. PhD thesis, Université Claude Bernard – Lyon 1.

Forret, A, Schweitzer, JM, Gauthier, T, Krishna, R & Schweich, D 2006 Scale up of slurry bubble reactors. *Oil & Gas Science and Technology-Revue de l'IFP* **61** (3), 443–458.

Gemello, L, Cappello, V, Augier, F, Marchisio, D & Plais, C 2018 Cfd-based scale-up of hydrodynamics and mixing in bubble columns. *Chemical Engineering Research and Design* **136**, 846–858.

Gibert, Mathieu, Pabiou, Hervé, Tisserand, J-C, Gertjerenken, Betina, Castaing, Bernard & Chillà, Francesca 2009 Heat convection in a vertical channel: Plumes versus turbulent diffusion. *Physics of Fluids* **21** (3), 035109.

Guan, Xiaoping, Gao, Yongxiang, Tian, Zhen, Wang, Lijun, Cheng, Youwei & Li, Xi 2015 Hydrodynamics in bubble columns with pin-fin tube internals. *Chemical Engineering Research and Design* **102**, 196–206.

Guan, Xiaoping & Yang, Ning 2017 Bubble properties measurement in bubble columns: From homogeneous to heterogeneous regime. *Chemical Engineering Research and Design* **127**, 103–112.

Guan, Xiaoping, Yang, Ning, Li, Zhaoqi, Wang, Lijun, Cheng, Youwei & Li, Xi 2016 Experimental investigation of flow development in large-scale bubble columns in the churn-turbulent regime. *Industrial & Engineering Chemistry Research* **55** (11), 3125–3130.

Hills, J.H. 1974 Radial non-uniformity of velocity and voidage in a bubble column. *Transactions of the Institution of Chemical Engineers* **52**, 1–9.

Ishii, Mamoru 1975 Thermo-fluid dynamic theory of two-phase flow. *NASA Sti/recon Technical Report A* **75**, 29657.

Ishii, Mamoru & Zuber, Novak 1979 Drag coefficient and relative velocity in bubbly, droplet or particulate flows. *AIChE journal* **25** (5), 843–855.

Joshi, JB, Parasu, UV, Prasad, CVS, Phanikumar, DV, Deshpande, NS & Thorat, BN 1998 Gas hold-up structures in bubble column reactors. *Proceedings of the Indian National Science Academy* **64** (4), 441–567.

Kantarci, Nigar, Borak, Fahir & Ulgen, Kutlu O 2005 Bubble column reactors. *Process biochemistry* **40** (7), 2263–2283.

Kawase, Y, Halard, B & Moo-Young, M 1987 Theoretical prediction of volumetric mass transfer coefficients in bubble columns for newtonian and non-newtonian fluids. *chemical Engineering science* **42** (7), 1609–1617.

Kawase, Y & Moo-Young, M 1986 Liquid phase mixing in bubble columns with newtonian and non-newtonian fluids. *chemical Engineering science* **41** (8), 1969–1977.

Kawase, Yoshinori & Moo-Young, Murray 1987 Theoretical prediction of gas hold-up in bubble columns with newtonian and non-newtonian fluids. *Industrial & engineering chemistry research* **26** (5), 933–937.

Kikukawa, Hiroshi 2017 Physical and transport properties governing bubble column operations. *International Journal of Multi-phase Flows* **93**, 115–129.

Krishna, R, Wilkinson, PM & Van Dierendonck, LL 1991 A model for gas holdup in bubble columns incorporating the influence of gas density on flow regime transitions. *Chemical Engineering Science* **46** (10), 2491–2496.

Lefebvre, Anthony, Gluck, Stéphane, Mezui, Yann, Obligado, Martin & Cartellier, Alain H 2019 A new optical sensor for bubble velocity and size measurements in heterogeneous bubbly flows. In *The 12th European Congress Of Chemical lEngineering*.

Lefebvre, Anthony, Mezui, Yann, Obligado, Martin, Gluck, Stéphane & Cartellier, Alain 2022 A new, optimized doppler optical probe for phase detection, bubble velocity

and size measurements: investigation of a bubble column operated in the heterogeneous regime. *Chemical Engineering Science* **250**, 117359.

Liepmann, HW & Robinson, MS 1953 Counting methods and equipment for mean-value measurements in turbulence research. *Tech. Rep.*. National advisory committee for aeronautics.

Lucas, D, Prasser, H-M & Manera, A 2005 Influence of the lift force on the stability of a bubble column. *Chemical Engineering Science* **60** (13), 3609–3619.

Lucas, D & Ziegenhein, T 2019 Influence of the bubble size distribution on the bubble column flow regime. *International Journal of Multiphase Flow* **120**, 103092.

Maxworthy, T, Gnann, C, Kürten, M & Durst, F 1996 Experiments on the rise of air bubbles in clean viscous liquids. *Journal of fluid mechanics* **321**, 421–441.

McClure, Dale D, Kavanagh, John M, Fletcher, David F & Barton, Geoffrey W 2017 Experimental investigation into the drag volume fraction correction term for gas-liquid bubbly flows. *Chemical Engineering Science* **170**, 91–97.

Menzel, Thomas, In der Weide, Thomas, Staudacher, Oliver, Wein, Ondra & Onken, Ulfert 1990 Reynolds shear stress for modeling of bubble column reactors. *Industrial & engineering chemistry research* **29** (6), 988–994.

Metais, B & Eckert, ERG 1964 Forced, mixed, and free convection regimes. *Journal of Heat Transfer* .

Mezui, Yann, Cartellier, Alain H & Obligado, Martin 2018 Characterization of bubbles clusters in bubble column. In *Dispersed Two-Phase Flows 2018, SHF colloquium*.

Monchaux, Romain, Bourgoin, Mickaël & Cartellier, Alain 2010 Preferential concentration of heavy particles: A voronoï analysis. *Physics of Fluids* **22** (10), 103304.

Mora, Daniel Odens, Aliseda, A, Cartellier, Alain & Obligado, M 2018 Pitfalls measuring 1d inertial particle clustering. In *iTi Conference on Turbulence*, pp. 221–226. Springer.

Mora, Daniel Odens, Aliseda, Alberto, Cartellier, Alain & Obligado, Martin 2019 Characterizing 1d inertial particle clustering. *arXiv preprint arXiv:1906.09896* .

Mora, Daniel Odens, Obligado, Martin, Aliseda, Alberto & Cartellier, Alain 2021 Effect of re λ and rouse numbers on the settling of inertial droplets in homogeneous isotropic turbulence. *Physical Review Fluids* **6** (4), 044305.

Nedeltchev, Stoyan 2020 Precise identification of the end of the gas maldistribution in bubble columns equipped with perforated plate gas distributors. *Chemical Engineering Journal* **386**, 121535.

Panicker, Nithin, Passalacqua, Alberto & Fox, Rodney O 2020 Computational study of buoyancy driven turbulence in statistically homogeneous bubbly flows. *Chemical Engineering Science* **216**, 115546.

Raimundo, Pedro Maximiano 2015 Analyse et modélisation de l'hydrodynamique locale dans les colonnes à bulles. PhD thesis, Université Grenoble Alpes (ComUE).

Raimundo, P Maximiano, Cartellier, A, Beneventi, Davide, Forret, Ann & Augier, Frédéric 2016 A new technique for in-situ measurements of bubble characteristics in bubble columns operated in the heterogeneous regime. *Chemical Engineering Science* **155**, 504–523.

Raimundo, P Maximiano, Cloupet, Ann, Cartellier, A, Beneventi, Davide & Augier, Frédéric 2019 Hydrodynamics and scale-up of bubble columns in the heterogeneous regime: Comparison of bubble size, gas holdup and liquid velocity measured in 4 bubble columns from 0.15 m to 3 m in diameter. *Chemical Engineering Science* **198**, 52–61.

Risso, Frédéric 2018 Agitation, mixing, and transfers induced by bubbles. *Annual Review of Fluid Mechanics* **50**, 25–48.

Roghair, I, Lau, YM, Deen, NG, Slagter, HM, Baltussen, MW, Annaland, M Van Sint & Kuipers, JAM 2011 On the drag force of bubbles in bubble swarms at intermediate and high reynolds numbers. *Chemical engineering science* **66** (14), 3204–3211.

Rollbusch, Philipp, Bothe, Melanie, Becker, Marc, Ludwig, Martina, Grünewald, Marcus, Schlüter, Michael & Franke, Robert 2015 Bubble columns operated under industrially relevant conditions – current understanding of design parameters. *Chemichal Engineering Science* **126**, 660–678.

Rusaouen, E, Riedinger, X, Tisserand, J-C, Seychelles, F, Salort, J, Castaing, B

& Chillà, F 2014 Laminar and intermittent flow in a tilted heat pipe. *The European Physical Journal E* **37** (1), 1–8.

Ruzicka, MC 2013 On stability of a bubble column. *Chemical Engineering Research and Design* **91** (2), 191–203.

Ruzicka, MC, Drahoš, J, Fialova, M & Thomas, NH 2001 Effect of bubble column dimensions on flow regime transition. *Chemical Engineering Science* **56** (21-22), 6117–6124.

Ruzicka, MC & Thomas, NH 2003 Buoyancy-driven instability of bubbly layers: analogy with thermal convection. *International Journal of Multiphase Flow* **29** (2), 249–270.

Sharaf, Safa, Zednikova, Maria, Ruzicka, Marek C & Azzopardi, Barry J 2016 Global and local hydrodynamics of bubble columns–effect of gas distributor. *Chemical Engineering Journal* **288**, 489–504.

Shu, Shuli, Vidal, David, Bertrand, François & Chaouki, Jamal 2019 Multiscale multiphase phenomena in bubble column reactors: A review. *Renewable Energy* **141**, 613–631.

Simonnet, M, Gentric, C, Olmos, E & Midoux, N 2007 Experimental determination of the drag coefficient in a swarm of bubbles. *Chemical Engineering Science* **62** (3), 858–866.

Sumbekova, Sholpan, Aliseda, Alberto, Cartellier, Alain & Bourgoin, Mickael 2016 Clustering and settling of inertial particles in turbulence. In *Proceedings of the 5th International Conference on Jets, Wakes and Separated Flows (ICJWSF2015)*, pp. 475–482. Springer.

Sumbekova, Sholpan, Cartellier, Alain, Aliseda, Alberto & Bourgoin, Mickael 2017 Preferential concentration of inertial sub-kolmogorov particles: the roles of mass loading of particles, stokes numbers, and reynolds numbers. *Physical Review Fluids* **2** (2), 024302.

Uhlmann, Markus 2020 Voronoï tessellation analysis of sets of randomly placed finite-size spheres. *Physica A: Statistical Mechanics and its Applications* **555**, 124618.

Vial, Ch, Laine, R, Poncin, S, Midoux, N & Wild, G 2001 Influence of gas distribution and regime transitions on liquid velocity and turbulence in a 3-d bubble column. *Chemical engineering science* **56** (3), 1085–1093.

Wang, Lian-Ping & Maxey, Martin R 1993 Settling velocity and concentration distribution of heavy particles in homogeneous isotropic turbulence. *Journal of fluid mechanics* **256**, 27–68.

Wilkinson, Peter M, Spek, Arie P & van Dierendonck, Laurent L 1992 Design parameters estimation for scale-up of high-pressure bubble columns. *AIChE Journal* **38** (4), 544–554.

Xue, Junli, Al-Dahhan, Muthanna, Dudukovic, MP & Mudde, RF 2008 Bubble velocity, size, and interfacial area measurements in a bubble column by four-point optical probe. *AIChE journal* **54** (2), 350–363.

Yao, BP, Zheng, C, Gasche, HE & Hofmann, H 1991 Bubble behaviour and flow structure of bubble columns. *Chemical Engineering and Processing: Process Intensification* **29** (2), 65–75.

Zehner, P & Benfer, R 1996 Modelling fluid dynamics in multiphase reactors. *Chemical engineering science* **51** (10), 1735–1744.